

The University of Yaoundé 1

Faculty of Science

Department of Physics

**Dynamical analysis of autonomous electrical circuits
based on the shunted Josephson junction**

Thesis Submitted and defended for the award of Doctorat/Ph.D.
in Physics

Option: Electrics and electronics systems.

By

MONKAM Ybriss Joël

Master in Physics

Registration Number: 17T5924



Under the supervision of

WOAFO Paul

Professor

University of Yaoundé 1

TCHITNGA Robert

Associate Professor

University of Dschang

Laboratory of Energy, electrics and electronics systems

ybrissjoelmonkam@yahoo.fr

© Year 2024

UNIVERSITÉ DE YAOUNDÉ
THE UNIVERSITY OF YAOUNDE I



FACULTÉ DES SCIENCES
FACULTY OF SCIENCES

DÉPARTEMENT DE PHYSIQUE
DEPARTMENT OF PHYSICS

ATTESTATION DE CORRECTION DE LA THÈSE DE DOCTORAT/Ph.D

Nous, Professeur BODO Bertrand et Professeur ESSIMBI ZOBO Bernard, respectivement Examineur et Président du jury de la Thèse de Doctorat/PhD de Monsieur MONKAM Ybriss Joël, Matricule 1715924, préparée sous la direction des Professeurs WOAFU Paul (Université de Yaoundé I) et TCHITNGA Robert (Université de Dschang), intitulée : « Dynamical analysis of autonomous electrical circuits based on the shunted Josephson junction », soutenue le Jeudi, 11 Janvier 2024, en vue de l'obtention du grade de Docteur/PhD en Physique, Spécialité Systèmes électriques et électroniques, attestons que toutes les corrections demandées par le jury de soutenance ont été effectuées.

En foi de quoi, la présente attestation lui est délivrée pour servir et valoir ce que de droit.

Fait à Yaoundé, le 09 février 2024

Examineur

Le Président du jury

Le Chef du Département de Physique

Pr BODO Bertrand

Pr ESSIMBI ZOBO Bernard



Pr NDIJAK Jean-Marie

DEDICATION

DEDICATION

..... To my mother **Mrs. YOSSA Thérèse**, for its unconditional supports moral, material, and financial, which have favored the achievement of this work.

.....To my late father **Mr. ZEMAHO François**, who has always encouraged me from the moment when I started to go to school until the end of this thesis. Father, rest in peace.

ACKNOWLEDGMENTS

ACKNOWLEDGMENTS

Although I am registered at the Laboratory of energy, electric and electronic systems of the University of Yaoundé I, this work has been carried out at the Laboratory of Modelling and Simulation in Engineering, Biomimetics and Prototypes (LaMSEBP), Faculty of Science, University of Yaoundé I.

I thank the Almighty God for all the strength and Mercy He has been giving me and the health He has always granted me till today.

I would like to express my sincere thanks to **Professor WOAFO Paul**, my Ph.D. supervisor who held me during this adventure. Professor, during all these years of the thesis, you have grown in me good scientific, which, I hope, will always help me during my scientific career. You inculcated good human values in me, Thanks for all that.

I would like to express my gratitude and profound thankfulness to **Professor TCHITNGA Robert**, my Ph.D. co-supervisor, for his constant support, advice, and encouragement during this research. Professor, from my Master thesis up to now, you have sown in me good qualities which, I hope, will make me a great person. Beyond the role of co-supervisor, you have been like a father to me.

I am indebted to **Professor TAKOUGANG KINGNI SIFEU** of the University of Maroua, for all the discussions we had together concerning this work and his availability in every instant. Thanks also Professor, for the valuable exchanges and advice. Receive my gratitude.

Thanks to **Professor NDJAKA Jean-Marie Bienvenu**, Head of Department of Physics, Faculty of Science, UYI, and the teaching staff of at department for their valuable teaching and their fruitful advice.

My sincere thanks are intended for the **jury members** for having accept to evaluate my work.

I took advantage of the advice and multiple helps of other doctors trained in LaMSEBP: **Dr. TALLA Alain Francis, Dr. NWAGOUM TUWA Péguy, Dr. METSEBO Jules, Dr. SIMO Hervé, Dr. NDEMANOU Péguy, Dr. CHAMGOUÉ CHÉAGÉ André, Dr. DONGMO Eric,**

ACKNOWLEDGMENTS

Dr. TCHAKUI Murielle, Dr. TSAPLA Rolande, Dr MAKOUO Lucienne, Dr SIMO DOMGUIA Ulrich, Dr THEPI SIEWE Raoul, Dr GOUABO Ulrich.

I express my gratitude to my classmate, **Dr. MBOU SOH Guy Bertrand** for the friendly atmosphere and team spirit. We teamed together on a lot of projects. Thank you again for these scientific discussions that we have always had, thus creating a link of fraternity.

Thanks also to all the Ph.D. students of the LaMSEBP, particularly **Mr KOUEMOU Cedric, Mrs KOUAMI Nadine, Mrs YOUMBI Dorota, Mrs ESSAMBA Ursule, Mrs NGATCHA Nelly, Mr MBOYO Rene, Mr KOUAM Fidel, Mr TEMGOUA Pavel**, for fruitful interactions during the laboratory seminars.

I would like to thank the teaching staff of the department of physics, Faculty of Sciences, University of Dschang, particularly : **Pr. FOTSIN Hilaire Bertrand, Pr. TCHOFFO Martin, Pr. YEMELE David, Pr. PELAP François, Pr. LOUODOP FOTSO Patrick Hervé, Dr. TALLA MBE Jimmi, and Pr. TALLA Pierre Kisito** for the quality of their teaching during my university curriculum in Dschang.

Thanks to **Dr KENGNE Romanic, Dr KAMDOUN Victor, Dr MEGAM NGOUONKADI Elie Bertrand, Dr MEZATIO Anicet, Mr NDASSI Hermann, Dr SOH Guy Dr NGAMSA TEGNITSAP Joakim Vianney, Dr FONKOU Rodrigue, Dr LEUTCHO Gervais, Mrs. TCHUYANG WANDA Valérie, Mr KENYENYEN Evaristus Moh** for their unconditional support and fruitful interactions, since my Master training at the University of Dschang.

I am grateful to all the scientific organizations in which I have been actively involved and for the different financial support, they provided to the group to carry out activities in secondary schools, universities, and conferences that helped me to grow scientifically during my Ph.D. Studies, notably the **Optical Society of America (OSA), the Society of Photonics, Instrumentation, and Engineering (SPIE), and the Institute of Electrical and Electronics Engineers (IEEE).**

I thank all the members of my family and especially my second mother **Mrs TIOGUE Yvonne**, my Uncle **Mr TEBEUKOU Duplex**, and her wife **Mrs TEBEUKOU Clementine** for

ACKNOWLEDGMENTS

their unconditional support and their encouragement. I thank **Mrs DONGMO Marie Claire, Mrs MAFEUKOUE Suzanne, Mrs KEUMENI Rose Eugenie, Mrs NGAMENI Victorine, Mrs TIEGOUM Hélène, Mr DEUMENI Joseph Carlos, Mr MONKAM Norbert.**

I would also like to thank my fiancée, **Miss YODJEU Marie Madeleine**, for her love and her tireless encouragement to hold on until the end of this work.

I thank all my brothers and sisters, **Mrs DJEUFEUDJIO ZEMAHO Jeannine Flore, Mrs TEDONDJEUN ZEMAHO Natalie Chancelle, Mr TIOZIA ZEMAHO Appolinaire, Miss NGUEMENI ZEMAHO Aimerance, Mr ZEMAHO TSEKA Guillaume, Miss NGUEMO ZEMAHO Viviane, Miss KENFACK Marie Claire and Mrs YODJEU Marie Madeleine** for their moral support and their encouragement which allowed me to always work without getting discouraged and to go to the end of this work. May this work feed in you the sense of effort and the perpetual quest for knowledge and perfection.

Thanks to the **ZEMAHO family**, and the **NGUIMINI family** for all the sympathy, support, and encouragement they granted me.

Finally, I express my sincere gratitude to all those whose names are not been mentioned here, but who have contributed in one way or in another to the success of this work.

TABLE OF CONTENTS

TABLE OF CONTENTS

DEDICATION	ii
ACKNOWLEDGMENTS.....	iii
TABLE OF CONTENTS	vi
LIST OF FIGURES.....	ix
LIST OF TABLES	xii
LIST OF ABBREVIATIONS	xiii
ABSTRACT	xv
RÉSUMÉ.....	xvi
GENERAL INTRODUCTION	1
CHAPTER 1: LITERATURE REVIEW	5
1.1. Introduction	5
1.2. Generalities on Josephson Junction (JJ): models and applications	5
1.2.1. Definition of a Josephson Junction.....	5
1.2.2. Importance of Josephson effect	8
1.2.3. Josephson junction models	9
1.2.3.1. Resistive-capacitive shunted junction (RCSJ) model.....	9
1.2.3.2. Resistive-capacitive-inductance shunted junction (RCLSJ) model.....	12
1.2.4. Applications of Josephson junctions	14
1.3. Electrical oscillators generating complex behaviors	15
1.3.1. Generalities	15
1.3.2. Some nonlinear electrical components and their use to generate complex behavior	18
1.3.2.1. Nonlinear resistor, the modified Van Der Pol–Duffing oscillator and the modified Chua’s circuit	18
1.3.2.2. The field-effect junction transistor (JFET) and the Single Op-Amp–Based Jerk Circuit	21
1.3.2.3. Memristor and memristive oscillator circuits	24
1.3.2.4. Nonlinear condenser and nonlinear Duffing oscillator	26
1.4. Problem statement of the thesis.....	28

TABLE OF CONTENTS

1.5. Conclusion.....	29
CHAPTER 2: METHODOLOGY	31
2.1. Introduction	31
2.2. Mathematical formalisms	31
2.2.1. Stability analysis of equilibrium points	31
2.2.2. Routh-Hurwitz criterion	33
2.3. Numerical methods	34
2.3.1. Fourth-order Runge-Kutta method for ordinary differential equations.....	35
2.3.1.1. Implementation for the first-order differential equation.....	35
2.3.1.2. Implementation for the m-order differential equation	35
2.3.2. Numerical tools for characterizing the dynamical states of non-linear systems	36
2.3.2.1. Time series	37
2.3.2.2. Phase portraits	37
2.3.2.3. Bifurcation diagrams.....	38
2.3.2.4. Lyapunov's exponent.....	39
2.3.2.5. Lyapunov's spectrum.....	41
2.3.3. Hardware and software	42
2.4. Analog and microcontroller simulation methods	42
2.4.1. Analog simulation method.....	42
2.4.1.1 Analog simulation operations	42
2.4.1.2. Analog simulation equipment	59
2.4.1.3. Electronic circuit simulators	61
2.4.2. Microcontroller simulation method	61
2.5. Conclusion.....	63
CHAPTER 3: RESULTS AND DISCUSSION	65
3.1. Introduction	65
3.2. Chaos and hyperchaos in Colpitts-Josephson junction-like circuit.....	65
3.2.1. Colpitts-Josephson junction like circuit and mathematical description	65
3.2.2. Equilibrium points and their stability analysis	67
3.2.3. Numerical simulations: chaos and hyperchaos.....	70

TABLE OF CONTENTS

3.2.4. Electronic implementation.....	73
3.2.4.1. Generating the sine nonlinearity	73
3.2.4.2. OrCAD-PSpice electronic simulation results	74
3.2.5. Microcontroller implementation of the Colpitts - Josephson junction circuit.....	77
3.3. Amplitude control and electronic implementation of the Colpitts Josephson junction Op amp circuit.....	78
3.3.1. Mathematical and numerical simulation of the Colpitts Josephson junction Op amp circuit	78
3.3.2. OrCAD-PSpice simulation of the Colpitts Josephson junction Op amp circuit.....	86
3.3.3. Partial and total amplitude controls of Colpitts Josephson junction Op amp circuit	89
3.3.3.1. Partial amplitude control.....	89
3.3.3.2. Total amplitude control.....	91
3.4. Conclusion.....	92
GENERAL CONCLUSION	93
EXTENSIONS AND FUTURE WORK.....	94
BIBLIOGRAPHY	95
LIST OF PUBLICATIONS OF THE THESIS	111

LIST OF FIGURES

LIST OF FIGURES

Figure 1.1 : JJ with two superconductors of the same kind separated by an insulator [88].....	6
Figure 1.2 : Basic structure of Josephson Junction (JJ) [93].....	8
Figure 1.3 : Schematic representation of, (a) the LRCSJ model, (b) the NRCLSJ model [4,67]	9
Figure 1.4 : Current-voltage characteristics at a temperature T (in Kelvin) of the intrinsic junction shunt resistance $R(V)$ [100]	11
Figure 1.5: Schematic representation of, (a) the NRCLSJ model, and (b) the LRCLSJ model [26]	12
Figure 1.6: (a) Nonlinear resistor symbol. (b) Physical realization of the nonlinear resistor [149]	18
Figure 1.7: Electrical model of the MVDPD oscillator [149].....	19
Figure 1.8: The normal Chua oscillator [149].....	20
Figure 1.9: a) N-channel JFET; b) P-channel JFET [183]	21
Figure 1.10: Schematic representation of the jerky oscillator. The nonlinear element is made of a JFET with the gate (G) and the source (S) electrodes short-circuited [161].....	23
Figure 1.11: (a) Representation of the memristor, (b) Equivalent circuit of the memristor [162].	24
Figure 1.12: Second-order nonautonomous inductor-free memristive chaotic circuit. (a) Circuit schematic diagram [162]	25
Figure 1.13: Model of the nonlinear condenser [164].....	26
Figure 1.14: Schematic of electromechanical device [166]	27
Figure 2.3: Circuit symbol of an ideal Op-amp	43
Figure 2.4: The Op-amp 741, a) Circuit symbol, b) Datasheet, c) Integrated circuit [180].....	46
Figure 2.5: Inverter circuit with Op-Amp.	46
Figure 2.6: Internal representation of inverter circuit with Op-Amp.....	47
Figure 2.7: Non-inverting circuit with Op-Amp.	48
Figure 2.8: Equivalent Potential Divider Network in non-inverting amplifier.	49
Figure 2.9: The voltage Follower circuit with Op-Amp.	50
Figure 2.13: The voltage multiplier type AD633JN series: a) Datasheet b) Integrated circuit [180].	58

LIST OF FIGURES

Figure 2.18: Materials use in this work: (a) Rigol digital oscilloscope; (b) Test board; (c) Computer; (d) Arduino Uno uboard; (e) Mutimeter; (f) Connection cables. [85, 180]	61
Figure 2.19: Illustration of the experimental method.....	62
Figure 2.20: Block diagram for the microcontroller simulation.	63
Figure 3.2: Stability boundaries of equilibrium point $E_1(0,0,0,0,0)$: (a) in parameter space spanning R and C_1 , and (b) the plot of initial condition x_6^* versus $R(\Omega)$ with $C_1 = 10nF$	69
Figure 3.3: (a) Lyapunov spectra of system (3.3) for the outputs 1 to 4 as a function of the parameter θ_2 ; (b) Corresponding bifurcation diagram displaying the local maximum (in black color) and local minimum (in red color) of x_1 as a function of θ_2 ; (c) Corresponding maximum Lyapunov diagram for $x_1(0) = x_2(0) = x_3(0) = 0.01$, $x_4(0) = x_5(0) = 0.001$, $x_6(0) = 0$, and parameter $C_1 = 10nF$ and $L = 0.8pH$	71
Figure 3.4: Zoom of the Lyapunov spectra of figure 3.3(a) to show places with two positive Lyapunov exponents	72
Figure 3.5: Phase portraits in the plane (x_2, x_4) and (x_1, x_3) for a hyperchaotic attractor (Figure 3.5 (a) for $\theta_2 = 13.60$) and chaotic attractor (Figure 3.5 (b) for $\theta_2 = 149.55$).....	73
Figure 3.6: a) Electric circuit with analogic sine function; b) Analog sine function curve with $R=1k\Omega$	73
Figure 3.8: OrCAD-PSpice phase portrait of hyper-chaotic and chaotic attractors in the planes (V_{C2}, I_L) and (V_J, I_S) for: (a) $\theta_2 = 13.60$ and (b) $\theta_2 = 149.55$	76
Figure 3.9 : Time evolution of the hyperchaotic signal x_2 (Figure 3.9 (a) for $\theta_2 = 13.6$) and that of the chaotic dynamics (Figure 3.9 (b) for $\theta_2 = 149.55$).....	77
Figure 3.10: Phase portraits (x_2, x_4) obtained from the microcontroller simulation: (a) hyperchaotic signal for $\theta_2 = 13.6$ and (b) chaotic attractors for $\theta_2 = 149.55$	78
Figure 3.12 : (a) Stability diagram of the equilibrium point E_I in parameter space spanning R and C_1 . (b) Stability diagram of the steady-state x_5^* (the initial condition of variable x_5) associated	

LIST OF FIGURES

with the equilibrium point E_I versus R for $C_I = 0.1 \text{ nF}$. The other parameters are set to $I_c = 0.55 \text{ mA}$; $C_J = 35 \text{ pF}$; $R_J = 0.061 \text{ } \Omega$; $C_2 = 10 \text{ nF}$; $L = 0.8 \text{ pH}$	81
Figure 3.13: Lyapunov spectra as a function of resistor $R(\Omega)$ (a) and the corresponding bifurcation diagram displaying the local maxima (b) of x_1 as a function of resistor R for $C_I=0.1 \text{ nF}$ and $L=0.8 \text{ pH}$	83
Figure 3.14: Zoom of the Lyapunov spectra of Figure 3.13 (a).....	84
Figure 3.15: Hyperchaotic and chaotic attractors in the plane (x_2, x_4) and (x_3, x_5) :.....	85
Figure 3.17: OrCAD-PSpice phase portrait of hyper-chaotic and chaotic attractors in the planes (V_{C_2}, I_L) and (V_J, φ) for (a) $R = 61.78 \times 10^{-2} \text{ } \Omega$ and (b) $R = 1.50 \text{ } \Omega$	88
Figure 3.18: (Color online) The average values of the state variables x_1 (black), x_2 (blue), x_3 (red), x_4 (yellow), and x_5 (green) versus boosting controller γ for $R = 0.6178 \text{ } \Omega$	90
Figure 3.19: (Colour online) Phase portraits in the plane (x_1, x_2) and time series of the signal x_1 of system (3.20) for $R = 0.6178 \text{ } \Omega$ and different values of control parameter γ : $\gamma = -10$ (black), $\gamma = 1$ (blue) and $\gamma = 12$ (red); Initial conditions $x_1(0) = 0.02$, $x_2(0) = 0.01$, $x_3(0) = 0.01$, $x_4(0) = 0.01$, $x_5(0) = 0.001$	90
Figure 3.20 : (Colour online) Phase portraits in the planes (x_1, x_2) , (x_2, x_4) and (x_3, x_5) of system (12) for $R = 0.6178 \text{ } \Omega$ and different values of control parameter ε : $\varepsilon = 0.5$ (black), $\varepsilon = 1.5$ (blue) and $\varepsilon = 2$ (red); Initial conditions $x_1(0) = 0.02$, $x_2(0) = 0.01$, $x_3(0) = 0.01$, $x_4(0) = 0.01$, $x_5(0) = 0.001$	92

LIST OF TABLES

LIST OF TABLES

Table 2.1: Characteristics of the various attractors for four-dimensional flow [211].....	41
Table 3.1: Values of resistors for the analog Colpitts-Josephson junction-like circuit with $\omega_0 = 10^4$, $C = 100nF$ and $u_0 = 1V$	87
Table 3.2: Values of resistors of the LCC-JJ-Op amp circuit with $\omega_0 = 10^4$ and $C = 100 nF$	87

LIST OF ABBREVIATIONS

LIST OF ABBREVIATIONS

AC:	Alternative Current
CCDs:	Charge Coupled Devices
CLC:	Capacitive-Inductance- Capacitive
DC:	Direct Current
DAC:	Digital to Analog Converter
EMS:	Electro-Mechanical System
FORTTRAN:	FOR mular TRAN lator
HB:	Hopf Bifurcation
ICSP:	In Circuit Serial Programming
IDE:	Integrated Development Environment
JFET:	Junction Field Effect Transistor
JJ:	Josephson Junction
KCL:	Kirchhoff Current Law
KVL:	Kirchhoff Voltage Law
LCC-JJ:	Inductance-Capacitive-Capacitive Josephson Junction
LE:	Lyapunov Exponent
LRCLSJ:	Linear Resistive-Capacitive-Inductance Shunted Junction
LRCSJ:	Linear Resistive-Capacitive Shunted Junction
MAPLE:	Mostly Annoying Programmable Language Ever
MATLAB:	MATrix LABoratory.
MVDPD:	Modified Van Der Pol–Duffing
NLE:	Non-Linear Element
NR:	Negative Resistor.
ODEs:	Ordinary Differential Equations
Op-Amp:	Operational Amplifier
PSpice:	Personal Simulation Program with Integrated Circuit Emphasis.
PWM:	Pulse Width Modulation
PWNL:	PieceWise NonLinearity

LIST OF ABBREVIATIONS

RCLSJ:	Resistive-Capacitive-Inductance Shunted Junction
RCSJ:	Resistive-Capacitive Shunted Junction
RK:	Runge Kutta
RSFQ:	Rapid Single Flux Quantum
SQUIDs:	Superconducting Quantum Interference Devices
SHeQUIDs:	Superfluid Helium Quantum Interference Devices
STJs:	Superconducting Tunnel Junction Detectors
S-I-S J:	Superconductor-Insulator-Superconductor Junction
Spice:	Simulation Program with Integrated Circuit Emphasis.
USB:	Universal Serial Bus

ABSTRACT

ABSTRACT

This thesis deals with the dynamical characterization of autonomous electrical circuits based on the shunted Josephson Junction (JJ). Two models of JJ are used. A linear resistive-capacitive-inductance shunted junction (LRCLSJ) model and a linear resistive and capacitive shunted junction model (LRCSJ) model. Each of those junction models is used in a Colpitts-like CLC circuit made of two capacitors, an inductance with its internal resistor though operating at low frequencies. The circuits proposed display Hopf bifurcation, periodic oscillations, chaotic as well as hyperchaotic attractors. The electronic implementation of these circuits using OrCAD-PSpice software is presented to confront the results of the numerical simulations. A good qualitative agreement is revealed by comparing the analog and numerical simulation results. The microcontroller implementation is presented in the LRCLSJ model, by using an Arduino UNO board. The results obtained are in good agreement with the numerical simulation results. The partial and total control of the amplitude of its signals are studied by introducing two additional parameters in one of the proposed circuits. This work contributes to the understanding of complex behaviors occurring in autonomous electrical circuits based on the shunted JJ.

Keywords: *Josephson junction, chaotic attractor, hyperchaotic oscillator, Hopf bifurcation, electronic simulation, microcontroller implementation, partial and total amplitude controls.*

RÉSUMÉ

Cette thèse traite de la caractérisation dynamique de circuits électriques autonomes basés sur la Jonction de Josephson (JJ) shuntée. Deux modèles de JJ sont utilisés dans ce travail : un modèle de jonction shuntée linéaire résistive-capacitive-inductive (LRCLSJ) et un modèle de jonction shuntée linéaire résistive-capacitive (LRCSJ). Chacun de ces modèles de jonction est utilisé dans un circuit CLC de type Colpitts composé de deux condensateurs, d'une inductance et de sa résistance interne, mais fonctionnant à basse fréquence. Les différents circuits proposés présentent des bifurcations de Hopf, des oscillations périodiques et des attracteurs chaotiques et hyperchaotiques. L'implémentation électronique de ces circuits à l'aide du logiciel OrCAD-PSpice est présentée pour confronter les résultats des simulations numériques. Un bon accord qualitatif est révélé en comparant les résultats des simulations analogiques et numériques. La simulation par microcontrôleur pour le modèle LRCLSJ est faite en utilisant une carte Arduino UNO. Les résultats obtenus sont en bon accord avec les résultats de la simulation numérique. Le contrôle partiel et total de l'amplitude de ses signaux est étudié en introduisant deux paramètres supplémentaires dans un des circuits proposés. Ce travail contribue à la compréhension des comportements complexes se produisant dans les circuits électriques autonomes basés sur la JJ shunté.

Mots clés : *Jonction de Josephson, attracteurs chaotiques, oscillateur hyperchaotique, bifurcation de Hopf, simulation électronique, simulation par microcontrôleur, contrôles partiel et total d'amplitude*

GENERAL INTRODUCTION

The dynamical study of electrical circuits is of vital interest for the understanding of certain phenomena in many fields of science and technologic, such as physics, chemistry, biology, and engineering. Many problems in these domains are related to nonlinear self-excited oscillators [1,2]. Two self-sustained oscillators based on JJ will be investigated in this thesis. Many researchers have studied Josephson junction (JJ) devices because they are very good candidates commonly exploited for the implementation of complex systems with specific applications [3-7].

Since the first full description of a chaotic system by Edward Lorenz through a set of three coupled first-order ordinary differential equations (ODEs) [8], a tremendous interest in developing deterministic chaos theory has boosted research in various directions. The quest for the simplest autonomous chaotic circuit has continuously arisen for various reasons [9-18]. One of the main reasons is that they can be used in many applications such as radar and sonar [19], secure chaotic communications [20], robotics [21], or random number generator [22]. A simplest autonomous circuit should minimize both the number of physical components and idealized elements in its mathematical model [23]. Chaos in superconducting JJ has been studied by many researchers [24-29]. Over the last three decades, the simplest chaotic circuits have been identified in circuits from five down to two components [9-18]. The simplest autonomous chaotic circuits in [9-18] required a passive or active nonlinear physical component. A two-element autonomous circuit has been realized using a nonlinear current-controlled meminductor [10]. One has assisted in the search for chaos and fractals in human and social and economic sciences [8, 30, 31], natural sciences [32-34], environmental sciences [35, 36], or medicine [37-39]. Applications of nonlinear sciences in various branches of engineering such as mechanics and mechatronics [40], electronics [41-43], optics, and telecommunication [44] have been reported, to name some. In ref. [11], a capacitor and a memristor have been required to obtain chaotic signals. Experimental evidence of chaotic signals in a circuit made of a junction field-effect transistor (JFET) and a tapped coil has been brought out by [12]. In ref. [13], a three-element autonomous circuit has been realized using a nonlinear active memristor. A four-component Chua's circuit proposed in [14] used an active nonlinear resistor. The authors of [15] demonstrated chaotic signals in a circuit made of one resistor, two capacitors, and an operational amplifier (Op-Amp) working in its nonlinear regime. Piper and Sprott introduced

GENERAL INTRODUCTION

two simple autonomous chaotic circuits using only op-amps and linear time-invariant passive components [16]. In [17, 18], three five-component autonomous chaotic circuits of a jerky type made of two capacitors, one resistor, one capacitor, one JFET, and one Op-Amp working in the linear regime have been proposed. With this increasing interest in a branch of science that is complex and somehow mathematically demanding, some researchers even expressed the view to see this science be taught earlier, say at the undergraduate level, for better dissemination. In this regard, [45] proposed a paper entitled Introducing chaotic circuits in an undergraduate electronic course. This thesis was reduced to showing visual proof of chaos in two simple electronics circuits. Later on, another author published a paper on Introducing nonlinear time series analysis in undergraduate courses [46]. This other contribution was not related to electronic circuitry. Recently [47] and [48] proposed approaches conciliating simple circuits and enough details that could explain chaos at the undergraduate level, including hyperchaos. However, the justification of hyperchaos in their circuits was partly due to the appearance of virtual impedances generally known as parasitic capacitors (or inductors) that occur at high frequencies in PN-junctions of semiconductor materials but disappear at low frequencies. These virtually present but physically absent impedances could make their circuits models non-realistic enough for undergraduates to understand hyperchaotic evidence in such circuits because equivalent circuits of active electronic components at high frequency may not have been taught yet. Because they need more than three energy tanks, autonomous hyperchaotic circuits generally result from modified chaotic circuits [49-51], coupling and synchronization of chaotic circuits [52-54], circuits with delay-line or analog development from mathematical equations [55], or even driving 3D systems to higher complexity [56,57]. Since the pioneering work of Chua [12], it is also known that chaotic circuits are nonlinear element (NLE) dependent. Such elements appear in circuits in the form of nonlinear resistances viewed as a single component (the example of a tunnel diode [58] or as a sub-circuit known as negative resistance [15,59]). They can also be encountered as nonlinear capacitors [60], or nonlinear inductors such as ferromagnetic inductors [61-64] and Josephson junctions (JJ) [65-67] or memristors [27,11]. With the rapid development in fabrication technology and low- (or high-) temperature superconducting materials, the investigations on JJ have attracted much attention due to its potential applications, such as voltage standards and microwave devices [70-72].

GENERAL INTRODUCTION

In this work, we will consider an NLE of the JJ type for its potential importance in engineering. It is present in quantum computation, where it contributes as superconducting quantum bits in quantum two-level systems. In microwave oscillators and digital electronics, its capacity to quickly change in bistable voltage state enables the realization of ultra-fast switching electronic components [73–76]. It is also used as voltage-controlled oscillators or magnetic field sensors for application in medical engineering, material science, geophysics, etc [73,77]. An interesting autonomous circuit based on JJ [78] indicates that the authors could control chaos using delayed linear feedback. We choose this model circuit as a candidate to compensate for the limitation mentioned above concerning the circuits in Refs [47] and [48]. Delay-line can be very cumbersome [79]. Thus, we propose replacing this with very simple nondelayed linear feedback that can be easier to implement. The new circuit recalls the chaotic single op-amp jerk circuit of Ref [81], where the predominant active component is made of a field-effect transistor with short-circuited gate-source electrodes that became a piece-wise NLE. Notwithstanding its simplicity compared to [78,79], it harbors hyperchaotic signals resulting from the contribution of the JJ described by its linear resistive-capacitive-inductive shunted junction (LRCLSJ) model, where its counterpart [80] with the same number of physical impedances generates chaos. The present work will provide additional tools to justify hyperchaos in autonomous circuits with less than four physical linear capacitors and/or inductors and operating at low frequency.

Inspired by [16-18], this thesis also proposes a five-component autonomous circuit made of two capacitors, one resistor, one inductor, one Op-Amp working in its linear regime, and a JJ described by a linear resistive and capacitively shunted JJ model. A JJ is a quantum mechanical device made by sandwiching a thin layer of insulating material between two layers of superconducting material [23, 82]. Moreover, it has been demonstrated recently that the differential equations derived from complex electronic circuits can be implemented in microcontrollers to generate real electronic signals similar to the ones that can be delivered by the electronic circuits made of discrete or analog electronic components [81, 83-87]. Because of the high-frequency working regime of the Josephson junction, one can think of considering this is free of noise method to generate complex electrical signals.

In the framework of this thesis, we aim to:

GENERAL INTRODUCTION

- **demonstrate that a simple five-components autonomous circuit made of a Colpitts oscillator in which a Josephson junction is added can generate chaos and hyperchaos;**
- **simulate electronically the analog equivalent circuit derived from the equations describing the autonomous Colpitts-Josephson junction like circuit;**
- **simulate by microcontroller the differential equations of the circuits and compare with the results obtained numerically and confront results to those obtained by numerical simulation;**
- **realize the microcontroller simulation based on differential equations discretized and inserted appropriately in a microcontroller program;**
- **analyse the electronic implementation to use the electronic simulation for partial and total amplitude controls of a proposed LCC-JJ-Op amp circuit.**

The present work is divided into three chapters. Chapter one is devoted to the literature review on JJ, their applications, and the electronic oscillators generating complex behaviors. We will conclude this chapter by highlighting the problems to be solved in the thesis.

In Chapter Two, the methods used are presented. We explain the mathematical, and numerical methods used to solve nonlinear differential equations. We also explain the analog and microcontrollers simulation methods.

In chapter three, we present the results obtained. We end the thesis with a general conclusion

CHAPTER 1: LITERATURE REVIEW

1.1. Introduction

This chapter provides an overview of the literature and some generalities on electrical circuits based on some nonlinear electrical components and the problem statement. Section 1.2 presents the generalities on nonlinear electrical circuits. Section 1.3 deals with some models of JJ and their applications, while section 1.4 will give more details on electric circuits based on some electrical nonlinear components. The problem statement of the thesis will be underlined in section 1.5. Section 1.6 will conclude the chapter.

1.2. Generalities on Josephson Junction (JJ): models and applications

1.2.1. Definition of a Josephson Junction

A Josephson junction is created by sandwiching a skinny layer of a nonsuperconducting material between two layers of superconducting material. The device's area unit was named in reconnaissance Brian Josephson, who foretold in 1962 that pairs of superconducting electrons may "tunnel" throughout the no superconducting barrier from one superconductor to the other. He conjointly foretold the precise variety of the present and voltage relations for the junction. Experimental work confirm later on that he was right, and Josephson was awarded the 1973 honor in Physics for his work. In a Josephson junction, the nonsuperconducting barrier separating the two superconductors should be skinny [88]. If the barrier is stuff, it is to get on the order of thirty angstroms thick or less. If the barrier is another metal (nonsuperconducting), it should be the maximum amount as many microns thick. Till an important current is reached, a supercurrent will flow across the barrier; lepton pairs will tunnel across the barrier with no resistance. However, once the important current is exceeded, another voltage can develop across the junction. That voltage can depend upon time that is, it is an AC voltage. This successively causes a lowering of the junction's important current, inflicting even a lot of traditional current to flow and a larger AC voltage.

We consider the Josephson Junction with two superconductors of the same kind separated by an insulator as shown in figure 1.1 and that no magnetic field is present. The object of the insulator is to separate the superconductors and leave open a way of coupling them by tunneling. Assuming that the temperature is low enough, so that, it can be considered that all electrons are associated together in Cooper pairs. Hence, since the motion of the electrons is correlated, we will use Ψ_1 to represent their motion on one side of the insulating barrier and Ψ_2 to represent the motion on the other side of the insulating barrier.

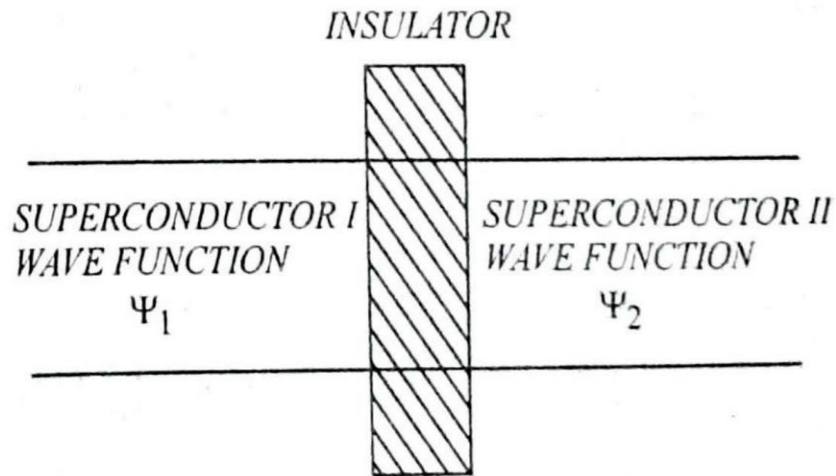


Figure 1.1 : JJ with two superconductors of the same kind separated by an insulator [88]

Let us assume that when the insulator is very thick so that both superconductors can act independently, then ψ_1 and ψ_2 satisfy Schrodinger-like equations

$$i\hbar \cdot \frac{\partial \psi_1}{\partial t} - H_1 \psi_1 = 0, \quad (1.1)$$

$$i\hbar \cdot \frac{\partial \psi_2}{\partial t} - H_2 \psi_2 = 0, \quad (1.2)$$

where H_1 and H_2 are operators and represent the energy on the two sides of the insulating barrier.

We consider the situation where the insulating barrier is not going thick so that the Cooper pairs are prevented from tunneling from one superconductor to the other.

This coupling will then be allowed by modifying the Schrodinger equations,

$$i\hbar \cdot \frac{\partial \psi_1}{\partial t} - H_1 \psi_1 = C \psi_2, \quad (1.3)$$

$$i\hbar \cdot \frac{\partial \psi_2}{\partial t} - H_2 \psi_2 = C \psi_2, \quad (1.4)$$

where C is a constant depending upon the material of the insulating barrier and its thickness as well. Since we are interested in the response of the Josephson junction to an applied voltage, so let us connect a potential difference V across the junction. If the charge of a Cooper pair is $q = 2e$, then

$$H_1 - H_2 - qV = 0. \quad (1.5)$$

If zero of potential energy is halfway between the two superconducting regions, then we have

$$i\hbar \cdot \frac{\partial \psi_1}{\partial t} - \frac{qV}{2} \psi_1 = C \psi_1, \quad (1.6)$$

$$i\hbar \cdot \frac{\partial \psi_2}{\partial t} - \frac{qV}{2} \psi_2 = C \psi_2, \quad (1.7)$$

The wave function can be written in terms of an amplitude and a phase as follows,

$$\Psi_i = \sqrt{\rho_i} \exp(iP_i), \quad (1.8)$$

where $\rho_i = |\psi_i|^2$ measures the density of a charge. Substituting equation (1.8) into equations (1.6) and (1.7) and separating real and imaginary parts, we get

$$\hbar \rho = 2C \sqrt{(\rho_1 \rho_2)} \cdot \sin \Delta, \quad (1.9)$$

$$\hbar(P_2 - P_1) = qV, \quad (1.10)$$

where Δ is the phase difference and is represented by

$$\Delta \equiv P_2 - P_1. \quad (1.11)$$

Since the rate at which the charge density begins to change should be proportional to the current density, therefore, we may have equation from (1.2) that,

$$J = J_0 \sin \Delta. \quad (1.12)$$

From equations (1.10) and (1.11), we get qV

$$\hbar\Delta = qV \text{ or } \Delta = \frac{qV}{\hbar}, \quad (1.13)$$

and hence by integrating equation (1.11), we find

$$\Delta(t) = \Delta_0 + \frac{q}{\hbar} \int_0^t V(t) dt. \quad (1.14)$$

Combining equations (1.12) and (1.14), we get a general expression for the current density in a JJ given by following equation.

$$J = J_0 \sin \left(\Delta_0 + \frac{q}{\hbar} \int_0^t V(t) dt \right). \quad (1.15)$$

Figure 1.2 illustrates the basic structure of one Josephson junction in a large series array; the junction is an overlap between two superconductors' thin films that are separated by a thin oxide barrier. The Josephson Effect [89, 90] is the remarkable effect of superconductivity, a macroscopic quantum phenomenon that appears at very low temperatures in some metals. In the superconductor state, the electrons attract two by two and form pairs, called Cooper Pairs [91]. The Josephson Effect is associated with the passage of these pairs by tunnel effect [92], through an insulating barrier placed between two superconductors, called Josephson Junction (figure 1.2b) (Superconductor-Insulator-Superconductor junction "S-I-S Josephson Junction").

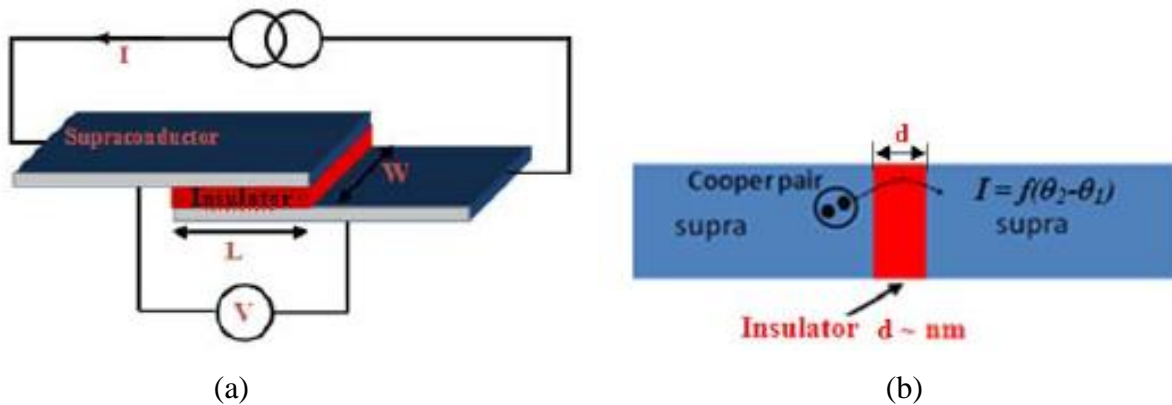


Figure 1.2 : Basic structure of Josephson Junction (JJ) [93]

1.2.2. Importance of Josephson effect

The Josephson effects are so important that they represent the quantum effects operating on a microscopic scale. To see the quantum effects on a macroscopic scale, we will be required to

have many particles in the same state, for example, photons are bosons and so we can get a man of them in the same state. Electrons are, however, fermions that must obey the Pauli principle. Hence it appears to be impossible to see the quantum effects of electrons on a macroscopic scale. However, in certain sense, the Cooper pairs having total spin zero do act like bosons and we can get several in the same state, which implies that it is possible to observe the quantum effects of superconductivity on a macroscopic scale.

1.2.3. Josephson junction models

In the literature, there are two main electrical rate-equations of JJ: Resistor and capacitor shunted JJ (RCSJJ) model, and resistor, capacitor, and inductive shunted JJ (RCLSJJ) model.

Recently, researchers have been extending chaos and nonlinear dynamics to Josephson junctions, particularly at the nanoscale, as these devices find applications as ultra-high-frequency oscillators, mixers, and filters that are of much use to encrypted telecommunication, information-protection intentions, and chaos-secured networks [20, 94]. Chaos has been observed in both theory and experiment in superconducting junctions and numerous models have been proposed, among which is the shunted resistive–capacitive–inductive Josephson junction (RCLSJ) [25, 95]. The latter is an extension of the semi-classical well-known RCSJ model [26, 98] and is receiving attention for the modeling structures used in millimeter-wave technology. These two models of JJ are presented as follows.

1.2.3.1. Resistive-capacitive shunted junction (RCSJ) model

The different RCSJ models are represented in the figure below.

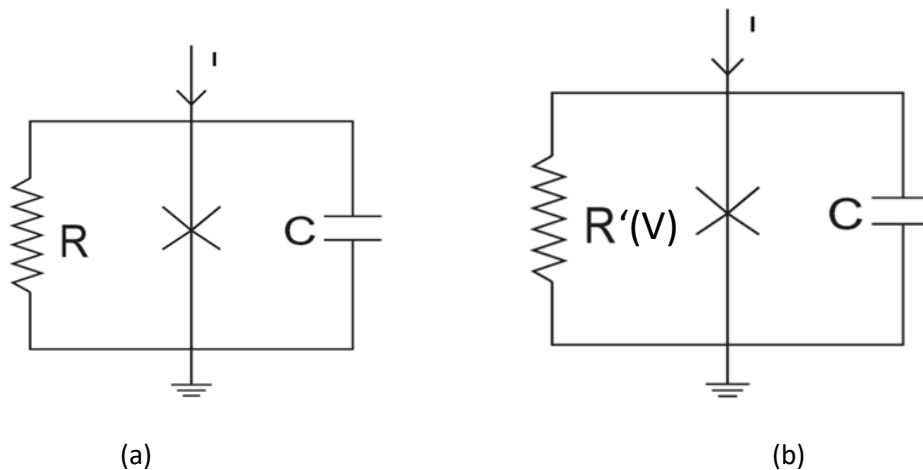


Figure 1.3 : Schematic representation of, (a) the LRCSJ model, (b) the NRCLSJ model [4,67]

The circuit of figure 1.3(a) consists of the external current source I , the capacitor C , the linear resistor R , and the JJ element connected in parallel. A voltage V is developed across the JJ by applying the Kirchhoff law, the following equations are obtained:

$$v = \frac{h}{2\pi e} \frac{d\phi}{dt'} \quad (1.16)$$

$$C \frac{dV}{dt'} + \frac{V}{R} + I_J = I, \quad (1.17)$$

where V is the voltage across the JJ, h is the Planck constant, t' is the time, e is the electron charge, $I_J = I_{JC} \sin \phi$ is the JJ current, and $\phi = \phi_2 - \phi_1$ is the phase difference. By introducing the following parameters:

$$t = \omega_0 t', \quad i(t) = I / I_C, \quad \omega_0 = (2\pi e I_{JC} / hC)^{1/2}, \quad V = v \sqrt{2\pi e C / h I_{JC}} \quad \text{and} \quad \beta_C = 2\pi e R^2 C I_C / h > 0,$$

The set of Eqs. (1.16, 1.17) can be normalized as:

$$\frac{d\phi}{dt} = V, \quad (1.18)$$

$$\frac{dV}{dt} = i(t) - V / \sqrt{\beta_C} - \sin(\phi), \quad (1.19)$$

where β_C is the capacitance of JJ.

The current-voltage (I-V) characteristic of the junction in figure 1.4 at a particular temperature T (in Kelvin) shows hysteresis (see figure 1.4) at a critical current I_C , where R_n is the junction normal state resistance and R_{sg} is the subgap resistance. I_{JC} the junction critical current, ϕ is the phase difference of the superconducting order parameter across the junction, R is the junction resistance and C is the junction capacitor. The complex dynamics in JJ arise due to the hysteresis in the current-voltage characteristic.

The modeling of the NRCSJ model (see figure 1.3(b)) is done in the same way. In NRCSJ and NRCLSJ models, a nonlinear resistance replaced the parallel linear resistance of the LRCSJ and LRCLSJ models, where the voltage-dependent junction resistance is defined by Eq. (1.20) and V_g is gap junction voltage. Whan et al. [26, 97] approximated the I-V characteristic as a step function between two junction resistances, which agrees with their experimental results.

$$R(V) = \begin{cases} R_n & \text{if } |V| > V_g \\ R_{sg} & \text{if } |V| \leq V_g \end{cases} \quad (1.20)$$

The intrinsic junction shunt nonlinear resistance $R(V)$ is modeled by a piecewise nonlinear resistor as shown in figure 1.4 below:

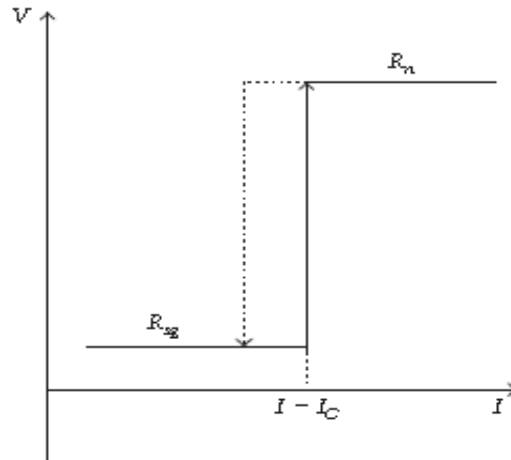


Figure 1.4 : Current-voltage characteristics at a temperature T (in Kelvin) of the intrinsic junction shunt resistance $R(V)$ [100]

The theoretical analysis and microcontroller implementation of the linear resistor-capacitor shunted Josephson junction model was studied by Ngatcha *et al.* [99], when the external current source is, firstly, considered as a DC, then secondly as an AC. These authors have shown that the rate-equations describing the linear resistive, capacitive shunted Josephson junction model have two or no equilibrium points relying on the external direct current source. They analyzed the stability of the two equilibrium points of the LRCSJJ model. They also showed that the increase of the capacitance of JJ led to an increase in the hysteresis loop of current-voltage curves. For given modulation parameters of external current source, linear resistor, capacitor shunted Josephson junction model displayed two different shapes of chaotic attractors, periodic attractors, limit cycle, and excitable mode. The existence of chaotic behaviors was confirmed by microcontroller results obtained from the microcontroller implementation of the linear resistor-capacitor shunted Josephson junction model.

1.2.3.2. Resistive-capacitive-inductance shunted junction (RCLSJ) model

The RCLSJ has been found to show complex and chaotic behavior crucially depending on the choice of system parameters. In the literature, we can find, the linear resistive-capacitive-inductance shunted junction (LRCSJ) model, nonlinear resistive-capacitive-inductance shunted junction model, and the NRCLSJ model [100–102]. The first two models show chaotic behaviors when driven by an external sinusoidal signal [77] while the NRCLSJ model generates chaotic oscillation with external dc bias only [117–119]. For large inductance, the NRCLSJ model behaves as a relaxation oscillator [25]. The NRCLSJ model [100, 101] is used to simulate JJ, resulting in a fairly good agreement with the experiment. The RCSJ model, however, fails to reproduce significant features on experimental I - V curves when the shunt of the JJ contains an inductance component [26, 104]. According to the results of these researchers, we will use the LRCSJ model in this thesis.

In their work [27], the authors, Sifeu Takougang Kingni *et al* consider the NRCLSJ model where the nonlinear resistance $R(V)$ is replaced by a linear resistance R . In figure 1.5(a), the shunted nonlinear resistance in figure 1.5(b) is replaced by a linear resistor R . The JJ is represented by the supercurrent channel I_c . I is the bias current applied to the JJ and C is the junction capacitance. A current I_s flows through the shunt inductance L_s and its internal resistance R_s .

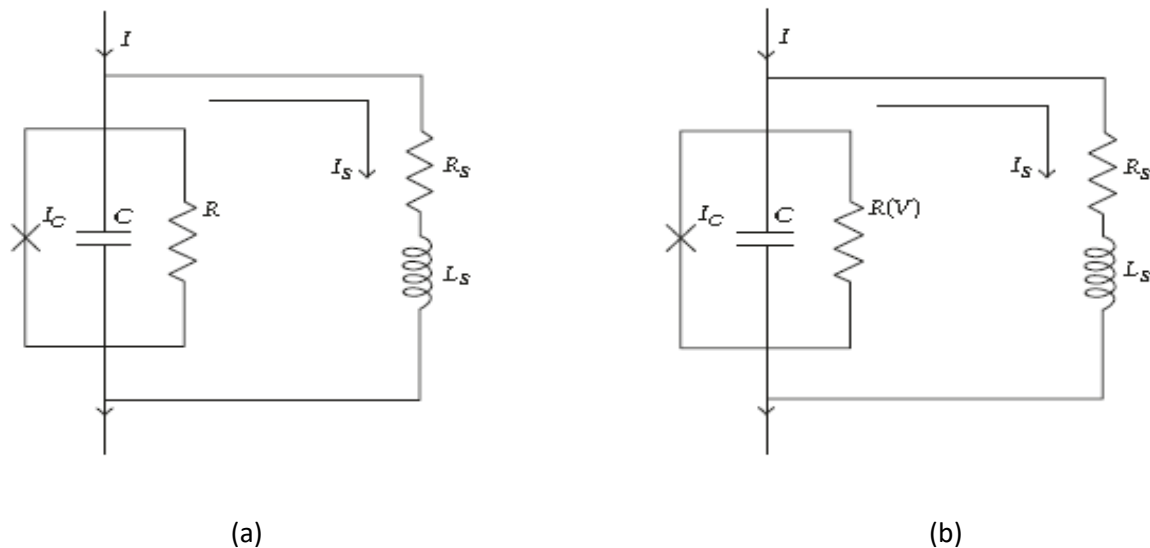


Figure 1.5: Schematic representation of, (a) the NRCLSJ model, and (b) the LRCLSJ model [26]

The application of the Kirchhoff laws to the circuit of Figure 1.5(a) leads to the following differential equation:

$$I = C \frac{dV}{dt} + \frac{V}{R} + I_C \sin \varphi + I_S, \quad (1.21a)$$

$$V = L_S \frac{dI_S}{dt} + R_S I_S, \quad (1.21b)$$

$$V = \frac{\hbar}{2e} \frac{d\varphi}{dt}, \quad (1.21c)$$

where ϕ denotes the phase difference of JJ and V the voltage across it.

Using the dimensionless variables,

$$V = x R_S I_C; \quad I_S = y I_C; \quad \varphi = z; \quad t' = \frac{t}{w_0}; \quad w_0 = \frac{2\pi e R_S I_C}{h}. \quad (1.22)$$

The dimensionless set of this system can be rewritten as

$$\dot{x} = \frac{1}{\beta_C} (i - y - \beta_R x - \sin z), \quad (1.23a)$$

$$\dot{y} = \frac{1}{\beta_L} (x - y), \quad (1.23b)$$

$$\dot{z} = x, \quad (1.23c)$$

with

$$\beta_R = \frac{R_S}{R}; \quad \beta_C = \frac{2\pi e C R_S^2 I_C}{h}; \quad \beta_L = \frac{2\pi e L_S I_C}{h}; \quad i = \frac{I}{I_C}. \quad (1.24)$$

Processing as in the case of figure 1.5(a), the mathematical equations governing the dynamics in figure 1.5(b) are given by the equation system below:

$$\begin{cases} \dot{x} = \frac{1}{\beta_C} (i - y - g(x)x - \sin z); \\ \dot{y} = \frac{1}{\beta_L} (x - y); \\ \dot{z} = x; \end{cases} \quad (1.25)$$

with the expressions of the parameters given by:

$$\beta_C = \frac{2\pi e C R_s^2 I_C}{h}; \quad \beta_L = \frac{2\pi e L_s I_C}{h}; \quad i = \frac{I}{I_C}. \quad (1.26)$$

The nonlinear function $g(x)$ is defined by:

$$g(x) = \begin{cases} \frac{R_s}{R_n} & \text{if } |x| < \frac{V_g}{R_s I_C} \\ \frac{R_s}{R_{sg}} & \text{if } |x| \geq \frac{V_g}{R_s I_C} \end{cases}. \quad (1.27)$$

In the ref [100], the authors investigated the dynamics of the LRCLSJ model by considering the effect of parameters on the system's behavior, to see if it can exhibit some of the dynamical behaviors of the NRCLSJ model. After investigation, the simulations show that for $i < 1.0$ the trajectories of the system converge to one of the equilibrium points $E_{1,2}$ while, for $i > 1.0$, the trajectories of the system display periodic or complex behaviors. It is interesting to note that, for $i > 1.0$, they also found regular spiking, intrinsic bursting, fast-spiking, and periodic bursting in the junction when the capacitive parameter β_C is kept fixed at $\beta_C = 0.007$, while the dc bias i , the inductive β_L , and resistive β_R parameters are varied.

1.2.4. Applications of Josephson junctions

The Josephson result has found wide usage, as an example within the following areas [67, 105]:

- ✓ SQUIDS, or superconducting quantum interference devices, area unit sensitive magnetometers that operate via the Josephson result. They are wide employed in science and engineering.
- ✓ In preciseness science, the Josephson result provides an associate in Nursing precisely duplicable conversion between frequency and voltage. Since the frequency is already outlined exactly and much by the atomic number 55 commonplace, the Josephson result is employed, for many sensible functions, to present the quality illustration of a V, the Josephson voltage commonplace.

- ✓ Single-electron transistors area units are typically created of superconducting materials, permitting users to be a product of the Josephson result to attain novel effects. The ensuing device is named a "superconducting single-electron transistor".
- ✓ The Josephson result is additionally used for the foremost precise measurements of elementary charge in terms of the Josephson constant and von Klitzing constant that is expounded to the quantum Hall result.
- ✓ RSFQ digital physics relies on shunted Josephson junctions. during this case, the junction shift event is associated with the emission of 1 magnetic flux quantum $1/2e.h$ that carries the digital information: the absence of shift is love zero, whereas one shift event carries a one.
- ✓ Josephson Junctions area unit integral in superconducting quantum computing as qubits like in a very flux qubit or others schemes wherever the section and charge act because the conjugate variables
- ✓ Superconducting tunnel junction detectors (STJs) might become a viable replacement for CCDs (charge-coupled devices) to be used in very astronomy in a few years. These devices are unit effective across a good spectrum from ultraviolet to infrared, and conjointly in x-rays. The technology has been tried out on the William Herschel Telescope within the SCAM instrument.
- ✓ Quiterons and similar superconducting shift devices.
- ✓ Josephson effect has also been observed in SHeQUIDs, the superfluid helium analog of a dc-SQUID.

1.3. Electrical oscillators generating complex behaviors

1.3.1. Generalities

Nonlinear electronic circuits have attracted appreciable attention because they can provide powerful experimental and analytical platforms for people to understand dynamic behaviors in physics [106], engineering [107, 108], electronic [109], and neurology [110]. Considering that a simple nonlinear electronic circuit can serve as a paradigm for a better understanding of bifurcation

and chaos, it is a significant research topic to simplify chaotic circuits by minimizing the number of dynamic elements and physical components [16,111-114].

The design of chaotic oscillator circuits has been a subject of increasing interest during the past few years because of the possible applications of chaos in several areas and particularly in communication. As an active topic of research, it has advanced significantly due to the pioneering contributions made by many authors [115–120]. The main thrust of this research is to discover new chaotic oscillator circuits and to further study the dynamics responsible for the generation of chaos in these circuits [115, 121, 122]. In the past three decades, a variety of nonlinear electronic oscillator circuits consisting of either real nonlinear physical devices such as nonlinear diodes, capacitors, inductors, and resistors or devices constructed with ingenious piecewise linear circuit elements [123] have been utilized as truth black boxes to explore different properties of chaotic dynamics. In particular, both autonomous and nonautonomous piecewise linear circuits have emerged as simple yet powerful experimental and analytical platforms for understanding bifurcation and chaos [115,124–126]. The nonautonomous circuits used by several authors [117,127–133] for this purpose are of second-order and incorporate the nonlinear element in terms of the well-known Chua's diode which exhibits two negative slopes in its I-V characteristic. Though its nonlinear behavior is mathematically tractable, its electronic implementation, using discrete components requires two op-amps and six linear resistors. Later, Lacy [131] proposed a simple nonautonomous circuit designed with a reduced number of nonlinear elements. In his circuit, he used one op-amp, three linear resistors, and two Zener diodes, and hence the total number of elements is reduced to six compared to two op-amps and six linear resistors in the case of Chua's diode. As the breakpoints depend on the total negative resistance of the circuit [121], the introduction of the Zener diode in this circuit sets the breakpoints at $\pm 1,0$ V. One of the present authors has already studied bifurcation and chaos in various simple second-order dissipative nonautonomous electronic circuits with Chua's diode as the nonlinear element [122,132]. In that study, he has reported quasiperiodicity, period-adding, Farey's sequences, intermittency, band-merging, etc. Very recently, Kurt [134] introduced numerically, a nonautonomous model of the nonlinear sub-circuit involving a nonautonomous Chua's diode (without minimizing the number of elements), which indicates the behavior of a nonlinear resistor and enhances the complexity of the standard Chua's diode. Thus, generating a new nonlinear chaotic electronic circuit with a reduced number of elements and with a new piecewise nonlinearity and further, understanding the

underlying physical mechanism has become an important and interesting topic of research in recent years [113]. Statistically speaking, nonautonomous circuits, one of the main forms of chaotic circuits, contain fewer dynamic elements than autonomous chaotic circuits since externally driven signals can replace a dynamic element or an oscillating unit in autonomous chaotic circuits [113].

Many autonomous chaotic circuits and non-autonomous nonlinear circuits can also exhibit many interesting dynamical phenomena [135-137]. Hyperchaotic systems appeared in many important fields of physics, engineering, and computer sciences, such as laser physics, control, flow dynamics, liquid mixing, electronic circuits, secure communications, and information sciences [138-140].

In 1982, Gibbon and McGuinness studied and stated the real and complex Lorenz equations in rotating fluids and lasers [141]. While, in 1983, Fowler *et al.* introduced complex Lorenz equations and their relevance to physical systems [142]. Zeglache and Mandel proposed complex nonlinear equations for detuned lasers [143]. The complex character of the state variables and parameters follows from purely physical considerations [144; 145]. Complex state variables (or quantities) are found in equations of problems in laser physics and thermal convection of liquid flows where the electric field and atomic polarization amplitudes are complex quantities, see [144, 146]. The real and imaginary parts of these variables can display chaotic and hyperchaotic dynamics. Mahmoud *et al.* [145] introduced complex Chen and Lü systems and studied their dynamics. The complex Lorenz, Chen, and Lü systems do not exhibit hyperchaotic dynamics. Therefore, one wishes to propose complex systems that display hyperchaotic behaviors. Special cases of complex systems have been studied in the recent literature. A system with more than one positive Lyapunov exponent is called a hyperchaotic system. The dynamics of hyperchaotic systems are complicated and rich in the sense that they exhibit chaotic and hyperchaotic behaviors as well as periodic and quasi-periodic solutions for wide and narrow ranges of system parameters. For example, chaotic behavior and chaos control for a class of complex partial differential equations have been studied in [147].

To have a complex dynamic as chaos and a possible hyperchaos in electrical circuits, there must be a nonlinear element in the circuit, i.e., the element with a nonlinear current-voltage characteristic, for example, nonlinear resistor, nonlinear capacitor, nonlinear inductor, memristor, diode, JJ, and many others. The simple examples of electric circuits where chaos appears are the

Van der Pol oscillator, and Chua's circuit [148]. Both circuits have one nonlinear element which is the nonlinear resistor. We will present some examples of circuits with complex behaviors in this section.

1.3.2. Some nonlinear electrical components and their use to generate complex behavior

1.3.2.1. Nonlinear resistor, the modified Van Der Pol–Duffing oscillator and the modified Chua’s circuit

a) Nonlinear resistor

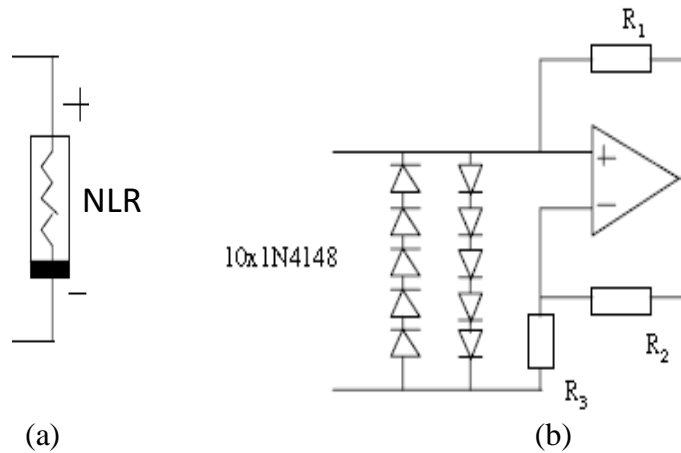


Figure 1.6: (a) Nonlinear resistor symbol. (b) Physical realization of the nonlinear resistor [149]

The physical realization of the nonlinear resistance for the MVDPD oscillator is shown in figure 1.6) [150, 151]. The operational amplifier (Op-Amp) mounted with the resistors R1, R2, and R3 realizes a piecewise-three region-linear resistance with a domain of negative resistance responsible of the birth of free oscillations, while the set of 10 signal diodes is used to introduce symmetrical nonlinearities in the current-voltage characteristics of the global nonlinear resistance which can therefore be approximated by a cubic function of the form. The I–V characteristic of the nonlinear resistor (NLR) is approximated by the cubic polynomial.

$$I(V) = t + aV + bV^3 \quad \text{with } (a < 0, b < 0). \quad (1.28)$$

Such a nonlinear element can be physically constructed using a set of diodes and an operational amplifier [152, 153].

b) Modified Van Der Pol–Duffing (MVDPD) oscillator

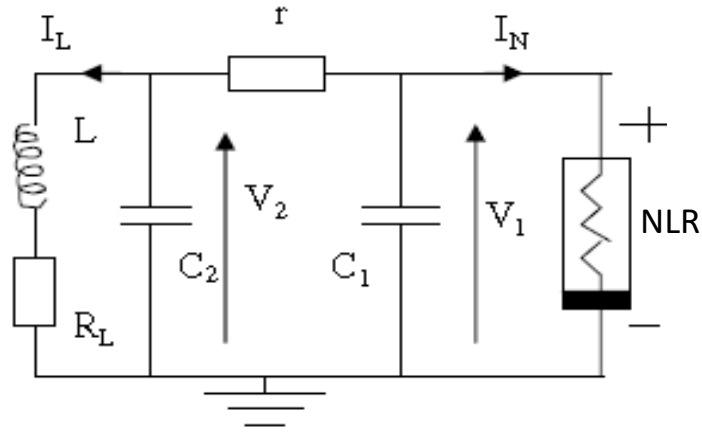


Figure 1.7: Electrical model of the MVDPD oscillator [149]

The modified Van der Pol–Duffing oscillator (MVDPD) is an improved model of an autonomous chaotic system introduced by King and Gaito in 1992 [149]. The authors proved in this work that the system has a chaotic dynamic.

By applying Kirchhoff’s laws to the equivalent circuit of figure 1.7, we obtain the following set of differential equations:

$$\begin{cases} \frac{dV_1}{dt} = \frac{1}{C_1} \left(\frac{1}{r} + a \right) V_1 + \frac{V_2}{rC_1} - \frac{b}{C_1} V_1^3 - \frac{v}{C_1}, \\ \frac{dV_2}{dt} = \frac{V_1}{rC_2} + \frac{V_2}{rC_1} - \frac{i_L}{C_2}, \\ \frac{di_L}{dt} = \frac{V_2}{L} - \frac{R_L}{L} i_L. \end{cases} \quad (1.29)$$

Note that since the parameter l is in general cancelled with the offset current of the op-amp, we further cancel it from our equations. With the selection of parameters $m = 100$, $a = 0.35$, $b = 300$ and $c = 0.2$, the MVDPD circuit has chaotic oscillations with a one-dimensional Lyapunov exponent $k_{max} = 0.96$. The initial values are chosen to be $(x_1(0), y_1(0), z_1(0)) = (0.2, 0.4, 0.5)$. [149].

c) Modified Chua's circuit

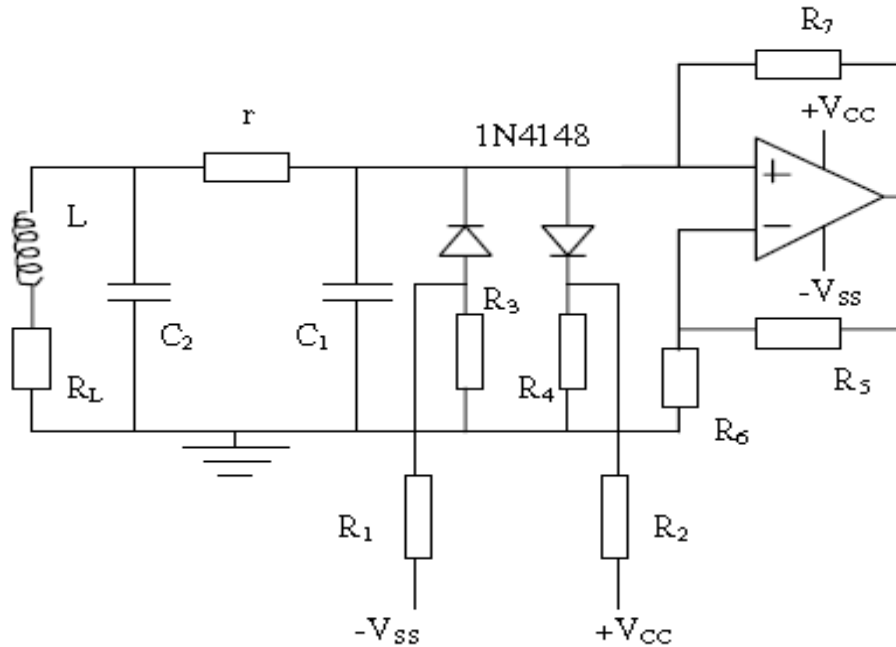


Figure 1.8: The normal Chua oscillator [149]

Figure 1.8 is derived from the well-known and famous Chua's circuit [178] where the nonlinear element (commonly called Chua's diode) is implemented using two diodes only, in addition to an op-amp and some resistors. Several other practical implementations of a Chua's diode characterized by a five-segment piecewise-linear current-voltage characteristic has been proposed [155]. An implementation of Chua's circuit with a cubic nonlinearity was first described by Zhong [180]. The advantages of cubic nonlinearity are that it requires no absolute-valued functions, it is smooth, and thus more suitable for mathematical calculations. Physically, the original Chua's circuit does not involve any resistor in series with the inductor. This resistor appears in the Chua's oscillator of [157]. The current-voltage characteristics of the nonlinear resistance are given by:

$$i(V) = v_C + a_2 V + b_2 V^3. \quad (1.30)$$

The modified Chua's circuit oscillator can thus be described by the following equations:

$$\begin{cases} \dot{x}_2 = a(y_2 - x_2^3 + cx_2), \\ \dot{y}_2 = x_2 - y_2 - z_2, \\ \dot{z}_2 = by_2. \end{cases} \quad (1.31)$$

In order to obtain the so-called double scroll attractor which is specific to the family of Chua's circuits, we use the same selection of parameters as in ref [158], that is, $a = 10$, $b = 16$ and $c = 0.143$. The initial values as $(x_2(0), y_2(0), z_2(0)) = (0.1, 0.3, 0)$. The associated one-dimensional Lyapunov exponent is $k_{\max} = 0.26$. The chaotic attractor obtained is displayed in as shown in ref [149].

1.3.2.2. The field-effect junction transistor (JFET) and the Single Op-Amp-Based Jerk Circuit

a) The junction field-effect transistor (JFET)



Figure 1.9: a) N-channel JFET; b) P-channel JFET [183]

A JFET is a three terminal semiconductor device in which current conduction is by one type of carrier i.e., electrons or holes. The JFET was developed about the same time as the transistor but it came into general use only in the late 1960s. In a JFET, the current conduction is either by electrons or holes and is controlled through an electric field between the gate electrode and the conducting channel of the device. The JFET has high input impedance and low noise levels [159, 160]. A JFET consists of a p -type or N -type silicon bar containing two PN junctions at the sides. The bar forms the conducting channel for the charge carriers. If the bar is of N -type, it is called n-channel JFET

(Figure 1.9a), and if the bar is of P-type, it is called a P-channel JFET (Figure 1.9b) The two PN junctions forming diodes are connected internally and a common terminal called gate is taken out. Other terminals are source and drain taken out from the bar as shown [159, 160]. Thus a JFET has essentially three terminals, gate (G), source (S), and drain (D). The voltage V_{GS} applied to the Gate controls the current flowing between the Drain and the Source terminals. V_{GS} refers to the voltage applied between the Gate and the Source while V_{DS} refers to the voltage applied between the Drain and the Source. Because a Junction Field Effect Transistor is a voltage controlled device, “NO current flows into the gate!” then the Source current (I_S) flowing out of the device equals the Drain current flowing into it and therefore ($I_D = I_S$).

The Drain current is zero when $V_{GS} = V_P$. For normal operation, V_{GS} is biased to be somewhere between V_P and 0. Then we can calculate the Drain current, I_D for any given bias point in the saturation or active region as follows:

$$I_D = I_{DSS} \left[1 - \frac{V_{GS}}{V_P} \right]^2, \tag{1.32}$$

where I_{DSS} is a maximum saturation current.

b) Single Op-Amp–Based Jerk Circuit

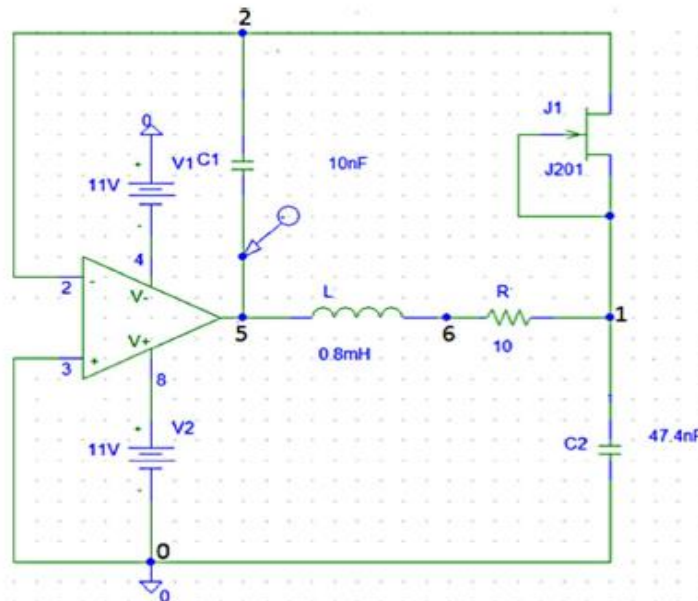


Figure 1.10: Schematic representation of the jerky oscillator. The nonlinear element is made of a JFET with the gate (G) and the source (S) electrodes short-circuited [161]

Figure 1.10 is based on a single Op-Amp as the only idealized component and carries a minimal number of five components. The key component of this oscillator circuit is a junction field-effect transistor operating in its triode region, which provides a nonlinear resistor of antisymmetrical current-voltage characteristic, emulating a Colpitts-like chaotic circuit. In their work, the authors proposed a simple system, which jerk function, although a bit complicated, resembles that of Chua's circuit aside from some parameters and has the sensible advantage to be governed by a Piece Wise Nonlinear (PWL NL) equation that can be used to perform exact analytical works. These equations govern the circuit depicted in figure 1.10 an oscillator with one Op-Amp, one junction field-effect transistor (JFET), two capacitors C_1 and C_2 , and one coil L with internal resistance R .

Let us consider $R_J \approx 750 \Omega$ to be the JFET small-signal resistance and $V_T \approx -0.66 \text{ V}$ to be the JFET gate-source voltage [62]. An appropriate choice of parameters, namely, $\alpha = C_1/C_2$, $\beta = R_J^2 C_1/L$, and $\gamma = R/R_J$, as well as $I = V_T \phi(y)/R_J$, $V_{C1} = xV_T$, $V_{C2} = yV_T$, $I_L = zV_T/R_J$, and $t = R_J C_1 \tau$, reveals the state equations of the circuit, obtained through application of Kirchhoff's laws.

$$\begin{cases} C_1 \dot{V}_{C1} = I, \\ C_2 \dot{V}_{C2} = I - I_L, \\ L \dot{I}_L = -(V_{C1} - V_{C2} + R I_L). \end{cases} \quad (1.33)$$

The necessary Nonlinear transistor (NLT) in the system for chaos is made of the PW NL form of the JFET current-voltage characteristic.

$$I = \frac{1}{R_J} \begin{cases} -V_{C_k} & \text{if } -V_{C_k} \geq V_T \\ V_T & \text{if } -V_{C_k} < V_T \end{cases}, \quad (1.34)$$

V_{C_k} , $k = 1, 2$, is the voltage difference at the electrodes of capacitor C_k , and I_L is the current flowing through the coil L . With some mathematical manipulations, it can be shown that (1.33) can be transformed into the jerk form

$$\begin{cases} i = W(v_0)v = -\frac{1}{R_3}(1 - gv_0^2)v, \\ C_0 \frac{dv_0}{dt} = \frac{-1}{R_1}v - \frac{1}{R_2}v_0. \end{cases} \quad (1.38)$$

where v and i are the voltage and current at the input terminal of the memristor with memductance $W(v_0)$, respectively. v_0 is the voltage across the integral capacitor C_0 , and g is the total gain of the two multipliers M_1 and M_2 .

b) Memristive oscillator circuit

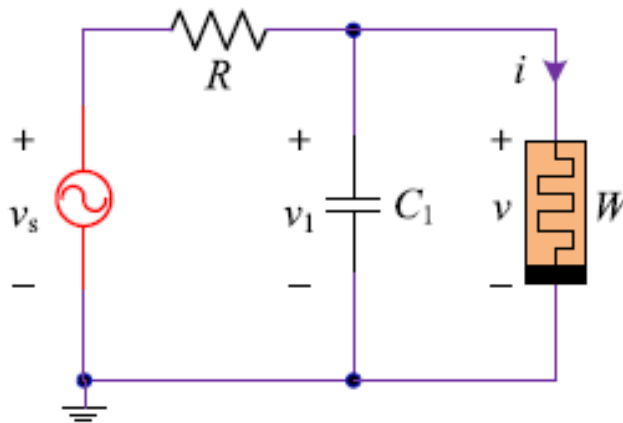


Figure 1.12: Second-order nonautonomous inductor-free memristive chaotic circuit. (a) Circuit schematic diagram [162]

Figure 1.12 represents the schematic diagram of a non-autonomous second-order memristive circuit. The proposed circuit is physically realizable and only consists of a capacitor C_1 , a resistor R , a sinusoidal voltage source v_s , and a voltage-controlled W .

The proposed circuit in figure 1.12 has only two dynamic elements, which are the capacitor C_1 and the active voltage controlled memristor with memductance $W(v_0)$, corresponding to two state variables of v_1 and v_0 , respectively. Thus, the proposed circuit in figure 1.12 can be modeled as:

$$\begin{cases} \frac{dv_1}{dt} = \frac{v_s - v_1}{RC_1} + \frac{(1 - gv_0^2)v_1}{R_3C_1}, \\ \frac{dv_0}{dt} = \frac{-v_1}{R_1C_0} - \frac{v_0}{R_2C_0}, \end{cases} \quad (1.39)$$

where $v_s = A\sin(2\pi ft)$, and A is the amplitude and f indicates the frequency.

Compared with the non-autonomous memristive circuits in [135-137], this circuit is a second-order and inductor-free realization with a simplified topological structure outstandingly. A memristor is a nonlinear circuit element, which is used to realize the nonlinearity of the circuit in figure 1.12. this simple circuit has dynamical behaviors of limit cycles with different periodicities and chaotic attractors with three different topological structures. The numerical results obtained in this literature work emulate the striking dynamical features of period and chaos emerging from the proposed circuit. The authors showed that their circuit can generate chaotic attractors with three different topological structures, which implies that the proposed circuit is chaotic genuinely.

1.3.2.4. Nonlinear condenser and nonlinear Duffing oscillator

a) Nonlinear condenser

In most experimental and theoretical works, the Duffing electrical nonlinearity in an electronic circuit is introduced via a varicap diode. We present here a simple device for which the Charge-Voltage (C-V) characteristic is like that of the varicap diode (see Figure 1.13).

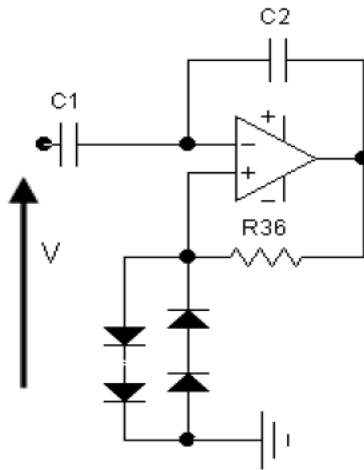


Figure 1.13: Model of the nonlinear condenser [164]

The C-V characteristic is then given as

$$V = \frac{q}{C_1} + nV_0 \sinh^{-1} \left(\frac{-q}{2R_{36}i_0C_2} \right). \quad (1.40)$$

A two terms Taylor expansion of sinh function gives

$$V = \left[\frac{1}{C_1} - \frac{nV_0}{2R_{36}i_0C_2} \right] q + \frac{nV_0}{48R_{36}^3i_0^3C_2^3} q^3 \quad \text{with} \quad R_{36} > \frac{nV_0C_1}{2i_0C_2}. \quad (1.41)$$

Other models of nonlinear elements can be found in some classical books such as [165].

b) The RLC circuit with nonlinear capacitor

In 2007, J. B. Mogo and P. Woafu [166] studied an electromechanical device with a pendulum arm. The electrical part of their proposed device is shown in the Figure 1.14 below:

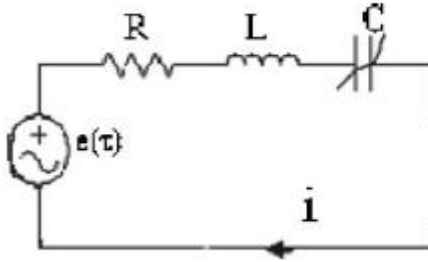


Figure 1.14: Schematic of electromechanical device [166]

The pendulum depicted in Figure 1.14 is a thin rod interdependent with a plate, on which electrical windings are applied. Connected to an electric circuit, its oscillations are due to the electromagnetic force resulting from two identical and repulsive permanent magnets. This setup is a system with two degrees of freedom: the charge q of the nonlinear condenser and the angular displacement θ of the pendulum. We will focus on just the electrical part of the Figure 1.14.

The electric oscillator used to drive the pendulum is an RLC series circuit with sinusoidal excitation $e(\tau) = v_0 \cos \Omega \tau$ (v_0 and Ω being, respectively, the amplitude and frequency, and τ the time). Denoting the forced mesh current i in the RLC circuit, as shown in Figure 1.14, applying Kirchhoff's rules, we find:

$$L \frac{di}{dt} + Ri + V_C(q) = e(\tau), \quad (1.42)$$

where $L (di / dt)$, Ri , and $V_c (q)$ are the voltages across the inductance L , the resistor R , and the nonlinear capacitor C , respectively. In our electromechanical model, the electrical nonlinear term is introduced by considering that the voltage of the capacitor is a nonlinear function of the instantaneous electrical charge q of the following form:

$$V_c(q) = \frac{1}{C_0} q + a_3 q^3, \quad (1.43)$$

where C_0 is the linear value of C and a_3 is the nonlinear coefficient depending on the type of capacitor used. This form of $V_c (q)$ is typical of nonlinear reactance components such as varactor diodes, widely used in electrical engineering especially to design, for example, parametric amplifiers, upconverters, mixers, low-power microwave oscillators, etc. [167]. Inserting Eq. (1.43) in Eq. (1.42), the electric part of the model is described by the following nonlinear differential equation:

$$\ddot{q} + \frac{R}{L} \dot{q} + \omega_e^2 q + \frac{a_3}{L} q^3 = \frac{v_0}{L} \cos(\Omega \tau), \quad (1.44)$$

where $\omega_e^2 = 1/LC_0$ is the resonance frequency of the electric oscillator, and overdots denote derivatives with respect to dimensional time τ .

The numerical simulation in this work shows that the system can lead to complex dynamical behaviors such as multiperiodic and chaotic states. It was observed that without the cubic nonlinearity, the system rarely shows a chaotic behavior with the chosen parameters. It is also found that there are various routes to chaos (such as sudden transition and period doubling transition) with several kinds of periodic windows.

1.4. Problem statement of the thesis

The analysis and modeling of nonlinear electrical circuits are of great interest for their dynamical responses. The dynamics of such circuits can be as simple and/or complex depending on the number of degrees of freedom and the type of nonlinear element they contain. Some rich dynamical behaviors, such as chaos and hyperchaos [168, 169], hyperchaotic multi-wing attractors [146, 147], coexisting multiple attractors [148, 149], hidden attractors [174], complex transient chaos and hyperchaos [136, 175], chaotic and hyperchaotic beats [135, 137], to mention a few,

have been revealed from many nonlinear electric circuits constituted of some nonlinear component like memristor, diode, nonlinear resistor, nonlinear capacitor, nonlinear inductor, and many others. But less studies have been conducted using a JJ with other nonlinear electronic components.

Motivated by those considerations **the first problem we solve in this thesis is the analysis of the behavior of electrical circuits based on a particular nonlinear element which is the JJ.** This study is scientifically new, since apart from the two works of Noel Freddy Fotie Foka et *al* [176, 192], most nonlinear electrical circuits are much more made of nonlinear elements such as a diode, memristor, and nonlinear resistors, capacitors, inductors, and others. These researchers have investigated the dynamical features and the digital implementation of a microcontroller JJ neuron model driven by a thermal signal and have obtained dynamics, namely, the chaos in their circuit. One of the particularities of the circuits studied in this thesis is that in addition to chaotic dynamics, they can also generate hyperchaotic dynamics which can offer a vast field of application. It was thus a question for us to propose electrical circuits able to generate chaotic and hyperchaotic dynamics at high-frequency thanks to the Josephson Junction.

The second problem to be solved in this thesis is to propose an autonomous nonlinear circuit based on the JJ. We will therefore try to introduce the JJ, as the only non-linear element (NLE), in a circuit and to make it oscillate without an external variable while hoping to obtain complex dynamics such as chaos and hyperchaos.

A microcontroller simulation of the circuit with JJ based on the mathematical equations governing their dynamics will be our third problem.

The JJ is a difficult component to find and manipulate in the optimal conditions of experimentation, but the analogical study is feasible. Thus, **the fourth and last problem to be solved is to realize the analog circuits, starting from the mathematical equations of the studied physical systems. Finally, we will make a partial and total control of the amplitude of an electric circuit.**

1.5. Conclusion

This chapter was developed to permit an understanding of the concepts which will be used in this thesis. The first part of the chapter talked about the literature review on JJ and its different electrical models. Secondly, we presented a review on nonlinear electrical circuits able to have

complex behaviors such as chaos and more particularly hyperchaos which are important for secure communications. We continued our analysis by doing a brief review on electric circuits based on some electrical nonlinear components. We also presented some essential works carried out in the literature. This presentation has allowed us to highlight the problems of the thesis.

The next chapter will be devoted to mathematical formalisms, numerical, analog, and microcontroller simulation methods used to analyze the dynamical states of the electric circuits proposed in this work.

CHAPTER 2: METHODOLOGY

2.1. Introduction

This chapter deals with the different methods used in this thesis which are organized as follows. In section 2.2, mathematical formalisms will be presented. This concerns the stability analysis of equilibrium points and the Routh-Hurwitz criteria have been elaborated to choose the one better adapted in the frame of this work. Another approach using numerical methods has been presented in section 2.3 because these theoretical methods can present some limitations in the analysis of nonlinear differential equations characterized by complex dynamic behaviors such as Chaos/hyperchaos. In this section, we will present chaos and hyperchaos characterization and Circuit analysis methods. Sections 2.4 is consecrated to electronic components, analog simulation method, and Principe of microcontroller simulation. In this section, we present some electronic components and the analog operations that will allow us to build electronic circuits mimicking the differential equations of an oscillator. Even though computers and software are used for simulations, analog circuits can provide concrete and accurate results for real applications. The last section is devoted to the conclusion.

2.2. Mathematical formalisms

2.2.1. Stability analysis of equilibrium points

Dynamical systems deal with systems that evolve. The term "system" refers to a set of state variables (whose value evolves with time) and the interactions between them. Their evolution over time is both causal and deterministic. For a deterministic evolution, the dynamic system can be modeled in two distinct ways, namely

- Continuous evolution in time, represented by a system of ordinary differential equations in the following form:

$$\dot{X}_1 = f(t, X, C), \tag{2.1}$$

where C is a column matrix characterizing the parameters of the system.

- ✓ A discrete evolution in time. In this case, the time is a discrete variable and the system of equations is then presented in the following form:

METHODOLOGY

$$X_{n+1} = f(t_n, X_n, C_n). \quad (2.2)$$

The stability of a dynamic system represents the property that a dynamic system has to remain in the same state despite small perturbations. Thus a system will be said to be stable when it returns to its initial state (which we assume to be a fixed point) after having undergone small perturbations and unstable in the opposite case. In other words, if we apply a perturbation to a fixed point, the Taylor expansion to the first order $F(X)$ is written:

$$F(X_0 + \delta X) = F(X_0) + J(X_0)\delta X + o(\delta X) \approx J(X_0)\delta X. \quad (2.3)$$

where $J(X_0)$ is the Jacobian matrix F calculated at the point X_0 .

$$J(X_0) = \left(\frac{\partial F_i}{\partial X_j} \Big|_{X_0} \right). \quad (2.4)$$

The solution is written in the form:

$$\delta X(t) = \sum_i a_i C_i \exp(\lambda_i t). \quad (2.5)$$

It appears that the fixed point is stable if and only if all the eigenvalues of J are with a negative real part. In this case, the perturbation decreases exponentially and the system returns to the equilibrium position. If one of the eigenvalues has a zero real part, the system is marginally stable (it does not move away). If at least one of the eigenvalues has a strictly positive real part, then the system is unstable since the perturbation tends to grow over time. In phase space, the representative point moves away from the fixed point in the direction of the corresponding eigenvector. The imaginary parts can be zero or not inducing an oscillation.

We classify the fixed points according to the real part of the eigenvalues λ_i

- ✓ If $\forall i, R(\lambda_i) < 0$, the fixed point is stable.
- ✓ If $\forall i, R(\lambda_i) > 0$, the fixed point is unstable.
- ✓ If $\exists i, R(\lambda_i) < 0$ and $\exists j, R(\lambda_j) > 0$ the fixed point is a saddle point (unstable),

where the λ_i represent the eigenvalues of the matrix J , the C_i corresponding eigenvectors a_i , and δX_0 depend on the initial conditions. In general, the λ_i are complex and the exponential involves two contributions: The real part $R(\lambda_i)$ leads to a contraction or a dilation δX depending on whether it is negative or positive.

2.2.2. Routh-Hurwitz criterion

The Routh-Hurwitz criterion is one of the important criteria that give necessary and sufficient conditions for all of the roots of the characteristic polynomial (with real coefficients) to lie in the left half of the complex plane. To derive the stability regions of a dynamical system, some conditions must be respected. In case the Routh-Hurwitz criterion as stated in Theorem 2.2.2.1 is satisfied, then any solution of the differential equation converges towards the investigated fixed point.

Theorem 2.2.2.1. Routh-Hurwitz criterion.

Given the polynomial obtained from the Jacobean matrix of a given system around one of its fixed points,

$$P(\lambda) = a_0\lambda^n + a_1\lambda^{n-1} + \dots + a_{n-1}\lambda + a_n, \quad (2.6)$$

where the coefficients a_i are real constants, $i = 0, \dots, n$, define the n Hurwitz matrices using the coefficients a_i of the characteristic polynomial:

$$H_1 = (a_1), \quad H_2 = \begin{pmatrix} a_1 & a_0 \\ a_3 & a_2 \end{pmatrix}, \quad H_3 = \begin{pmatrix} a_1 & a_0 & 0 \\ a_3 & a_2 & a_1 \\ a_5 & a_4 & a_3 \end{pmatrix}, \quad \text{and} \quad H_n = \begin{pmatrix} a_1 & a_0 & 0 & 0 & \dots & 0 \\ a_3 & a_2 & a_1 & a_0 & \dots & 0 \\ a_5 & a_3 & a_2 & a_1 & \dots & 0 \\ \dots & \dots & \dots & \dots & \dots & 0 \\ \dots & \dots & \dots & \dots & \dots & \dots \\ 0 & 0 & 0 & 0 & \dots & a_n \end{pmatrix}, \quad (2.7)$$

where $a_j = 0$ if $j > n$.

METHODOLOGY

All the roots of the polynomial $P(\lambda)$ are negative or have a negative real part if and only if the determinants of all the Hurwitz matrices are positive:

$$\det(H_j) > 0, \quad j = 1, 2, \dots, n. \quad (2.8)$$

As the dynamical equations studied in this thesis are of five and six order, regarding the Theorem 2.2.2.1, the Routh-Hurwitz criteria will be written as

$$\det(H_1) > 0, \det(H_2) > 0, \det(H_3) > 0, \det(H_4) > 0, \det(H_5) > 0, \text{ and } \det(H_6) > 0. \quad (2.9)$$

It is worth mentioning that there exists a corollary (necessary conditions but not sufficient) to Theorem 2.2.2.1, which helps to conclude more rapidly on the stability of the analyzed fixed points; it is stated as follows:

Corollary 2.2.2.1.1. *Suppose the coefficients of the characteristic polynomial are real. If all of the roots of the characteristic polynomial equation (2.6) are negative or have a negative real part, then the coefficients $a_i > 0$, for $i = 1, 2, \dots, n$.*

In this thesis, the Routh-Hurwitz criterion and its corollary are used to analyze the stability of all the proposed mathematical models.

2.3. Numerical methods

Numerical methods are based on an algorithm that is implemented through computers to solve different types of problems. Computers enable us to approximate the solutions to analytically intractable problems, and also to visualize those solutions. In this thesis, solutions (numerical integration of $x' = f(x)$) to each of our nonlinear dynamical systems will be investigated through the fourth-order Runge-Kutta algorithm.

2.3.1. Fourth-order Runge-Kutta method for ordinary differential equations

2.3.1.1. Implementation for the first-order differential equation

All this thesis is based on the analysis of nonlinear dynamical (chaotic and hyperchaotic) solutions in electronic circuits. Henceforth, only numerical integration of our nonlinear differential equations ($\dot{x} = f(t, x)$) can enable us to well approximate the solutions of analytically intractable problems, and also visualize those solutions. The accommodate algorithm is that of fourth-order Runge-Kutta. Indeed, among the plethora of numerical integration methods, the fourth-order Runge-Kutta offers a good balance between computational cost, stability, and efficiency [44]. The solution x_{n+1} in terms of x_n and t_n is given by the following scheme:

$$x_{n+1} = x_n + \frac{1}{6}(k_1 + 2k_2 + 2k_3 + k_4), \quad (2.10)$$

with,

$$\begin{aligned} k_1 &= f(t_n, x_n), \\ k_2 &= f\left(t_n + \frac{h}{2}, x_n + \frac{h}{2}k_1\right), \\ k_3 &= f\left(t_n + \frac{h}{2}, x_n + \frac{h}{2}k_2\right), \\ k_4 &= f(t_n + h, x_n + hk_3), \end{aligned} \quad (2.11)$$

where h represents the step of integration and t_n the time sampling at n^{th} iteration. All the numerical analysis and further investigations in this thesis will be first based on the fourth-order Runge-Kutta numerical integration of each of our systems (defined by the set of autonomous ordinary differential equations only).

2.3.1.2. Implementation for the m-order differential equation

In the case of an m-order differential equation, we have:

$$\begin{cases} \frac{d^m y}{dt^m} = f_m\left(t, y, \frac{dy}{dt}, \frac{d^2 y}{dt^2}, \frac{d^{m-1} y}{dt^{m-1}}\right), \\ \frac{d^k y}{dt^k}(t_0) = y_0^{(k)}. \end{cases}, \quad (2.12)$$

With successive variables change, the equation (2.12) can be written under the following form:

$$\left\{ \begin{array}{l} \frac{d^0 y}{dt^0} = u_0 = y = f_0(t, u_0, u_1, u_2, \dots, u_{m-1}), \\ \frac{dy}{dt} = \frac{du_0}{dt} = u_1 = f_1(t, u_0, u_1, u_2, \dots, u_{m-1}), \\ \frac{d^2 y}{dt^2} = \frac{du_1}{dt} = u_2 = f_2(t, u_0, u_1, u_2, \dots, u_{m-1}), \\ \vdots \\ \frac{d^{m-1} y}{dt^{m-1}} = \frac{du_{m-2}}{dt} = u_{m-1} = f_{m-1}(t, u_0, u_1, u_2, \dots, u_{m-1}), \\ \frac{d^m y}{dt^m} = \frac{du_{m-1}}{dt} = f_m(t, u_0, u_1, u_2, \dots, u_{m-1}) \\ \frac{d^k y}{dt^k}(t_0) = u_k(t_0) = y_0^{(k)}, k \in \{1, 2, 3, \dots, m-1\}. \end{array} \right. \quad (2.13)$$

With this general vectorial form, iterations can be performed to determine all the values of y and its derivative at a different time separated by the time step h using:

$$u_k(t+h) \leftarrow u_k(t) + \frac{1}{6}(L_1^k + 2(L_2^k + L_3^k) + L_4^k), \quad (2.14)$$

where

$$\begin{aligned} L_1^k &= hf_k \left[t, u_0(t), u_1(t), \dots, u_{m-1}(t) \right], \\ L_2^k &= hf_k \left[t + \frac{h}{2}, u_0(t) + \frac{L_1^0}{2}, u_1(t) + \frac{L_1^1}{2}, \dots, u_{m-1}(t) + \frac{L_1^{m-1}}{2} \right], \\ L_3^k &= hf_k \left[t + \frac{h}{2}, u_0(t) + \frac{L_2^0}{2}, u_1(t) + \frac{L_2^1}{2}, \dots, u_{m-1}(t) + \frac{L_2^{m-1}}{2} \right], \\ L_4^k &= hf_k \left[t + \frac{h}{2}, u_0(t) + \frac{L_3^0}{2}, u_1(t) + \frac{L_3^1}{2}, \dots, u_{m-1}(t) + \frac{L_3^{m-1}}{2} \right]. \end{aligned} \quad (2.15)$$

This generalized form can also serve to solve numerically first-order coupled ODEs.

2.3.2. Numerical tools for characterizing the dynamical states of non-linear systems

2.3.2.1. Time series

For as long as scientist have been recording data, time has been a crucial factor. In time series analysis, time is a significant variable of the data. Times series analysis helps us study our world and learn how we progress within it.

Time series analysis is a specific way of analyzing a sequence of data points collected over an interval of time. In time series analysis, analysts record data points at consistent intervals over a set period rather than just recording the data points intermittently or randomly. However, this type of analysis is not merely the act of collecting data over time. What sets time series data apart from other data is that the analysis can show how variables change over time. In other words, time is a crucial variable because it shows how the data adjusts throughout the data points as well as the final results. It provides an additional source of information and a set order of dependencies between the data. Time series analysis typically requires a large number of data points to ensure consistency and reliability. An extensive data set ensures you have a representative sample size and that analysis can cut through noisy data. It also ensures that any trends or patterns discovered are not outliers and can account for seasonal variance. Additionally, time-series data can be used for forecasting-predicting future data based on historical data.

2.3.2.2. Phase portraits

The region of the phase space towards which the trajectories of a dissipative dynamical system converge is called an "attractor". Attractors are geometrical shapes that characterize the long-term evolution of dynamical systems. There are four types of attractors: a point, a torus, a limit cycle, and a more complex fractal-like structure [212].

- The "fixed point" attractor is a point in the phase space towards which the trajectories tend and is, therefore, a constant stationary solution,
- The "limit cycle" attractor is a closed trajectory in phase space towards which the trajectories tend. It is therefore a periodic solution of the system,
- The "torus" attractor represents the motions resulting from two or more independent oscillations which are sometimes called quasi-periodic motions,
- Strange attractors are much more complex than the others.

2.3.2.3. Bifurcation diagrams

Another set of concepts useful for the analysis of dynamical systems is the theory of bifurcation. A bifurcation diagram shows the values visited or approached asymptotically (fixed points periodic orbits, or chaotic attractors) by a system as a function of the system control parameter. In dynamics systems, the bifurcation diagram provides model transitions and instabilities as some control parameters are varied [44]. This concept refers to the study of changes in the behavior of a system when its parameters change. Bifurcation means a qualitative change in the dynamics of the system that results from the change of one of the parameters of the system. There are several methods used to obtain the bifurcation diagrams. One way is to keep the same initial conditions for all the iterations of the control parameters. This method is suited to track parallel branches existing in systems. Another method consists of considering the final state at each iteration as initial conditions for the next iteration. This method is following the real experiment as initial conditions are changing when a control parameter is varying.

For example, the destabilization of a stable equilibrium, the appearance or disappearance of a cycle or an attractor, and many others. The value for which the bifurcation occurs is called the bifurcation point. There are several types of bifurcation. We can mention among others:

- The flip bifurcation or period splitting:

This bifurcation occurs when one of the eigenvalues of the system is equal to -1 . A cycle of order k which undergoes this bifurcation will change its nature and create a cycle of order $2k$ of the same nature.

- The fold bifurcation or node-col:

In this type of bifurcation, two equilibrium points exist (one is stable and the other is unstable) before the bifurcation. After the bifurcation, no equilibrium exists.

- The Hopf bifurcation:

A Hopf bifurcation occurs when a periodic solution cycle or limit cycle surrounding an equilibrium point emerges or disappears when a parameter μ varies. When a stable limit cycle surrounds an

unstable equilibrium point, it is called a supercritical Hopf bifurcation. If the limit cycle is unstable and surrounds a stable equilibrium point, it is called a subcritical Hopf bifurcation.

Moreover, some stable solutions like quasiperiodic oscillations can be misinterpreted from the bifurcation diagram as they are represented with dense points like chaos/hyperchaos solutions. Let us also note that hysteresis dynamics are tracked using this method by superimposing two sets of data corresponding respectively to increase and decrease values of the control parameter. Even though the bifurcation diagram helps to distinguish stable (periodic) solution areas from unstable (chaotic) ones; it doesn't provide any information about the kind of dynamic (chaos or hyperchaos) that is present in unstable areas.

Lyapunov exponents and phase portraits are some additional tools required to conclude the dynamics of the investigated system.

2.3.2.4. Lyapunov's exponent

To gain the most information from a dynamical system, one should look for its maximum Lyapunov exponent. Chaotic behavior is illustrated by a positive maximum Lyapunov exponent.

The evaluation of the maximum Lyapunov exponent can be done by observing the evolution of small perturbations of the system during its evolution over time. Thus, for a positive maximum Lyapunov exponent, a stretch occurs when initially neighboring points are separated: this is chaos. Moreover, for a negative exponent, there is a contraction or approach that characterizes a unique oscillatory or static state: this is regularity; and finally, for a zero exponent, we have a set of quasi-periodic waveforms: this is the torus.

The bifurcation is obtained from the numerical simulation. Under the same conditions, the chaotic behavior of the system can be characterized by using the Lyapunov exponent. Two methods exist to achieve this, the first is to perform the spectral calculation of the Lyapunov exponent for all dimensions of the system. This method consists in performing the one-dimensional calculation of the Lyapunov exponent whose plot specifies the zones of chaos and/or hyperchaos in a merged way. In the present case, the second method can be considered.

METHODOLOGY

Thus, if we perturb the system by introducing small variations on each of its axes, i.e. $\varepsilon_1, \varepsilon_2, \varepsilon_3, \varepsilon_4, \dots, \varepsilon_n$, with n the degree of the system, such that:

$$\begin{aligned}
 x_1 &\leftarrow x_1 + \varepsilon_1, \\
 x_2 &\leftarrow x_2 + \varepsilon_2, \\
 x_3 &\leftarrow x_3 + \varepsilon_3, \\
 x_4 &\leftarrow y_1 + \varepsilon_4, \\
 \vdots &\leftarrow \vdots, \\
 x_n &\leftarrow x_n + \varepsilon_n.
 \end{aligned} \tag{2.16}$$

Then, the maximum Lyapunov exponent will be defined by:

$$\lambda_{\max} = \lim_{x \rightarrow \infty} \frac{1}{t} \ln \left(\sqrt{\varepsilon_1 + \varepsilon_2 + \varepsilon_3 + \varepsilon_4 + \dots + \varepsilon_n} \right). \tag{2.17}$$

Furthermore, this maximum one-dimensional Lyapunov exponent λ_{\max} can be calculated using the following general formula:

$$\lambda_{\max} = \lim_{x \rightarrow +\infty} \frac{1}{m} \sum_{i=0}^{m-1} \ln |f(x_i)|, \tag{2.18}$$

with m the number of iterations

$$f(x_i) = M_J \times u, \tag{2.19}$$

where M_J is the Jacobian matrix associated with the system and u is the local variable used to describe the dynamics of this system in the vicinity of the equilibrium point.

There are two possible cases:

- ❖ $\lambda \leq 0$: In this case, we distinguish two sub-cases for which the oscillatory states are stable:
 - Case where $\lambda < 0$.

In this case, we have regular oscillations

- Case where $\lambda = 0$.

In this case, we have a toric orbit made up of a set of quasi-periodic waveforms.

- ❖ $\lambda > 0$: In this case, we have a toroidal orbit made of a set of quasi-periodic waveforms, which materializes the presence of a chaotic state.

METHODOLOGY

Note that the combination of the bifurcation diagram and the maximum Lyapunov exponent is an efficient tool to study the behavior (chaotic or not) of a dynamic system. The bifurcation diagram allows accounting for the qualitative state of the system while the maximum Lyapunov exponent allows accounting for the state of the system quantitatively. For this purpose, we will place the graph of the maximum Lyapunov exponent below the bifurcation diagram in all our work.

2.3.2.5. Lyapunov's spectrum

Another characterization tool that is always combined with the bifurcation diagram is the Lyapunov exponent (LE) spectrum. It is a more objective and quantitative measure than others. A characteristic feature of chaotic motion is the extreme sensitivity of the motion to small changes in initial conditions. For a chaotic motion, adjacent trajectories diverge exponentially, whereas for a regular motion trajectory is asymptotically stable and separate only linearly in time.

The rate of divergence of adjacent trajectories can be quantified conveniently in terms of Lyapunov exponents, which measure the mean rate of this exponential separation and describe the asymptotic stability properties of a trajectory. Unlike some other methods which only compute the largest Lyapunov exponent, the algorithm of [177] calculates the full spectrum of the Lyapunov exponents and thus allows one to distinguish between chaotic attractors marked by only one positive exponent and hyperchaotic attractors characterized by more than one positive exponent. Also, it contains more information about the dynamics than does the largest exponent by itself. Considering that each exponent can be negative, zero, or positive, that their sum cannot be positive for a bounded system, and that at least one exponent must be zero (this means that the trajectory always remains localized in time on a strange attractor) except for point attractors, there are five possible combinations for a four-dimensional state space. Table 1 shows the classification of attractors and the corresponding dynamics in a four-dimensional system (which is the focus of this thesis) in terms of LE [178].

Table 2.1: Lyapunov's exponents of different types of attractors for four-dimensional flow [178]

λ_1	λ_2	λ_3	λ_4	Attractor	Dimension (D_{KY})	Dynamic
-------------	-------------	-------------	-------------	-----------	------------------------	---------

METHODOLOGY

-	-	-	-	Equilibrium point	0	Static
0	-	-	-	Limit cycle	1	Periodic
0	0	-	-	Attracting 2-torus	2	2D Torus
0	0	0	-	Invariant torus	1 or 2	3D Torus
+	0	-	-	Strange]2;3[Chaotic
+	+	0	-	Strange	>3 (noninteger)	Hyperchaotic

2.3.3. Hardware and software

During this work, we used a laptop computer running Windows 10 operating system and three major software: Fortran, MATLAB, Arduino UNO, Maple, OrCAD PSpice, Proteus, and Arduino.

2.4. Analog and microcontroller simulation methods

2.4.1. Analog simulation method

Analog simulations are based on the properties of certain electronic components and they are built from, voltage multipliers, integrators, inverters, and adders built from an operational amplifier, resistor, and capacitor. All these blocks are designed with a basic electronic component called an operational amplifier. We firstly present the ideal type of operational amplifier that will be used in this work. Then we present some analog operations that we will use to build those analog circuits and the voltage multipliers.

2.4.1.1 Analog simulation operations

❖ Ideal Operational amplifiers

METHODOLOGY

Operational amplifiers are linear devices that have all the properties required for nearly ideal DC amplification and are therefore used extensively in signal conditioning, filtering, or to perform mathematical operations such as add, subtract, integration and differentiation. An Operational Amplifier, or op-amp for short, is fundamentally a voltage amplifying device designed to be used with external feedback components such as resistors and capacitors between its output and input terminals. These feedback components determine the resulting function or “operation” of the amplifier and under the different feedback configurations whether resistive, capacitive, or both, the amplifier can perform a variety of different operations, giving rise to its name of “Operational Amplifier”.

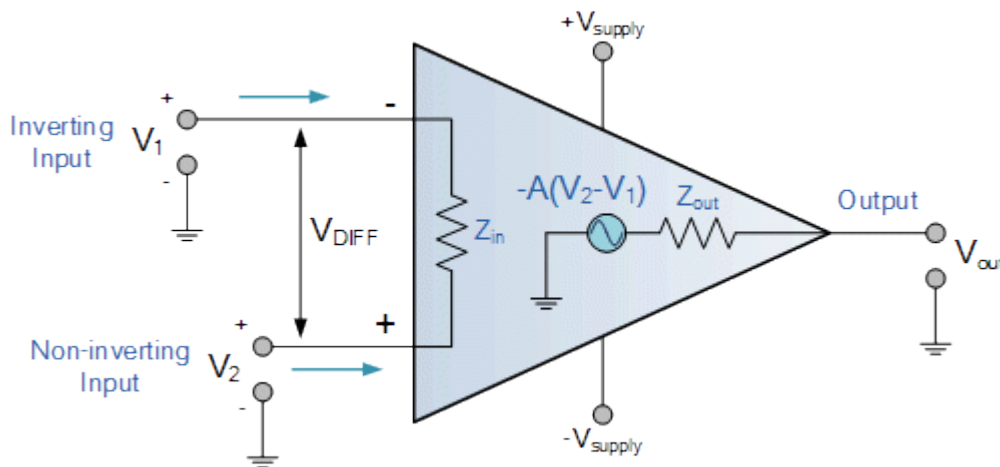


Figure 2.15: Circuit symbol of an ideal Op-amp

An Operational Amplifier is a three-terminal device that consists of two high impedance inputs. One of the inputs is called the Inverting Input, marked with a negative or “minus” sign, (-). The other input is called the Non-inverting Input, marked with a positive or “plus” sign (+).

A third terminal represents the operational amplifier's output port which can both sink and source either a voltage or a current. In a linear operational amplifier, the output signal is the amplification factor, known as the gain of the amplifier (A) multiplied by the value of the input signal, and depending on the nature of these input and output signals, there can be four different classifications of operational amplifier gain.

- Voltage – Voltage “in” and Voltage “out”
- Current – Current “in” and Current “out”

METHODOLOGY

- Transconductance – Voltage “in” and Current “out”
- Transresistance – Current “in” and Voltage “out”

Since most of the circuits dealing with operational amplifiers are voltage amplifiers, we will limit the tutorials in this section to voltage amplifiers only, (V_{in} and V_{out}).

The output voltage signal from an Operational Amplifier is the difference between the signals being applied to its two individual inputs. In other words, an op-amps output signal is the difference between the two input signals as the input stage of an Operational Amplifier is a differential amplifier as shown below.

❖ Op-amp Parameter and Idealised Characteristic

- ✓ Open Loop Gain, (A_{vo}) is **Infinite**

The main function of an operational amplifier is to amplify the input signal and the more open-loop gain it has the better. Open-loop gain is the gain of the op-amp without positive or negative feedback and for such an amplifier the gain will be infinite but typical real values range from about 20,000 to 200,000.

- ✓ Input impedance, (Z_{IN}) is **Infinite**

Input impedance is the ratio of input voltage to input current and is assumed to be infinite to prevent any current from flowing from the source supply into the amplifier's input circuitry ($I_{IN} = 0$). Real op-amps have input leakage currents from a few pico-amps to a few milli-amps.

- ✓ Output impedance, (Z_{OUT}) is **Zero**

The output impedance of the ideal operational amplifier is assumed to be zero acting as a perfect internal voltage source with no internal resistance so that it can supply as much current as necessary to the load. This internal resistance is effectively in series with the load thereby reducing the output voltage available to the load. Real op-amps have output impedances in the 100-20k Ω range.

- ✓ Bandwidth, (BW) is **Infinite**

An ideal operational amplifier has an infinite frequency response and can amplify any frequency signal from DC to the highest AC frequencies so it is therefore assumed to have infinite bandwidth. With real op-amps, the bandwidth is limited by the Gain-Bandwidth product (GB), which is equal to the frequency where the amplifier's gain becomes unity.

- ✓ Offset Voltage, (V_{IO}) is **Zero**

METHODOLOGY

The amplifier's output will be zero when the voltage difference between the inverting and the non-inverting inputs is zero, the same or when both inputs are grounded. Real op-amps have some amount of output offset voltage. From these “idealized” characteristics above, we can see that the input resistance is infinite, so no current flows into either input terminal (the “current rule”) and that the differential input offset voltage is zero (the “voltage rule”). It is important to remember these two properties as they will help us understand the workings of the Operational Amplifier concerning the analysis and design of op-amp circuits.

We know now that an Operational amplifier is a very high gain DC differential amplifier that uses one or more external feedback networks to control its response and characteristics. We can connect external resistors or capacitors to the op-amp in many different ways to form basic “building Blocks” circuits such as Inverting, Non-Inverting, Voltage Follower, Summing, Differential, Integrator, and Differentiator type amplifiers.

An “ideal” or perfect operational amplifier is a device with certain special characteristics such as infinite open-loop gain A_O , infinite input resistance R_{IN} , zero output resistance R_{OUT} , infinite bandwidth 0 to ∞ , and zero offsets (the output is exactly zero when the input is zero). There are a very large number of operational amplifier ICs available to suit every possible application from standard bipolar, precision, high-speed, low-noise, high-voltage, etc, in either standard configuration or with internal Junction FET transistors. Operational amplifiers are available in IC packages of either single, dual, or quad op-amps within one single device. The most commonly available and used of all operational amplifiers in basic electronic kits and projects is the industry standard μA -741.

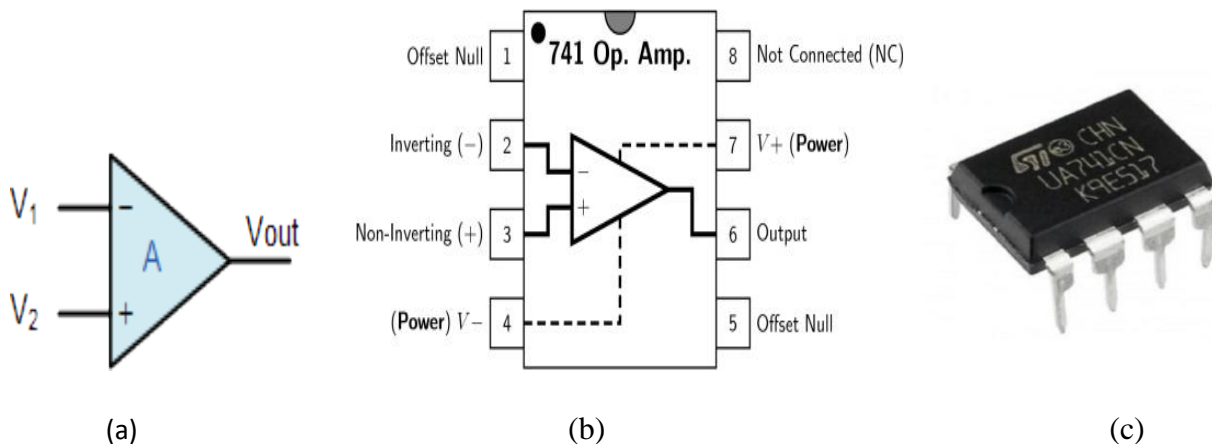


Figure 2.16: The Op-amp 741, a) Circuit symbol, b) Datasheet, c) Integrated circuit [180].

❖ Inverting Operational Amplifier

The Inverting Op-Amp configuration is one of the simplest and most commonly used op-amp topologies

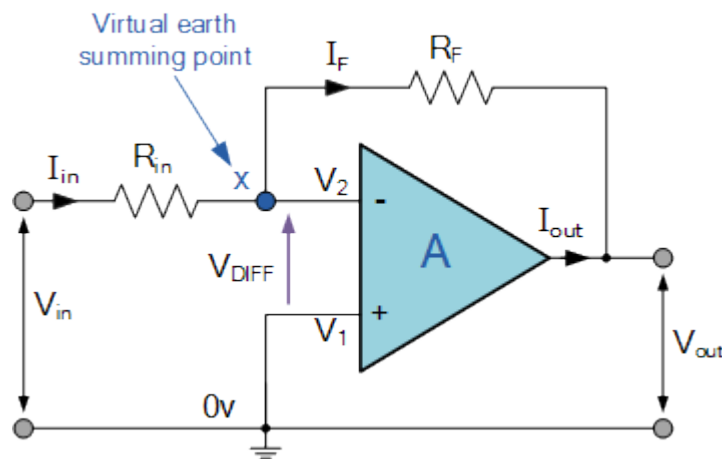


Figure 2.17: Inverter circuit with Op-Amp.

In this Inverting Amplifier circuit, the operational amplifier is connected with feedback to produce a closed-loop operation. When dealing with operational amplifiers there are two very important rules to remember about inverting amplifiers, these are: “No current flows into the input terminal” and “ V_1 always equals V_2 ”. However, in real-world op-amp circuits, both of these rules are slightly broken.

This is because the junction of the input and feedback signal (X) is at the same potential as the positive (+) input which is at zero volts or ground then, the junction is a “Virtual Earth”. Because of this virtual earth node, the input resistance of the amplifier is equal to the value of the input resistor, R_{in} and the closed-loop gain of the inverting amplifier can be set by the ratio of the two external resistors.

We said above that there are two very important rules to remember about inverting Amplifiers or any operational amplifier for that matter and these are.

METHODOLOGY

- No Current Flows into the Input Terminals
- The Differential Input Voltage is Zero as $V_1 = V_2 = 0$ (Virtual Earth)

Then by using these two rules we can derive the equation for calculating the closed-loop gain of an inverting amplifier, using first principles.

Current (i) flows through the resistor network as shown.

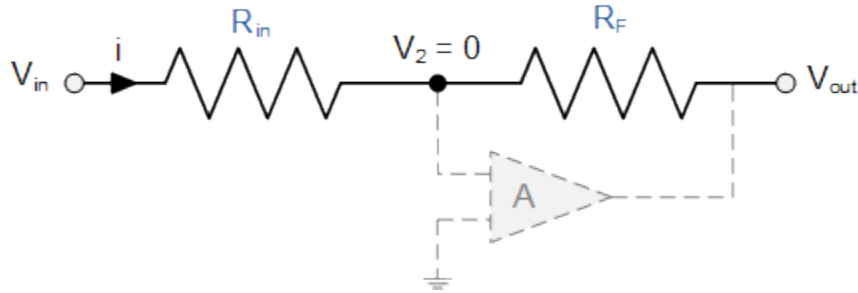


Figure 2.18: Internal representation of inverter circuit with Op-Amp

$$i = \frac{V_{in} - V_{out}}{R_{in} + R_f}, \quad (2.23)$$

therefore,

$$i = \frac{V_{in} - V_2}{R_{in}} = \frac{V_2 - V_{out}}{R_f}, \quad (2.24)$$

so,

$$\frac{V_{in}}{R_{in}} = V_2 \left[\frac{1}{R_{in}} + \frac{1}{R_f} \right] - \frac{V_{out}}{R_f}, \quad (2.25)$$

and as

$$i = \frac{V_{in} - 0}{R_{in}} = \frac{0 - V_{out}}{R_f} \quad \Leftrightarrow \quad \frac{R_f}{R_{in}} = -\frac{V_{out}}{V_{in}}, \quad (2.26)$$

the closed Loop Gain (A_v) of an Inverting Amplifier is given as,

$$A_v = \frac{V_{out}}{V_{in}} = -\frac{R_f}{R_{in}}, \quad (2.27)$$

and this can be transposed to give V_{out} as:

$$V_{out} = -\frac{R_f}{R_{in}} V_{in}. \quad (2.28)$$

❖ **Non-inverting Operational Amplifier**

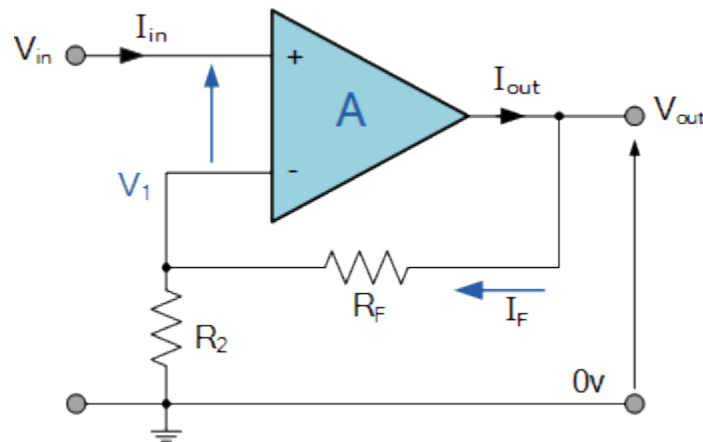


Figure 2.19: Non-inverting circuit with Op-Amp.

In this configuration, the input voltage signal, (V_{in}) is applied directly to the non-inverting (+) input terminal which means that the output gain of the amplifier becomes “Positive” in value in contrast to the “Inverting Amplifier” circuit we saw in the last tutorial whose output gain is negative in value. The result of this is that the output signal is “in-phase” with the input signal.

Feedback control of the non-inverting operational amplifier is achieved by applying a small part of the output voltage signal back to the inverting (–) input terminal via an $R_F - R_2$ voltage divider network, again producing negative feedback. This closed-loop configuration produces a non-inverting amplifier circuit with very good stability, a very high input impedance, R_{in} approaching infinity, as no current flows into the positive input terminal, (ideal conditions) and a low output impedance, R_{out} as shown below.

METHODOLOGY

In the previous Inverting Amplifier tutorial, we said that for an ideal op-amp “No current flows into the input terminal” of the amplifier and that “ V_1 always equals V_2 ”. This was because the junction of the input and feedback signal (V_1) is at the same potential.

In other words, the junction is a “virtual earth” summing point. Because of this virtual earth node, the resistors, R_F and R_2 form a simple potential divider network across the non-inverting amplifier with the voltage gain of the circuit being determined by the ratios of R_2 and R_F as shown below.

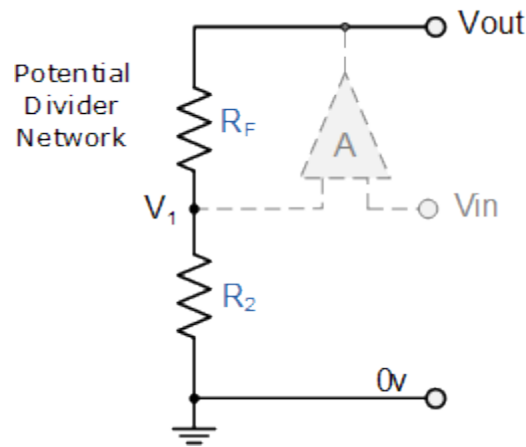


Figure 2.20: Equivalent Potential Divider Network in non-inverting amplifier.

Then using the formula to calculate the output voltage of a potential divider network, we can calculate the closed-loop voltage gain (A_V) of the non-inverting Amplifier as follows:

$$V_1 = \frac{R_2}{R_2 + R_F} V_{out}. \quad (2.29)$$

Ideal summing point :

$$V_1 = V_{in}. \quad (2.30)$$

Voltage Gain (A_V) is equal to:

$$A_V = \frac{V_{out}}{V_{in}} = \frac{R_2 + R_F}{R_2}. \quad (2.31)$$

METHODOLOGY

Then the closed-loop voltage gain of a Non-inverting Operational Amplifier will be given as:

$$A_V = \frac{V_{out}}{V_{in}} = 1 + \frac{R_F}{R_2}. \quad (2.32)$$

We can see from the equation above, that the overall closed-loop gain of a non-inverting amplifier will always be greater but never less than one (unity), it is positive and is determined by the ratio of the values of R_F and R_2 .

If the value of the feedback resistor R_F is zero, the gain of the amplifier will be exactly equal to one (unity). If resistor R_2 is zero the gain will approach infinity, but in practice, it will be limited to the operational amplifier's open-loop differential gain, (A_O).

We can easily convert an inverting operational amplifier configuration into a non-inverting amplifier configuration by simply changing the input connections as shown.

❖ Voltage Follower (Unity Gain Buffer)

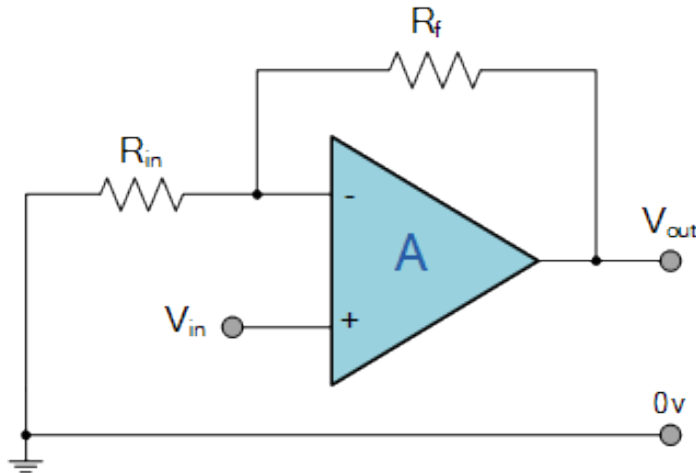


Figure 21: The voltage Follower circuit with Op-Amp.

If we made the feedback resistor, R_f equal to zero, ($R_f = 0$), and resistor R_2 equal to infinity, ($R_2 = \infty$), then the resulting circuit would have a fixed gain of “1” (unity) as all the output voltage

METHODOLOGY

is fed back to the inverting input terminal (negative feedback). This configuration would produce a special type of the non-inverting amplifier circuit called a Voltage Follower, also known as a “unity gain buffer”.

As the input signal is connected directly to the non-inverting input of the amplifier the output signal is not inverted resulting in the output voltage being equal to the input voltage, thus $V_{out} = V_{in}$. This then makes the voltage follower circuit ideal as a constant voltage source or voltage regulator because of its input to output isolation properties.

The advantage of the unity gain voltage follower configuration is that it can be used when impedance matching or circuit isolation is more important than voltage or current amplification as it maintains the input signal voltage at its output terminal. Also, the input impedance of the voltage follower circuit is extremely high, typically above $1M\Omega$ as it is equal to that of the operational amplifier's input resistance times its gain ($R_{in} \times A_O$). The op-amps output impedance is very low since an ideal op-amp condition is assumed so is unaffected by changes in load.

❖ The summing Amplifier circuit

The Summing Amplifier is another type of operational amplifier circuit configuration that is used to combine the voltages present on two or more inputs into a single output voltage.

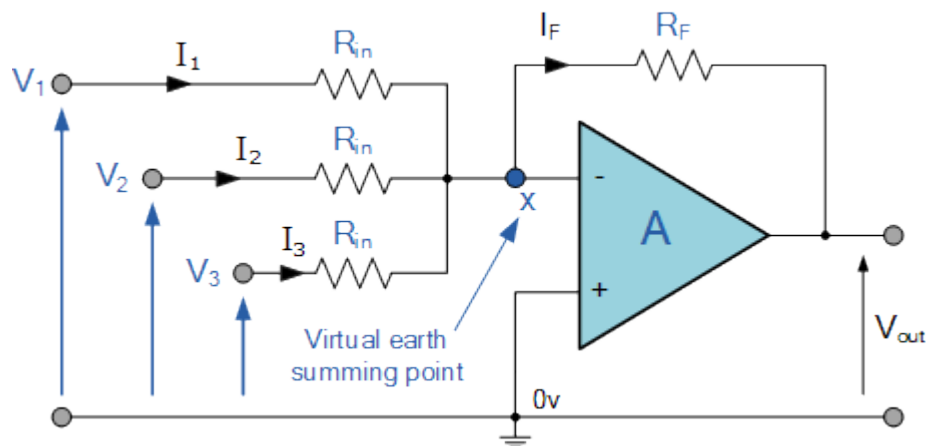


Figure 2.10: Adder circuit with Op-Amp.

METHODOLOGY

In this simple summing amplifier circuit, the output voltage, (V_{out}) now becomes proportional to the sum of the input voltages, V_1 , V_2 , V_3 , etc. Then we can modify the original equation for the inverting amplifier to take account of these new inputs thus:

$$I_F = I_1 + I_2 + I_3 = \left[\frac{V_1}{R_{in}} + \frac{V_2}{R_{in}} + \frac{V_3}{R_{in}} \right], \quad (2.33)$$

Inverting equation:

$$V_{out} = -\frac{R_F}{R_{in}} V_{in}, \quad (2.34)$$

then,

$$-V_{out} = \left[\frac{R_F}{R_{in}} V_1 + \frac{R_F}{R_{in}} V_2 + \frac{R_F}{R_{in}} V_3 \right]. \quad (2.35)$$

However, if all the input impedances, (R_{in}) are equal in value, we can simplify the above equation to give an output voltage of:

$$-V_{out} = \frac{R_F}{R_{in}} [V_1 + V_2 + V_3 + \dots etc]. \quad (2.36)$$

We now have an operational amplifier circuit that will amplify each input voltage and produce an output voltage signal that is proportional to the algebraic “SUM” of the three individual input voltages V_1 , V_2 , and V_3 . We can also add more inputs if required as each input “sees” their respective resistance, R_{in} as the only input impedance.

This is because the input signals are effectively isolated from each other by the “virtual earth” node at the inverting input of the op-amp. A direct voltage addition can also be obtained when all the resistances are of equal value and R_F is equal to R_{in} .

Note that when the summing point is connected to the inverting input of the op-amp the circuit will produce the negative sum of any number of input voltages. Likewise, when the summing point is

connected to the non-inverting input of the op-amp, it will produce the positive sum of the input voltages.

❖ The integrator Amplifier

The integrator Op-amp produces an output voltage that is both proportional to the amplitude and duration of the input signal

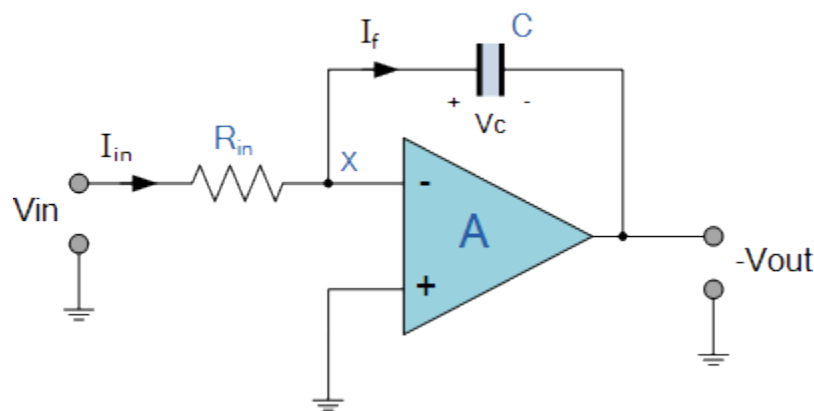


Figure 2.11: The integrated circuit with Op-Amp.

Operational amplifiers can be used as part of a positive or negative feedback amplifier or as an adder or subtractor type circuit using just pure resistances in both the input and the feedback loop. But what if we were to change the purely resistive (R_F) feedback element of an inverting amplifier with a frequency dependant complex element that has a reactance, (X), such as a Capacitor, C . What would be the effect on the op-amps voltage gain transfer function over its frequency range as a result of this complex impedance. By replacing this feedback resistance with a capacitor, we now have an RC Network connected across the operational amplifiers feedback path producing another type of operational amplifier circuit commonly called **an** Op-amp Integrator circuit as shown below.

As its name implies, the Op-amp Integrator is an operational amplifier circuit that performs the mathematical operation of Integration, that is we can cause the output to respond to changes in the input voltage over time as the op-amp integrator produces an output voltage that is proportional

METHODOLOGY

to the integral of the input voltage. In other words, the magnitude of the output signal is determined by the length of time a voltage is present at its input as the current through the feedback loop charges or discharges the capacitor as the required negative feedback occurs through the capacitor. When a step voltage, V_{in} is firstly applied to the input of an integrating amplifier, the uncharged capacitor C has very little resistance and acts a bit like a short circuit allowing maximum current to flow via the input resistor, R_{in} as potential difference exists between the two plates. No current flows into the amplifier's input and the point X is virtual earth resulting in zero output. As the impedance of the capacitor at this point is very low, the gain ratio of X_C/R_{IN} is also very small giving an overall voltage gain of less than one, (voltage follower circuit).

As the feedback capacitor, C begins to charge up due to the influence of the input voltage, its impedance X_c slowly increases in proportion to its rate of charge. The capacitor charges up at a rate determined by the RC time constant, (τ) of the series RC network. Negative feedback forces the op-amp to produce an output voltage that maintains virtual earth at the op-amp's inverting input.

We know from the first principles that the voltage on the plates of a capacitor is equal to the charge on the capacitor divided by its capacitance giving Q/C . Then the voltage across the capacitor is output V_{out} therefore: $-V_{out} = Q/C$. If the capacitor is charging and discharging, the rate of change of voltage across the capacitor is given as:

$$V_C = \frac{Q}{C}; \quad V_C = V_x - V_{out} = 0 - V_{out} \quad \Leftrightarrow \quad -\frac{dV_{out}}{dt} = \frac{1}{C} \frac{dQ}{dt}. \quad (2.37)$$

But dQ/dt is electric current and since the node voltage of the integrating op-amp at its inverting input terminal is zero, $X = 0$, the input current I_{in} flowing through the input resistor, R_{in} is given as:

$$I_{in} = \frac{V_{in} - 0}{R_{in}} = \frac{V_{in}}{R_{in}}. \quad (2.38)$$

The current flowing through the feedback capacitor C is given as:

$$I_f = C \frac{dV_{out}}{dt} = C \frac{dQ}{Cdt} = \frac{dQ}{dt} = \frac{dV_{out} \cdot C}{dt}. \quad (2.39)$$

Assuming that the input impedance of the op-amp is infinite (ideal op-amp), no current flows into the op-amp terminal. Therefore, the nodal equation at the inverting input terminal is given as:

$$I_{in} = I_f = \frac{V_{in}}{R_{in}} = \frac{dV_{out}C}{dt} \Leftrightarrow \frac{V_{in}}{V_{out}} \times \frac{dt}{R_{in}C} = 1. \quad (2.40)$$

From which we derive an ideal voltage output for the Op-amp Integrator as:

$$V_{out} = -\frac{1}{R_{in}C} \int_0^t V_{in} dt = \int_0^t V_{in} \frac{dt}{R_{in}C}. \quad (2.41)$$

To simplify the math's a little, this can also be re-written as:

$$V_{out} = -\frac{1}{j\omega RC} V_{in}. \quad (2.42)$$

Where: $\omega = 2\pi f$ and the output voltage V_{out} is a constant $1/RC$ times the integral of the input voltage V_{in} concerning time.

Thus the circuit has the transfer function of an inverting integrator with the gain constant of $-1/RC$. The minus sign ($-$) indicates a 180° phase shift because the input signal is connected directly to the inverting input terminal of the operational amplifier.

❖ The Differentiator Amplifier

The basic operational amplifier differentiator circuit produces an output signal which is the first derivative of the input signal

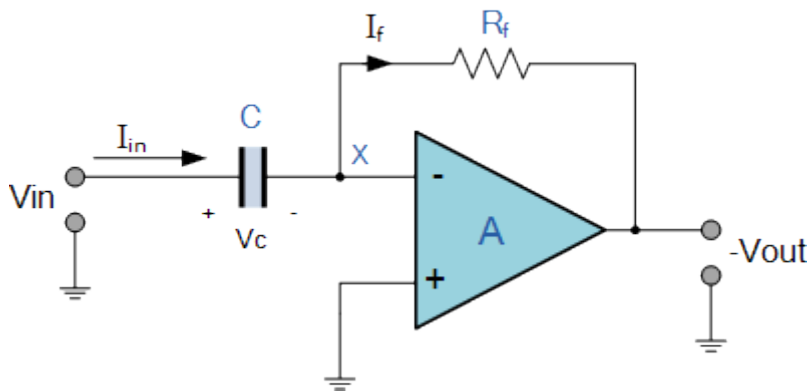


Figure 2.12: The Differentiator circuit with Op-Amp.

Here, the position of the capacitor and resistor have been reversed and now the reactance, X_C is connected to the input terminal of the inverting amplifier while the resistor, R_f forms the negative feedback element across the operational amplifier as normal. This operational amplifier circuit performs the mathematical operation of differentiation, that is it “produces a voltage output which is directly proportional to the input voltage’s rate-of-change concerning time. In other words, the faster or larger the change to the input voltage signal, the greater the input current, and the greater will be the output voltage change in response, becoming more of a “spike” in shape. As with the integrator circuit, we have a resistor and capacitor forming an RC Network across the operational amplifier and the reactance (X_C) of the capacitor plays a major role in the performance of an Op-amp Differentiator. The input signal to the differentiator is applied to the capacitor. The capacitor blocks any DC content so there is no current flow to the amplifier summing point, X resulting in zero output voltage. The capacitor only allows AC-type input voltage changes to pass through and whose frequency is dependent on the rate of change of the input signal.

At low frequencies, the reactance of the capacitor is “High” resulting in a low gain (R_F/X_C) and low output voltage from the op-amp. At higher frequencies, the reactance of the capacitor is much lower resulting in a higher gain and higher output voltage from the differentiator amplifier.

However, at high frequencies, an op-amp differentiator circuit becomes unstable and will start to oscillate. This is due mainly to the first-order effect, which determines the frequency response of the op-amp circuit causing a second-order response that, at high frequencies gives an output voltage

METHODOLOGY

far higher than what would be expected. To avoid this the high-frequency gain of the circuit needs to be reduced by adding a small value capacitor across the feedback resistor R_f .

Since the node voltage of the operational amplifier at its inverting input terminal is zero, the current, i flowing through the capacitor will be given as:

$$I_{in} = I_F \text{ and } I_F = -\frac{V_{out}}{R_f}. \quad (2.42)$$

The charge on the capacitor equals Capacitance times Voltage across the capacitor

$$Q = C \times V_{in}. \quad (2.43)$$

Thus the rate of change of this charge is:

$$\frac{dQ}{dt} = C \frac{dV_{in}}{dt}, \quad (2.44)$$

but dQ/dt is the capacitor current, i

$$I_{in} = C \frac{dV_{in}}{dt} = I_F \Leftrightarrow -\frac{V_{out}}{R_f} = C \frac{dV_{in}}{dt}, \quad (2.45)$$

from which we have an ideal voltage output for the op-amp differentiator is given as:

$$-V_{out} = -R_f C \frac{dV_{in}}{dt}. \quad (2.46)$$

Therefore, the output voltage V_{out} is a constant $-R_f C$ time the derivative of the input voltage V_{in} concerning time. The minus sign ($-$) indicates a 180° phase shift because the input signal is connected to the inverting input terminal of the operational amplifier.

One final point to mention, the Op-amp differentiator circuit in its basic form has two main disadvantages compared to the previous operational amplifier integrator circuit. One is that it suffers from instability at high frequencies as mentioned above, and the other is that the capacitive input makes it very susceptible to random noise signals and any noise or harmonics present in the source circuit will be amplified more than the input signal itself. This is because the output is

METHODOLOGY

proportional to the slope of the input voltage so some means of limiting the bandwidth to achieve closed-loop stability is required.

❖ Voltage multipliers

In this thesis, we will use the AD633JN multipliers, but let's note that there are several categories of voltage multipliers. The design of such a circuit requires resistors of equal value. This is not easy to realize technically. However, there are discrete components like the AD633 (and its equivalents) which are voltage multipliers. This circuit works with symmetrical power supplies of values between $\pm 8\text{V}$ and $\pm 18\text{V}$ with a typical value of $\pm 15\text{V}$. Its average consumption is 4mA , and its output is permanently short-circuited proof. With a bandwidth of one MHz, a differential input impedance of 10M and a voltage swing of $\pm 11\text{V}$, the dynamic characteristics of this circuit are excellent. Its pinout, which also serves as a symbol, and its actual structure are shown in figure 2.13a.

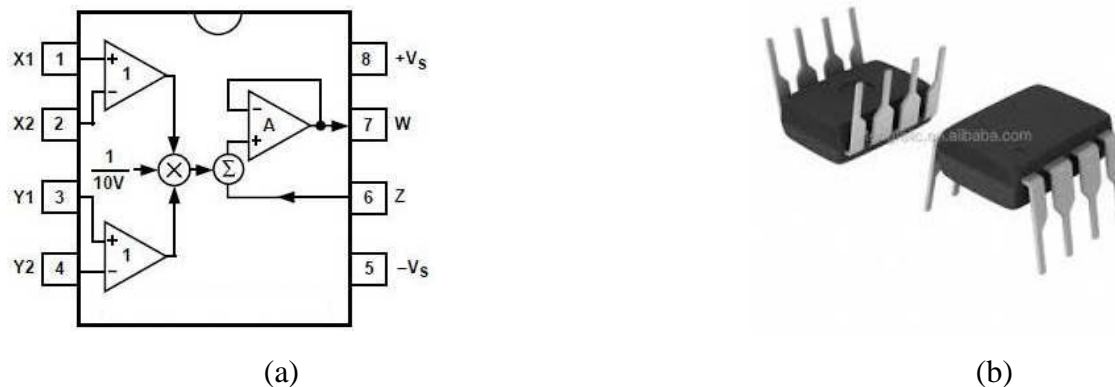


Figure 2.22: The voltage multiplier type AD633JN series: a) Datasheet b) Integrated circuit [180].

The transfer function of a voltage multiplier circuit is given by the following relationship:

$$W = \frac{(x_1 - x_2)(y_1 - y_2)}{V_{ref}} + z, \quad (2.47)$$

where W represents the output voltage of the multiplier whereas the quantities are denoted by $x_1, x_2, y_1,$ and y_2 representing the input voltages of the multiplier. z is an additional input generally connected to the ground. V_{ref} is scaling voltage whose value is 10V .

2.4.1.2. Analog simulation equipment

The real simulation by microcontroller carried out in this work required some materials such as Arduino UNO board, oscilloscope, multimeter, computer, connection cables, and test board on which we built the R-2R circuit for the conversion of digital signal coming out from Arduino into an analog signal that can be viewed in the oscilloscope.

It is very important to know how to use a test plate and to understand the principles of use. It is very useful to make electronic assemblies without soldering. The test plate is used with straps (single-stranded copper wires) of different sizes and lengths. The ends of the straps must be stripped for about 1 cm. All the points of the same column of the power bus (in red and blue on the diagram) are connected. All the points of a half-line are connected.

❖ A multimeter (sometimes called a universal controller)

It is a set of electrical measuring devices in a single box, usually consisting of a voltmeter, an ammeter, and an ohmmeter. The voltmeter and ammeter functions are available in DC and AC (see figure 2.18(e)).

❖ Oscilloscope, or oscillograph

It is a measuring instrument designed to visualize an electrical signal, most often variable over time. It is used by many scientists to visualize either electrical voltages or various other physical quantities previously transformed into voltage using an adapted converter or sensors. The rendering curve of an oscilloscope is called an oscillogram. The main purpose of an oscilloscope is to measure and display voltage as a function of time. They are widely used for electrical/electronic design, testing, and debugging of most objects that work with electricity. In this thesis, we used Rigol digital oscilloscope (see figure 2.18(a)).

❖ Arduino Uno board module

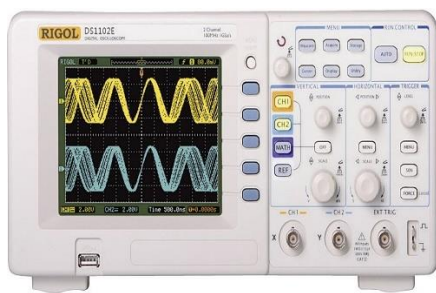
METHODOLOGY

The Arduino Uno module is a board based on the ATmega328 microcontroller with the following specifications: a power jack used to supply the needed voltage, a 16 MHz quartz used as a crystal oscillator, an ICSP header used to load programs, 14 digital pins which can be set as input or output, 6 analog inputs and 6 digital pins which can be used as PWM outputs, a USB connection for communication with computer via the open-source Arduino 1.6.11 software Integrated Development Environment (IDE), and a reset button (see Figure. 2.1.8(d)) [85]. The programming language used here in the Arduino software IDE is the “C/Arduino”, which is very closed and compatible with the “C” programming language.

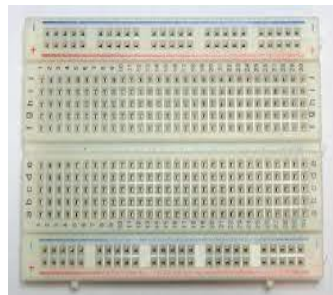
❖ The computer

It is used to program the mathematical equations governing the dynamics of the oscillator. The result of the resolution is exported in hexadecimal and then uploaded to the Arduino board through a USB cable (see figure 2.18(c)).

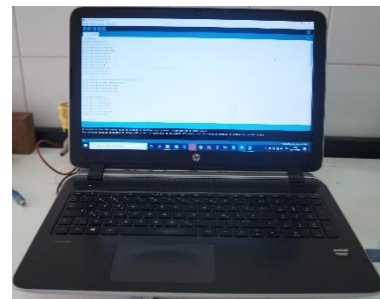
The images of these materials are shown in the following figure.



(a)



(b)



(c)



(d)



(e)



(f)

Figure 2.23: Materials use in this work: (a) Rigol digital oscilloscope; (b) Test board; (c) Computer; (d) Arduino Uno uboard; (e) Mutimeter; (f) Connection cables. [85, 180]

2.4.1.3. Electronic circuit simulators

The Analog simulation principle is universal and its elementary operations are direct consequences of physics laws [218]. Among these elementary operations we have: summation, multiplication, and integration. To design these operations, one needs to combine the basic electrical components such as resistors, capacitors, operational amplifiers, and analogs multiplier.

An electronic circuit simulator is a simulation software for modeling circuit operation and is an invaluable analysis tool, which uses mathematical models to replicate the behavior of an actual electronic circuit or device. Due to its highly accurate modeling capability, many Colleges and Universities use this type of software for the teaching of electronics technicians and electronics engineering programs. The most well-known analog simulator is SPICE and many software simulations have integrated this analog simulator; among them, P-SPICE, MultiSIM, and so on. In the thesis, we are going to use P-SPICE software.

2.4.2. Microcontroller simulation method

The microcontroller simulation procedure is to discretize the set of equations describing the dynamics of each of our oscillators, and then program the nonlinear differential equations through the RK₄ method, using the software Arduino compiler or mikroC which are both similar to C and C++. The program is then inserted in the Arduino which delivers its output signal through the converter R-2R resistors network placed at its output ports. Then the real electrical signal is visualized in the oscilloscope.

The Arduino Uno module board has been used in this thesis because of its simplicity and precision. The Arduino Uno module is a board based on the ATmega328 microcontroller with the following specifications: a power jack used to supply the needed voltage, a 16 MHz quartz used as a crystal oscillator, an ICSP header used to load programs, 14 digital pins which can be set as input or output, 6 analog inputs and 6 digital pins which can be used as PWM outputs, a USB connection for

METHODOLOGY

communication with computer via the open-source Arduino 1.8.5 software Integrated Development Environment (IDE), and a reset button. The programming language used here in the Arduino software IDE is the “C/Arduino”, which is very closed and compatible with the “C” programming language.

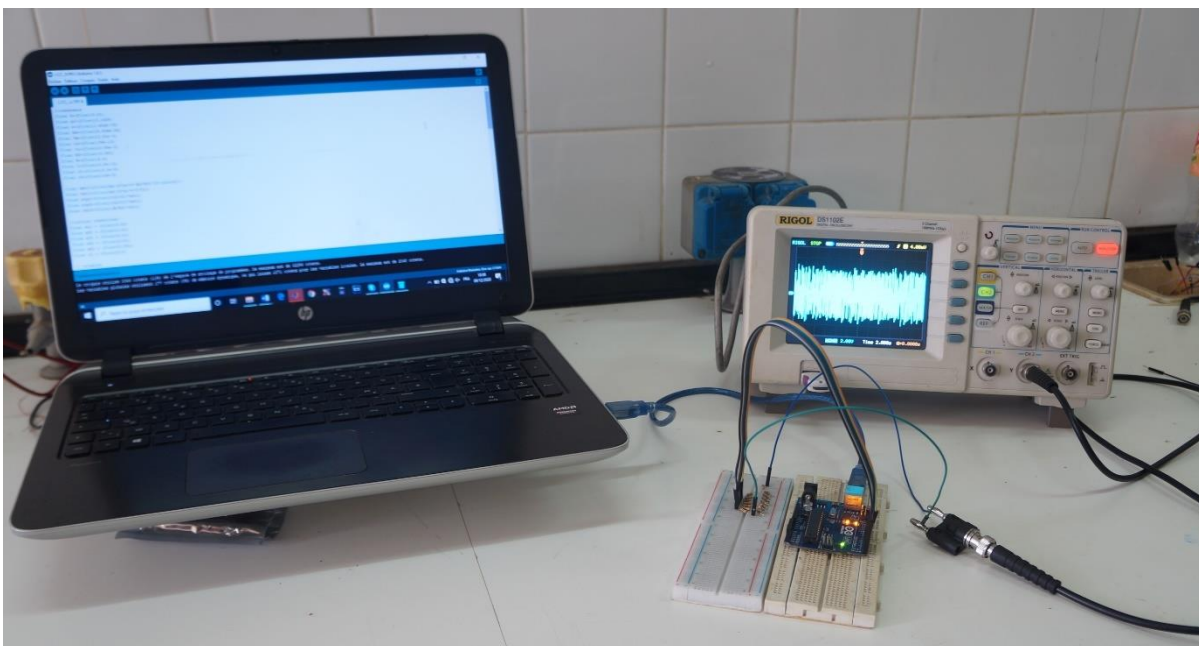


Figure 2.24: Illustration of the experimental method.

In this work, we use the Arduino Uno platform and R-2R ladder resistors network connected on a breadboard, which is acting as a DAC (digital to analog converter) with resistors $R = 1k\Omega \pm 5\%$ and $2R = 2k\Omega \pm 5\%$ respectively. The platforms communicate each with a computer via a USB connection. The outputs of the R-2R resistors network are connected to the two channels X and Y of the Rigol DS1052E digital oscilloscope as shown in figure 2.19. These channels receive the analog signals after their conversion through the R-2R network. Special jacks have been designed to directly connect all the 8 pins of digital inputs/outputs D0 to D7 of the Port D to the R-2R resistors network. The digital calculations performed by the microcontroller are sent to Port D which is connected to the R-2R network. The R-2R networks in turn convert the digital signals into analog signals; transmit them to the oscilloscope which displays them. As soon as the programs are loaded, the computer plays the role of the power supply, providing a voltage of 5 V and a maximum current of 40 mA. Each Arduino is connected to a computer separately if another observation is needed (velocity). In so doing, each platform will be able to freely call its needed current.

METHODOLOGY

The 8 pins of digital inputs/outputs D0 to D7 of the Port D are set as a digital output. Through a simple four order Runge-Kutta discretization, a program is written in C / Arduino language to perform calculations of the time trace, or time derivative if needed. The constants of the differential equations, the initial conditions, and the variables are all defined in the discretization program code. The nonlinear dynamical states of the oscillators are calculated inside the microcontroller before being displayed on the Rigol digital oscilloscope. The block diagram appears in Figure 9. The equations are discretized using the fourth-order Runge-Kutta method and then inserted into the microcontroller using the mikroC language. With the R-2R resistors network, the conversion from digital to analog signal takes place and analog signals are sent to the oscilloscope. Some details on this scheme can also be seen in Refs. [81, 83-86].

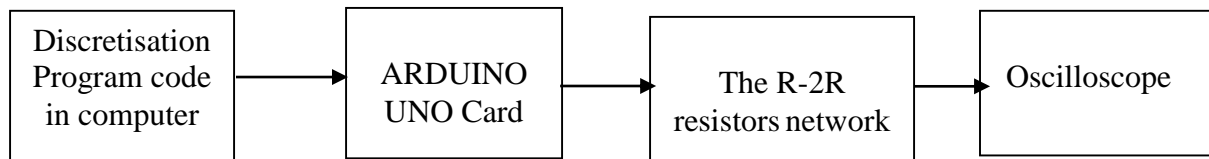


Figure 2.25: Block diagram for the microcontroller simulation.

This method of the study of nonlinear dynamical systems had advantage because of its simplicity in generating real electrical signals which cannot be obtained from the classical numerical simulation or which can be obtained using expensive and more complex experimental set-ups from the electronic circuits with analogic and discrete electronic components. The goal is to mimic the behavior of our systems (oscillators) and to have at the microcontrollers output electrical signals similar to those obtained using analog circuits.

2.5. Conclusion

This chapter has presented the mathematical formalisms needed for theoretical investigations and the numerical methods used to integrate the ordinary differential rate equations of an autonomous system. We started by presenting the stability analysis of equilibrium points and the Routh-Hurwitz criteria. After that, the numerical methods and some computational techniques both used to solve the ODEs and to characterize the dynamical behavior of the system have been

METHODOLOGY

described. Finally, we carried out the presentation of some electronic components, the analog simulation method, and the microcontroller simulation principle. The next chapter focuses on the results and discussions.

CHAPTER 3: RESULTS AND DISCUSSION

3.1. Introduction

In this chapter, we present, analyze and discuss the results obtained in our thesis. Section 3.2 will be devoted to the Generation of chaos and hyperchaos in the Colpitts-Josephson junction-like circuit. In this part, we will present the electric circuit and derivation of equations, the numerical simulations, electronic implementation, and the microcontroller real implementation of the Colpitts-Josephson junction-like circuit. Section 3.3 will focus on amplitude control and electronic implementation of the LCC-JJ-Op amp circuit. In this section, we will firstly present the analytical and numerical analysis. Then the electronic implementation and partial and total amplitude controls will be presented. Finally, Section 3.4 will be devoted to the conclusion.

3.2. Chaos and hyperchaos in Colpitts-Josephson junction-like circuit

3.2.1. Colpitts-Josephson junction like circuit and mathematical description

Figure 3.1 depicts the electronic circuit under study here. It consists of one operational amplifier, two capacitors C_1 , and C_2 ; one inductor L with internal resistor R , and a JJ diode. The Op-amp is considered ideal; thus it operates as a linear component. The only nonlinear element in the circuit is therefore the JJ. The model use here is given in chapter 1 (see figure 1.5(a)). It is made of the following component: one linear resistor R_J , one capacitors C_J , and one shunt L_S , with internal resistor R_S . The current that flows through L_S is names I_s .

RESULTS AND DISCUSSION

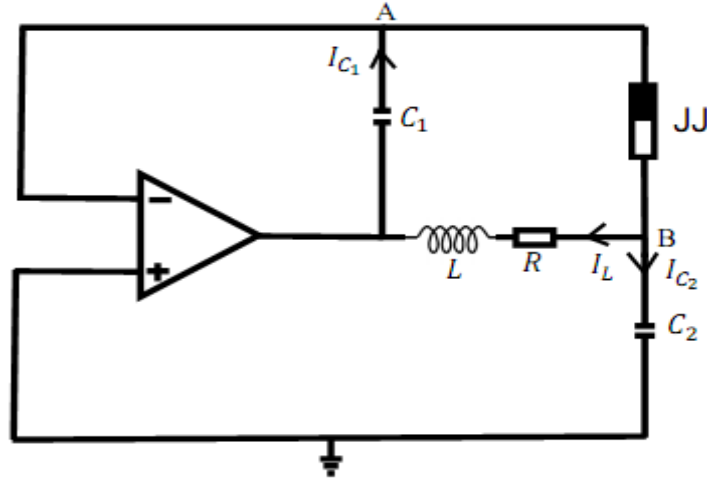


Figure 3.1: Electric circuit of CLC single operational amplifier-based oscillator with JJ nonlinearity

The application of the Kirchoff's laws to the circuit of Figure. 3.1 leads to the following differential equations:

$$\begin{aligned}
 C_1 \frac{dV_{C_1}}{dt} &= \frac{C_2}{R_J(C_2 + C_J)} V_J + \frac{I_C C_2}{C_2 + C_J} \sin \varphi + \frac{C_J}{C_2 + C_J} I_L + \frac{C_2}{C_2 + C_J} I_S, \\
 (C_2 + C_J) \frac{dV_{C_2}}{dt} &= -\frac{V_{C_2}}{R_J} + I_C \sin \varphi - I_L + I_S, \\
 (C_2 + C_J) \frac{dV_J}{dt} &= -\frac{V_J}{R_J} - I_C \sin \varphi + I_L - I_S, \\
 L \frac{dI_L}{dt} &= -(V_{C_1} - V_{C_2} + R I_L), \\
 L_S \frac{dI_S}{dt} &= V_J - R_S I_S, \\
 \frac{\hbar}{2e} \frac{d\varphi}{dt} &= V_J,
 \end{aligned} \tag{3.1}$$

where V_J , V_{C_1} , and V_{C_2} are the electric voltage respectively across the Josephson junction, the capacitor C_1 , and the capacitor C_2 ; I_L is the current flowing through the inductance L . φ denotes the quantum phase difference between the two superconductors. One can observe a symmetry in the system of equations (3.1) since it remains the same when inverting the signs of different variables.

Using the following dimensionless variables:

RESULTS AND DISCUSSION

$$\begin{aligned}
 V_{C_1} &= x_1 R_S I_C; \quad V_{C_2} = x_2 R_S I_C; \quad V_J = x_3 R_S I_C; \quad I_L = x_4 I_C; \quad I_S = x_5 I_C; \quad \varphi = x_6; \quad t = \frac{\tau}{w_0}; \\
 w_0 &= \frac{2\pi e R_S I_C}{h}; \quad \alpha_1 = \frac{C_2}{C_1} \beta_1; \quad \alpha_2 = \frac{C_2}{C_1} \beta_2; \quad \alpha_3 = \frac{C_J}{C_1} \beta_2; \quad \beta_2 = \frac{\beta_1}{R_S}; \quad \theta_1 = \frac{a_1}{L}; \quad \theta_2 = \frac{R}{L} a_2; \quad (3.2) \\
 \beta_1 &= \frac{h}{2\pi e (C_2 + C_J) R_S R_J I_C}; \quad \beta_L = \frac{2\pi e L_S I_C}{h}; \quad a_1 = \frac{h}{2\pi e I_C}; \quad a_2 = \frac{a_1}{R_S},
 \end{aligned}$$

and after some mathematical manipulations, Eq. (3.1) can be rewritten as follows:

$$\begin{aligned}
 \dot{x}_1 &= \alpha_1 x_3 + \alpha_2 (\sin(x_6) + x_5) + \alpha_3 x_4, \\
 \dot{x}_2 &= -\beta_1 x_2 + \beta_2 (\sin(x_6) - x_4 + x_5), \\
 \dot{x}_3 &= -\beta_1 x_3 - \beta_2 (\sin(x_6) - x_4 + x_5), \\
 \dot{x}_4 &= -\theta_1 (x_1 - x_2) - \theta_2 x_4, \\
 \dot{x}_5 &= \frac{1}{\beta_L} (x_3 - x_5), \\
 \dot{x}_6 &= x_3.
 \end{aligned} \tag{3.3}$$

System (3.3) has a symmetry under the following transformation:

$$S(x_1, x_2, x_3, x_4, x_5, x_6) \rightarrow (-x_1, -x_2, -x_3, -x_4, -x_5, -x_6),$$

3.2.2. Equilibrium points and their stability analysis

When the time derivatives in Eq. (3.3) are put to zero, the system presents two equilibrium points: $E_1(0,0,0,0,0,0)$ and $E_2(0,0,0,0,0,\pi)$. The characteristic equation of system (3.3) evaluated at the equilibrium point E_1 is:

$$\lambda^6 + a_{11}\lambda^5 + a_{12}\lambda^4 + a_{13}\lambda^3 + a_{14}\lambda^2 + a_{15}\lambda^1 + a_{16} = 0, \tag{3.4}$$

where the expressions of a_{1i} ($i = 1; 2; 3; 4; 5; 6$) are worth :

RESULTS AND DISCUSSION

$$\begin{aligned}
a_{11} &= \theta_2 + \theta_3 + 2\beta_1, \\
a_{12} &= (\alpha_3 + \beta_2)\theta_1 + (\beta_2 + \theta_2)\theta_3 + \beta_2 + 2\beta_1(\theta_2 + \theta_3) + \beta_1^2, \\
a_{13} &= \theta_1\theta_3(\alpha_3 + \beta_2) + \beta_2\theta_2(1 + \theta_3) + \beta_2\theta_3 + \theta_1(\alpha_1\beta_2 + 2\alpha_3\beta_1 + \beta_1\beta_2) + \beta_1\theta_3(\beta_2 + 2\theta_2) \\
&\quad + \beta_1\beta_2 + \beta_1^2(\theta_2 + \theta_3), \\
a_{14} &= \beta_2\theta_1(\alpha_2\theta_3 + \alpha_3\theta_3 + \alpha_2 + \alpha_3) + \beta_2\theta_2\theta_3 + \theta_1\theta_3(\alpha_1\beta_2 + 2\alpha_3\beta_1 + \beta_1\beta_2) \\
&\quad + \beta_1\beta_2(\theta_2\theta_3 + \theta_2 + \theta_3) + \alpha_1\beta_1\beta_2\theta_1 + \alpha_3(\beta_1^2\theta_1 + \beta_1^2\theta_2\theta_3), \\
a_{15} &= \beta_2\theta_1\theta_3(\alpha_2 + \alpha_3) + \beta_1\beta_2\theta_1(\alpha_2\theta_3 + \alpha_3\theta_3 + \alpha_2 + \alpha_3) + \beta_1\beta_2\theta_2\theta_3 + \alpha_1\beta_1\beta_2\theta_1\theta_3 + \alpha_3\beta_1^2\theta_1\theta_3, \\
a_{16} &= \beta_1\beta_2\theta_1\theta_3(\alpha_2 + \alpha_3),
\end{aligned} \tag{3.5}$$

with $\theta_3 = 1/\beta_L$.

At the equilibrium point E_2 , the characteristic equation is

$$\lambda^6 + a_{21}\lambda^5 + a_{22}\lambda^4 + a_{23}\lambda^3 + a_{24}\lambda^2 + a_{25}\lambda + a_{26} = 0, \tag{3.6}$$

with the expressions of a_{2i} ($i = 1; 2; 3; 4; 5; 6$) given below:

$$\begin{aligned}
a_{21} &= \theta_2 + \theta_3 + 2\beta_1, \\
a_{22} &= (\alpha_3 + \beta_2)\theta_1 + (\beta_2 + \theta_2)\theta_3 - \beta_2 + 2\beta_1(\theta_2 + \theta_3) + \beta_1^2, \\
a_{23} &= \theta_1\theta_3(\alpha_3 + \beta_2) + \beta_2\theta_2(\theta_3 - 1) - \beta_2\theta_3 + \theta_1(\alpha_1\beta_2 + 2\alpha_3\beta_1 + \beta_1\beta_2) + \beta_1\theta_3(\beta_2 + 2\theta_2) \\
&\quad - \beta_1\beta_2 + \beta_1^2(\theta_2 + \theta_3), \\
a_{24} &= \beta_2\theta_1(\alpha_2\theta_3 + \alpha_3\theta_3 - \alpha_2 - \alpha_3) - \beta_2\theta_2\theta_3 + \theta_1\theta_3(\alpha_1\beta_2 + 2\alpha_3\beta_1 + \beta_1\beta_2) \\
&\quad + \beta_1\beta_2(\theta_2\theta_3 - \theta_2 - \theta_3) + \alpha_1\beta_1\beta_2\theta_1 + \alpha_3(\beta_1^2\theta_1 + \beta_1^2\theta_2\theta_3), \\
a_{25} &= -\beta_2\theta_1\theta_3(\alpha_2 + \alpha_3) - \beta_1\beta_2\theta_1(-\alpha_2\theta_3 - \alpha_3\theta_3 + \alpha_2 + \alpha_3) + \beta_1\beta_2\theta_2\theta_3 + \alpha_1\beta_1\beta_2\theta_1\theta_3 + \alpha_3\beta_1^2\theta_1\theta_3, \\
a_{26} &= -\beta_1\beta_2\theta_1\theta_3(\alpha_2 + \alpha_3),
\end{aligned} \tag{3.7}$$

with $\theta_3 = 1/\beta_L$.

The application of the Routh–Hurwitz conditions shows that all roots of Eqs. (3.4) and (3.6) have negative real parts if and only if $a_{1i} > 0$ ($i = 1; 2; 3; 4; 5; 6$), and $a_{2i} > 0$ ($i = 1; 2; 3; 4; 5; 6$). Then all the discriminants of Routh are therefore strictly positive.

RESULTS AND DISCUSSION

In this work, we consider the effect of the varying parameters R and C_1 on the system as shown in Figure 3.2, and we keep all other parameters fixed at $I_C = 0.55mA$; $C_J = 35pF$; $R_J = 0.061\Omega$; $C_2 = 47.4nF$; $L = 0.8pH$.

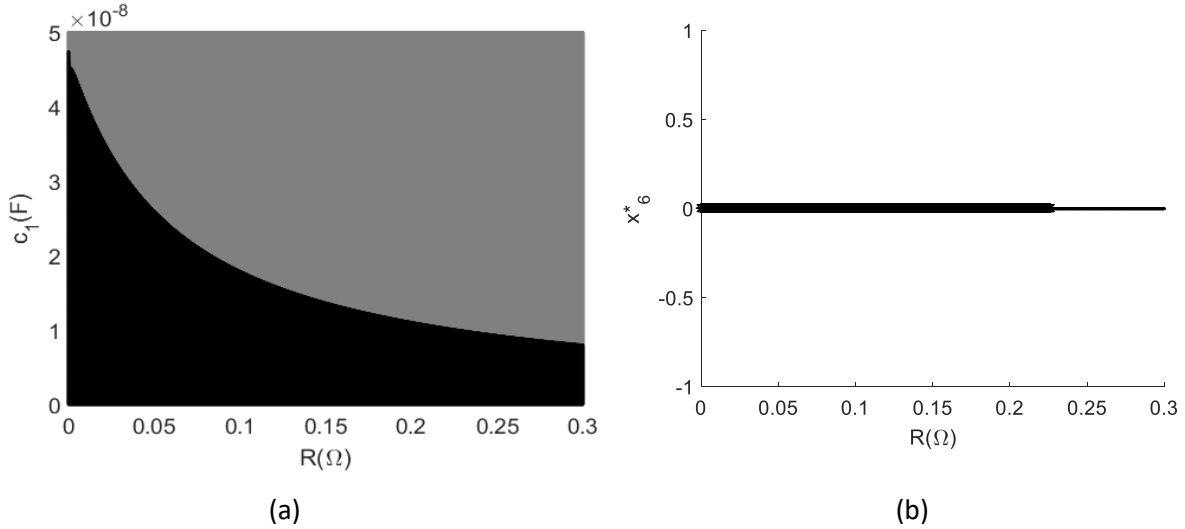


Figure 3.2: Stability boundaries of equilibrium point $E_1(0,0,0,0,0,0)$: (a) in parameter space spanning R and C_1 , and (b) the plot of initial condition x_6^* versus $R(\Omega)$ with $C_1 = 10nF$.

By varying the capacitor C_1 from 0 to $50nF$ and the resistor R from $9 \times 10^{-4}\Omega$ to $3 \times 10^{-1}\Omega$, which corresponds to varying the value of θ_2 from 12.0000 to 311.2022, the stability of the equilibrium point $E_1(0,0,0,0,0,0)$ appears as depicted in Figure 3.2(a). Here “black color” represents the unstable zone while “gray color” corresponds to the stable zone of the equilibrium point E_1 . Also in Figure 3.2(b), the “thick line” represents the values of R for which the equilibrium point E_1 is unstable, and the “slimline” represents the values of R for which the equilibrium point E_1 is stable. Furthermore, Figure 3.2(b) shows the existence of Hopf bifurcation at $R \approx 0.2289 \Omega$ ($\theta_2 = 311.2022$) where the equilibrium point E_1 changes its stability. For $R = 0.2200 \Omega$ ($\theta_2 = 299.1021$), system (3.3) displays a limit cycle while for

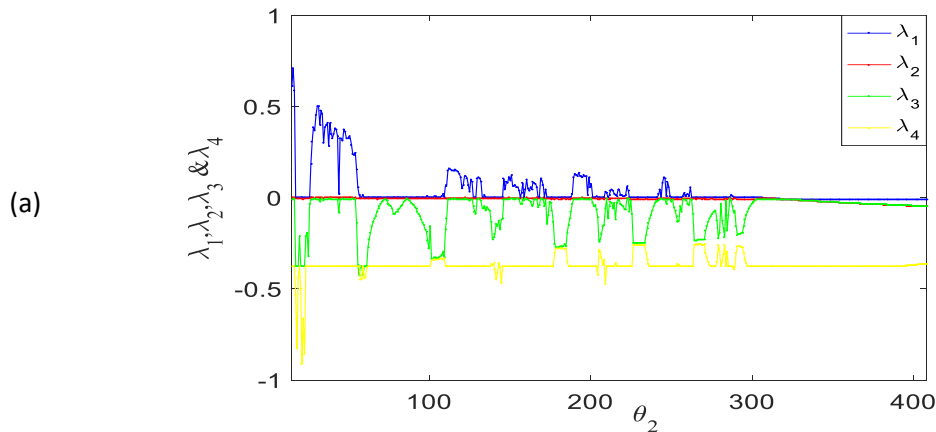
RESULTS AND DISCUSSION

$R = 0.2300 \Omega$ ($\theta_2 = 312.7000$), the trajectories of system (3.3) converge to the equilibrium point E_1 (not shown). Repeating a similar stability analysis around the equilibrium point $E_2(0,0,0,0,0,\pi)$, we found out that it is unconditionally unstable.

3.2.3. Numerical simulations: chaos and hyperchaos

To uncover the dynamical behavior of a system (3.3), the Lyapunov spectra and its corresponding bifurcation diagram versus the resistor embedded into the dimensionless parameter θ_2 are plotted in Figure 3.3.

Figure 3.3 presents the Lyapunov spectra (Figure 3.3(a)), the corresponding bifurcation diagram (Figure 3.3 (b)) and the maximal Lyapunov diagram (Figure 3.3(c)) where the maxima (in black dots) and the minima (red dots) are represented as a function of θ_2 varying from 12 to 408. When the θ_2 varies from 12.0000 to 299.1021, the bifurcation diagram of $x_1(\tau)$ exhibits chaotic and hyper-chaotic regions interspersed with periodic windows. For $299.1022 < \theta_2 \leq 408.0000$, the state of non-oscillations is observed in the system. These dynamics are confirmed by the Lyapunov spectra (Figure 3.3 (a)) and could, later on, be observed by plotting the attractor for different values of the control parameter θ_2 or R in the experimental case.



RESULTS AND DISCUSSION

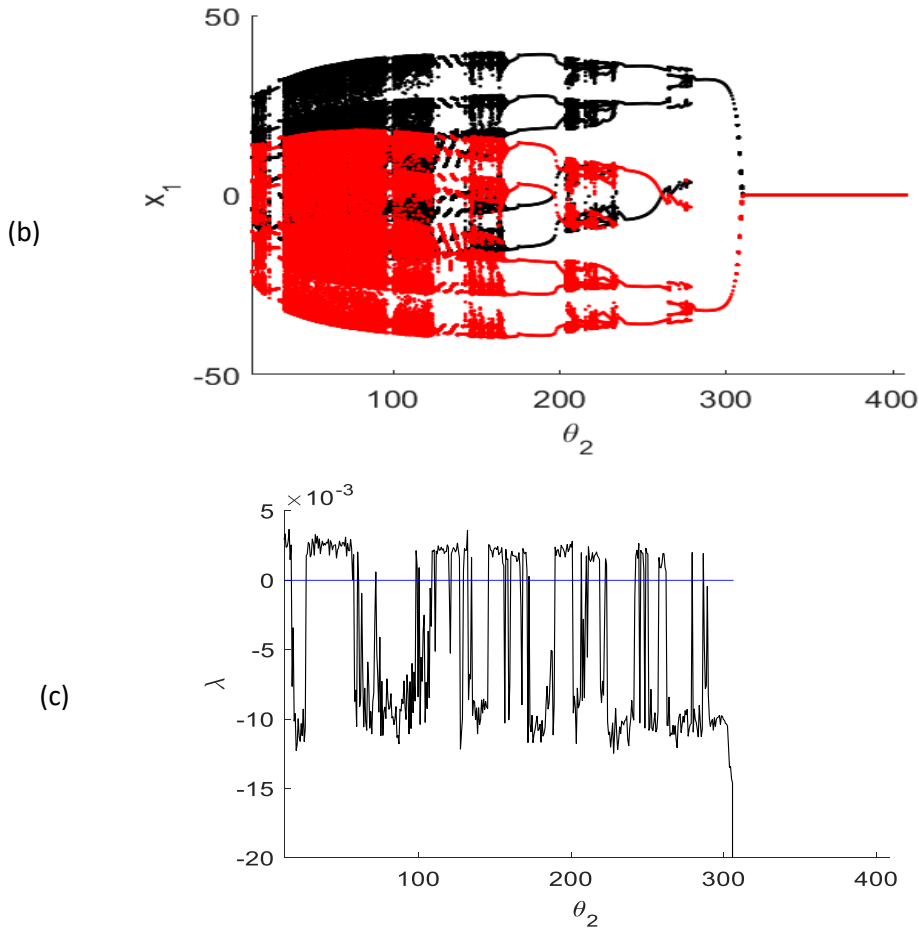


Figure 26: (a) Lyapunov spectra of system (3.3) for the outputs 1 to 4 as a function of the parameter θ_2 ; (b) Corresponding bifurcation diagram displaying the local maximum (in black color) and local minimum (in red color) of x_1 as a function of θ_2 ; (c) Corresponding maximum Lyapunov diagram for $x_1(0) = x_2(0) = x_3(0) = 0.01$, $x_4(0) = x_5(0) = 0.001$, $x_6(0) = 0$, and parameter $C_1 = 10 nF$ and $L = 0.8 pH$.

In order to see the signature of hyperchaotic behavior in system (3.3), a zoom of Figure 3.3(a) depicts two positive Lyapunov exponents λ_1 (blue color) and λ_2 (red color) for some windows space of $\theta_2 < 200$ illustrated in Figure 3.4. Thus, system (3.3) presents a 2D hyperchaoticity (two positive Lyapunov exponents) even though it is a 6D system (6 degrees of freedom). It is worth mentioning that Lyapunov exponents λ_5 and λ_6 are not plotted because they have very large negative amplitudes compared to that of the four others.

RESULTS AND DISCUSSION

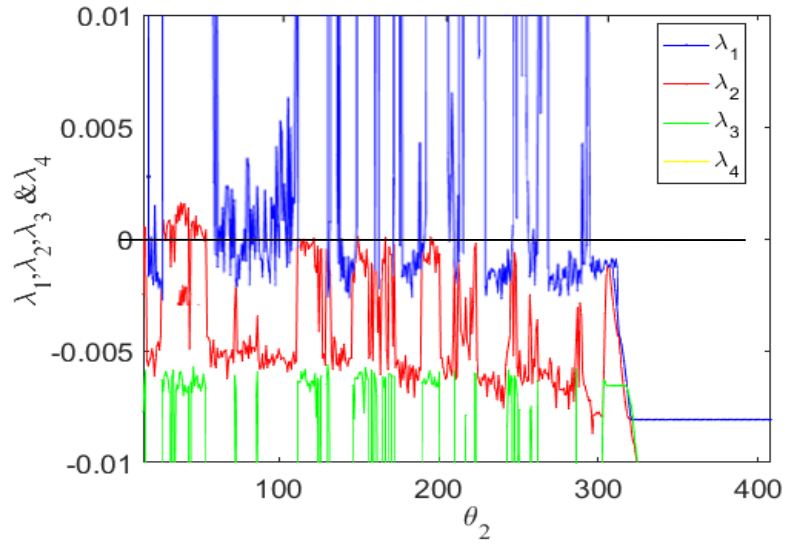
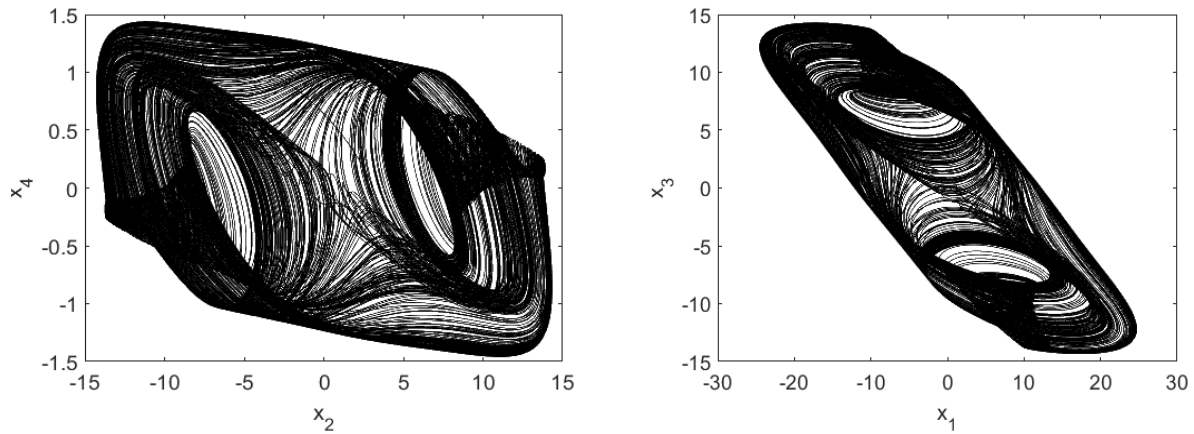


Figure 27: Zoom of the Lyapunov spectra of figure 3.3(a) to show places with two positive Lyapunov exponents

Examples of phase portraits are plotted for hyperchaotic and chaotic signals at $\theta_2 = 13.60$ respectively $\theta_2 = 149.55$ in Figure 3.5.



RESULTS AND DISCUSSION

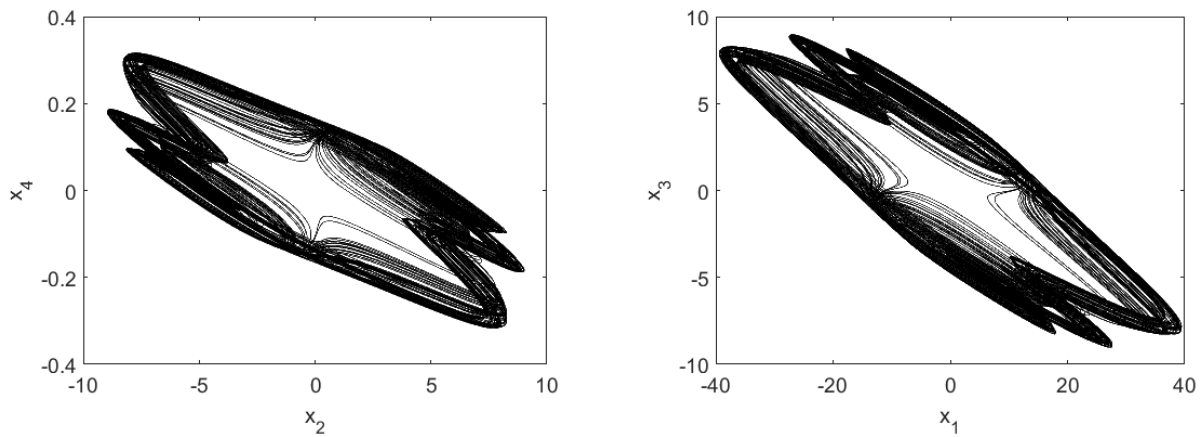


Figure 3.28: Phase portraits in the plane (x_2, x_4) and (x_1, x_3) for a hyperchaotic attractor (Figure 3.5 (a) for $\theta_2 = 13.60$) and chaotic attractor (Figure 3.5 (b) for $\theta_2 = 149.55$)

3.2.4. Electronic implementation

3.2.4.1. Generating the sine nonlinearity

Let us consider Figure 3.6 (a). Introducing this circuit in OrCAD PSpice simulator and varying the continuous voltage V from 0 V to 25 V with a step of 0.001 V, Figure 3.6 (b) has been obtained. It clearly shows the sine function. The circuit in figure 3.6 (a) will thus be used to generate the Josephson junction nonlinear term.

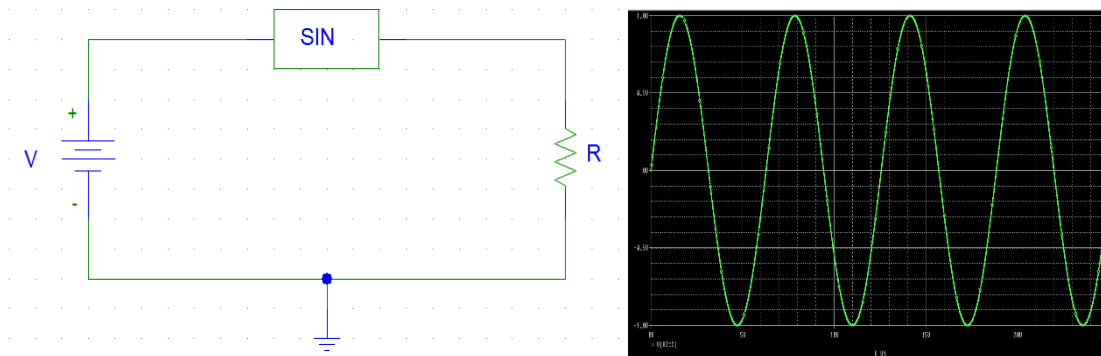


Figure 29: a) Electric circuit with analogic sine function; b) Analog sine function curve with $R=1 \text{ k}\Omega$

RESULTS AND DISCUSSION

The SIN block is an analogic sine function incorporated in OrCAD PSpice as a component. It receives a signal at its input and returns the sine of that signal at its output.

3.2.4.2. OrCAD-PSpice electronic simulation results

We develop in Figure 3.7 an electronic implementation of the five-component autonomous JJ-based circuit derived from its mathematical description in Eq. (3.3) using the integrated approach based on operational amplifiers [184, 185].

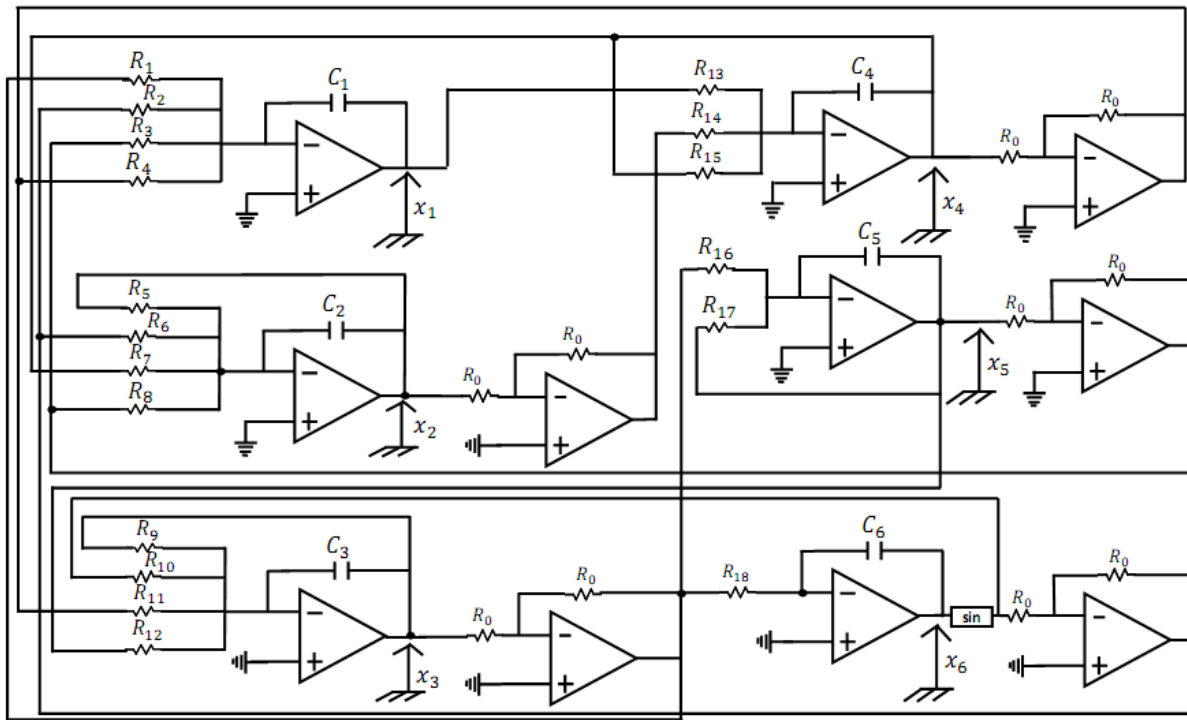


Figure 3.7: Analog circuit of the Colpitts-Josephson junction-like circuit

Figure 3.7 consists of eighteen resistors (from R_1 to R_{18}), an analogical sinus function, and five reverser circuits built using operational amplifiers and two identical resistors R_0 for each. The variables x_1 , x_2 , x_3 , x_4 , x_5 , and x_6 are represented by the voltages across the capacitors of the different integrators. All these capacitors are identical because they have the same value. Therefore, we can write $C_1 = C_2 = C_3 = C_4 = C_5 = C_6 = C$. By applying Kirchhoff's laws to the electronic circuit of Figure 3.7, its state equations can be derived as follows:

RESULTS AND DISCUSSION

$$\begin{aligned}
 \dot{x}_1 &= \frac{1}{R_1 C \omega_0} x_3 + \frac{\sin(x_6)}{R_2 C \omega_0 u_0} + \frac{x_5}{R_3 C \omega_0} + \frac{x_4}{R_4 C \omega_0}, \\
 \dot{x}_2 &= -\frac{1}{R_5 C \omega_0} x_2 + \frac{\sin(x_6)}{R_6 C \omega_0 u_0} - \frac{x_5}{R_7 C \omega_0} + \frac{x_4}{R_8 C \omega_0}, \\
 \dot{x}_3 &= -\frac{1}{R_9 C \omega_0} x_3 - \frac{\sin(x_6)}{R_{10} C \omega_0 u_0} + \frac{x_5}{R_{11} C \omega_0} - \frac{x_4}{R_{12} C \omega_0}, \\
 \dot{x}_4 &= -\frac{x_1}{R_{13} C \omega_0} + \frac{x_2}{R_{14} C \omega_0} - \frac{x_4}{R_{15} C \omega_0}, \\
 \dot{x}_5 &= \frac{x_3}{R_{16} C \omega_0} - \frac{x_5}{R_{17} C \omega_0}, \\
 \dot{x}_6 &= \frac{x_3 u_0}{R_{18} C \omega_0}.
 \end{aligned} \tag{3.8}$$

By identification between the Eqs. (3.3) and (3.8), we can define the values of the eighteen resistors mentioned above:

$$\begin{aligned}
 R_1 &= \frac{1}{\alpha_1 C \omega_0}; R_2 = \frac{1}{\alpha_2 C \omega_0 u_0}; R_3 = \frac{1}{\alpha_2 C \omega_0}; R_4 = \frac{1}{\alpha_3 C \omega_0}; R_5 = \frac{1}{\beta_1 C \omega_0}; \\
 R_6 &= R_{10} = \frac{1}{\beta_2 C \omega_0 u_0}; R_7 = R_8 = \frac{1}{\beta_2 C \omega_0}; R_9 = \frac{1}{\beta_1 C \omega_0}; R_{11} = R_{12} = \frac{1}{\beta_2 C \omega_0}; \\
 R_{13} &= \frac{1}{\theta_1 C \omega_0}; R_{14} = \frac{1}{\theta_1 C \omega_0 u_0}; R_{15} = \frac{1}{\theta_2 C \omega_0}; R_{16} = R_{17} = \frac{\beta_L}{C \omega_0}; R_{18} = \frac{u_0}{C \omega_0}.
 \end{aligned} \tag{3.9}$$

According to the values of parameters used for the numerical simulations, the values of the resistors from R_1 to R_{18} are given in Table 3.1.

Table 3.1: Values of resistors for the analog Colpitts-Josephson junction-like circuit with $\omega_0 = 10^4$,

$$C = 100 \text{ nF} \text{ and } u_0 = 1 \text{ V}$$

Resistors	Values (Ω)	Resistors	Values (Ω)
R_1	561.26	$R_6 = R_7 = R_8 = R_{10} = R_{11} = R_{12}$	47.97
R_2	10.12	$R_{13} = R_{14}$	668.67
R_3	10.12	R_{15} varying with control parameter θ_2	73.56
R_4	13.70 k	$R_{16} = R_{17}$	1.25 G
$R_5 = R_9$	2.66 k	$R_{18} = R_0$	1.00 k

RESULTS AND DISCUSSION

Figure 3.8 presents the phase portraits obtained from the analog circuit from Figure 3.7 by using the OrCAD-PSpice. One finds a good qualitative agreement between the PSpice results and numerical simulation results (see figure 3.9).

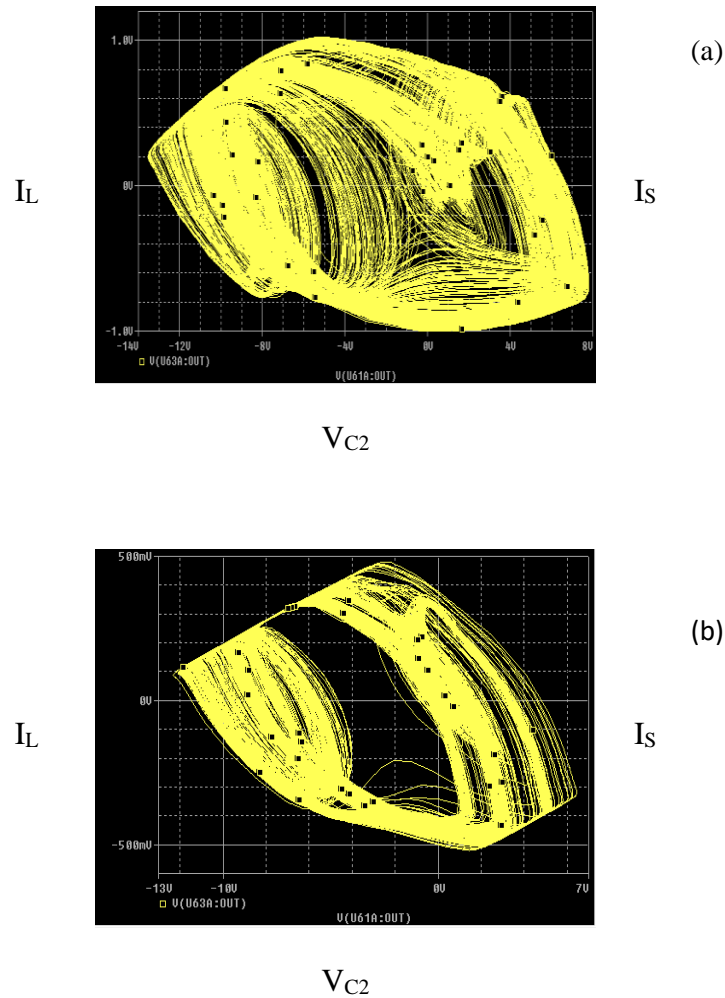


Figure 30: OrCAD-PSpice phase portrait of hyper-chaotic and chaotic attractors in the planes (V_{C2}, I_L) for: (a) $\theta_2 = 13.60$ and (b) $\theta_2 = 149.55$

RESULTS AND DISCUSSION

3.2.5. Microcontroller implementation of the Colpitts - Josephson junction circuit

The RIGOL digital oscilloscope curves are displayed instantly after the programs have been loaded. This gives a very high speed in obtaining the experimental results. The manipulations only require programming and loading into the microcontrollers. All data from the experimental simulations can be stored in the RIGOL digital oscilloscope and saved in a USB key for processing purposes. Figure 3.9 presents some time traces of the signals observed in the oscilloscope. It presents the time evolution of the signal x_2 in the case of hyperchaotic and chaotic dynamics. The corresponding phase portraits are displayed in Figure 3.10. To plot these phase portraits, we collected the temporal evolution of the data and used MATLAB software.

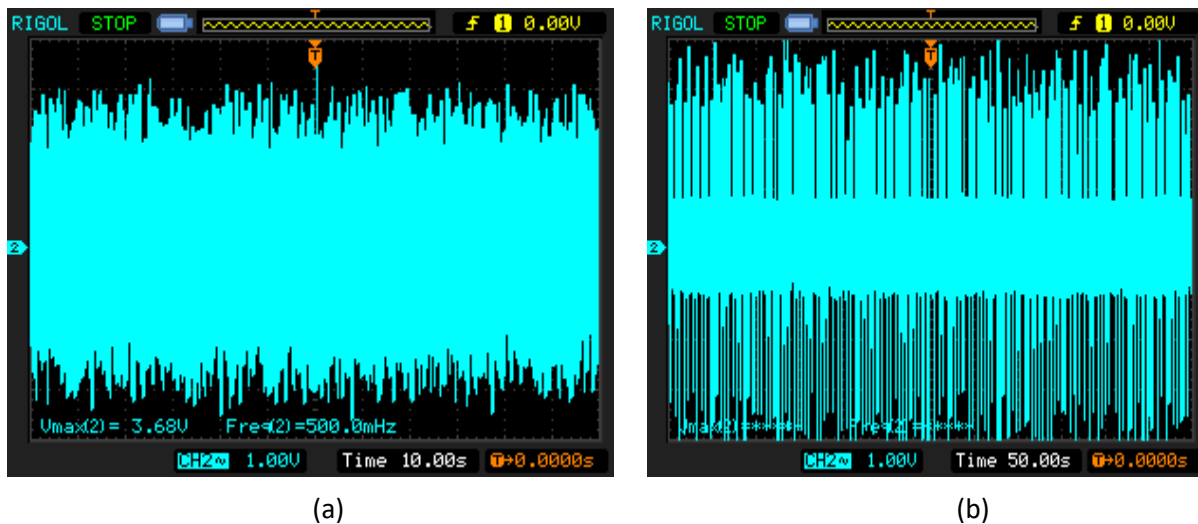


Figure 31 : Time evolution of the hyperchaotic signal x_2 (Figure 3.9 (a) for $\theta_2 = 13.6$) and that of the chaotic dynamics (Figure 3.9 (b) for $\theta_2 = 149.55$).

To produce a phase portrait showing this dynamic, we have to use two microcontrollers Arduino Uno board. The first Arduino Uno board connected to the X channel is responsible for visualizing the time trace, while the second, linked to the Y channel, is responsible for visualizing the time derivative

RESULTS AND DISCUSSION

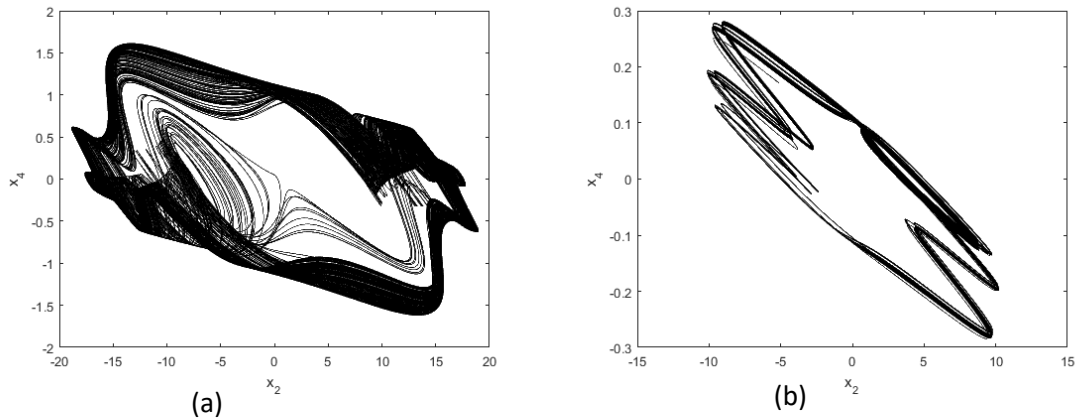


Figure 32: Phase portraits (x_2, x_4) obtained from the microcontroller simulation: (a) hyperchaotic signal for $\theta_2 = 13.6$ and (b) chaotic attractors for $\theta_2 = 149.55$.

3.3. Amplitude control and electronic implementation of the Colpitts Josephson junction Op amp circuit

3.3.1. Mathematical and numerical simulation of the Colpitts Josephson junction Op amp circuit

The LCC-JJ-Op amp circuit is presented in figure 3.11

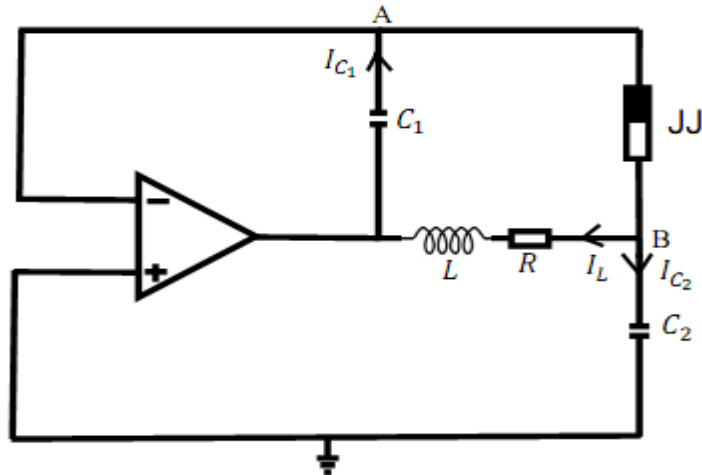


Figure 3.11: The schematic representations of Colpitts Josephson junction Op amp.

The circuit of figure 3.11 is made of: a single operational amplifier, two capacitors C_1 , and C_2 ; one inductor L with internal resistor R , and an LRCSJ model of JJ presented in Figure 1.3 of

RESULTS AND DISCUSSION

chapter 1. The Op-amp is considered ideal, so it operates as a linear component. The application of Kirchhoff's laws to the circuits of Figure 3.11 leads to the following differential equations:

$$C_1 \frac{dV_{C_1}}{dt} = \frac{C_2}{R_J(C_2 + C_J)} V_J + \frac{I_C C_2}{C_2 + C_J} \sin \varphi + \frac{C_J}{C_2 + C_J} I_L, \quad (3.10a)$$

$$(C_2 + C_J) \frac{dV_{C_2}}{dt} = -\frac{V_{C_2}}{R_J} + I_C \sin \varphi - I_L, \quad (3.10b)$$

$$(C_2 + C_J) \frac{dV_J}{dt} = -\frac{V_J}{R_J} - I_C \sin \varphi + I_L, \quad (3.10c)$$

$$L \frac{dI_L}{dt} = -(V_{C_1} - V_{C_2} + R I_L), \quad (3.10d)$$

$$\frac{\hbar}{2e} \frac{d\varphi}{dt} = V_J. \quad (3.10e)$$

Here, φ (phi) represents the quantum phase difference between the two superconductors constituting the Josephson junction and the critical current I_C . V_J , V_{C_1} , and V_{C_2} are the respective electrical voltages at the boundaries of the Josephson junction. C_1 , C_2 , and L are the capacitors and the inductance building the physical resonant energy tanks of the oscillator, with I_L the current flowing through L .

By inserting the following new variables and parameters in the set of Eqs. (3.10):

$$V_{C_1} = x_1 R_J I_C; \quad V_{C_2} = x_2 R_J I_C; \quad V_J = x_3 R_J I_C; \quad I_L = x_4 I_C; \quad \varphi = x_5; \quad t = \frac{\tau}{w_0}; \quad w_0 = \frac{2\pi e R_J I_C}{h}; \quad (3.11)$$

$$\alpha_1 = \frac{C_2}{C_1} \beta_1; \quad \alpha_2 = \frac{C_J}{C_1} \beta_1; \quad \theta_2 = \frac{R}{R_J} \theta_1; \quad \beta_1 = \frac{h}{2\pi e (C_2 + C_J) R_J I_C}; \quad \theta_1 = \frac{h}{2\pi e L I_C},$$

after some mathematical manipulations, the set of Eqs. (3.10) can be written as:

RESULTS AND DISCUSSION

$$\dot{x}_1 = \alpha_1(x_3 + \sin(x_5)) + \alpha_2 x_4, \quad (3.12a)$$

$$\dot{x}_2 = -\beta_1(x_2 - \sin(x_5) + x_4), \quad (3.12b)$$

$$\dot{x}_3 = -\beta_1(x_3 + \sin(x_5) - x_4), \quad (3.12c)$$

$$\dot{x}_4 = -\theta_1(x_1 - x_2) - \theta_2 x_4, \quad (3.12d)$$

$$\dot{x}_5 = x_3. \quad (3.12e)$$

The LCC-JJ-Op amp circuit described by system (3.12) has symmetry under the following transformation: $S(x_1, x_2, x_3, x_4, x_5) \rightarrow (-x_1, -x_2, -x_3, -x_4, -x_5)$. This system has two equilibrium points: $E_1(0, 0, 0, 0, 0)$ and $E_2(0, 0, 0, 0, \pi)$. The characteristic equation of system (3.12) evaluated at the equilibrium point E_1 is:

$$\lambda^5 + a_1 \lambda^4 + a_2 \lambda^3 + a_3 \lambda^2 + a_4 \lambda + a_5 = 0, \quad (3.13)$$

where the expressions of the a_i ($i = 1; 2; 3; 4; 5$) are given below:

$$\begin{aligned} a_1 &= R\theta_1/R_j + 2\beta_1, \\ a_2 &= (\alpha_2 + \beta_1)\theta_1 + \beta_1(1 + 2R\theta_1/R_j) + \beta_1^2, \\ a_3 &= \beta_1\theta_1(\alpha_1 + 2\alpha_2 + \beta_1) + \beta_1 R\theta_1(1 + \beta_1)/R_j + \beta_1^2, \\ a_4 &= (\alpha_1 + \alpha_2)(\beta_1^2\theta_1 + \beta_1\theta_1) + \beta_1^2 R\theta_1/R_j, \\ a_5 &= \beta_1^2\theta_1(\alpha_1 + \alpha_2). \end{aligned} \quad (3.14)$$

RESULTS AND DISCUSSION

Based on the Routh–Hurwitz conditions, Eq. (3.13) has all roots with negative real parts if and only if: $a_i > 0$ ($i = 1; 2; 3; 4; 5$) and all discriminant of Routh greater than zero. The stability diagram of the equilibrium point E_1 versus the resistor R and the capacitor C_1 is shown in Figure 3.12.

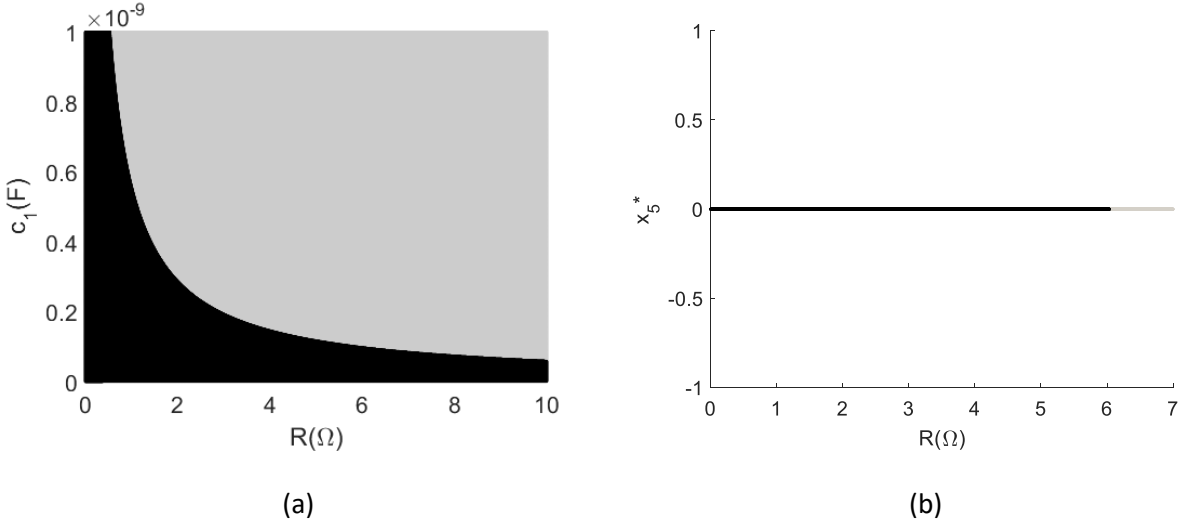


Figure 33 : (a) Stability diagram of the equilibrium point E_1 in parameter space spanning R and C_1 . (b) Stability diagram of the steady-state x_5^* (the initial condition of variable x_5) associated with the equilibrium point E_1 versus R for $C_1 = 0.1 \text{ nF}$. The other parameters are set to $I_c = 0.55 \text{ mA}$; $C_J = 35 \text{ pF}$; $R_J = 0.061 \text{ } \Omega$; $C_2 = 10 \text{ nF}$; $L = 0.8 \text{ pH}$.

The black color respectively grey color represents the unstable respectively the stable zone of the system around the critical point. The equilibrium point E_1 can be stable or unstable depending on the resistor R and the capacitor C_1 , as shown in Figure 3.12(a). According to the stability analysis of the equilibrium point E_1 as a function of the resistor R in figure 3.12(b), E_1 is unstable for $R < 6.038 \Omega$. The equilibrium point E_1 changes its stability at $R \approx 6.038 \Omega$ for which system (3.12) has either Hopf bifurcation or transcritical bifurcation. It is important to note that by varying the capacitor C_1 from $7 \times 10^{-5} \text{ pF}$ to 1 nF and the resistor R from $52 \times 10^{-3} \text{ } \Omega$ to $7 \text{ } \Omega$, the equilibrium point E_2 is always unstable.

Theorem: System (3.12) has a Hopf bifurcation at the equilibrium point E_1 when the resistor R crosses the critical value $R \approx 6.038 \Omega$.

RESULTS AND DISCUSSION

Proof: Substituting $\lambda = i\omega_0$ (with $\omega_0 > 0$ and $i^2 = -1$) into Eq. (3.13), then separating real and imaginary parts leads to:

$$\omega_{01} = \frac{1}{2}\sqrt{-2\sqrt{a_2^2 - 4a_4} + 2a_2} \quad \text{or} \quad \omega_{02} = \frac{1}{2}\sqrt{2\sqrt{a_2^2 - 4a_4} + 2a_2}. \quad (3.15)$$

By substituting ω_{01} in Eq. (3.13), the value of critical the point $R_H = 6.038999998 \Omega$ is figured out. Meanwhile by substituting ω_{02} in Eq. (3.13) leads to the negative value of the critical point $R_H = -6.038999998 \Omega$. This latter case is not interesting because it is not possible to have a negative resistance in the reality. By considering the case with ω_{01} and differentiating both sides of Eq. (3.13) concerning R , it follows that:

$$\frac{d\lambda}{dR} = \frac{(\theta_1/R_J)\lambda^4 + (2\beta_1\theta_1/R_J)\lambda^3 + (\beta_1\theta_1(1+\beta_1)/R_J)\lambda^2 + (\beta_1^2\theta_1/R_J)\lambda}{5\lambda^4 + 4a_1\lambda^3 + 3a_2\lambda^2 + 2a_3\lambda + a_4}, \quad (3.16)$$

then

$$\text{Re} \left(\frac{d\lambda}{dR} \Big|_{R=R_H, \lambda=i\omega_0} \right) = \frac{h_1h_3 + h_2h_4}{h_3^2 + h_4^2} \neq 0, \quad (3.17)$$

with $h_1 = b_1w_0^4 - b_3w_0^2$, $h_2 = b_2w_0^3 - b_4w_0$, $h_3 = 5w_0^4 - 3a_2w_0^2 + a_4$, $h_4 = 4a_1w_0^3 - 2a_3w_0$, $b_1 = \theta_1/R_J$, $b_2 = 2\beta_1\theta_1/R_J$, $b_3 = \beta_1\theta_1(1+\beta_1)/R_J$, $b_4 = \beta_1^2\theta_1/R_J$. Since the Jacobian matrix of system (3.12) at the equilibrium point E_1 has two purely imaginary eigenvalues and the real part of the eigenvalue satisfies $\text{Re} \left(\frac{d\lambda}{dR} \Big|_{R=R_H, \lambda=i\omega_0} \right) \neq 0$, all the conditions for the Hopf bifurcation to occur are verified.

Therefore, system (3.12) has a Hopf bifurcation at E_1 when $R_H \approx 6.038\Omega$, and a periodic solution will exist in a neighborhood of the point R_H . When $R < R_H$, system (3.12) exhibits a limit cycle

RESULTS AND DISCUSSION

whereas, for $R > R_H$, the trajectories of system (3.12) converge to the equilibrium point E_1 (not shown).

In order to know the dynamical behavior of the system (3.12), the Lyapunov spectra and its corresponding bifurcation diagram versus the resistor R are plotted in figure 3.13.

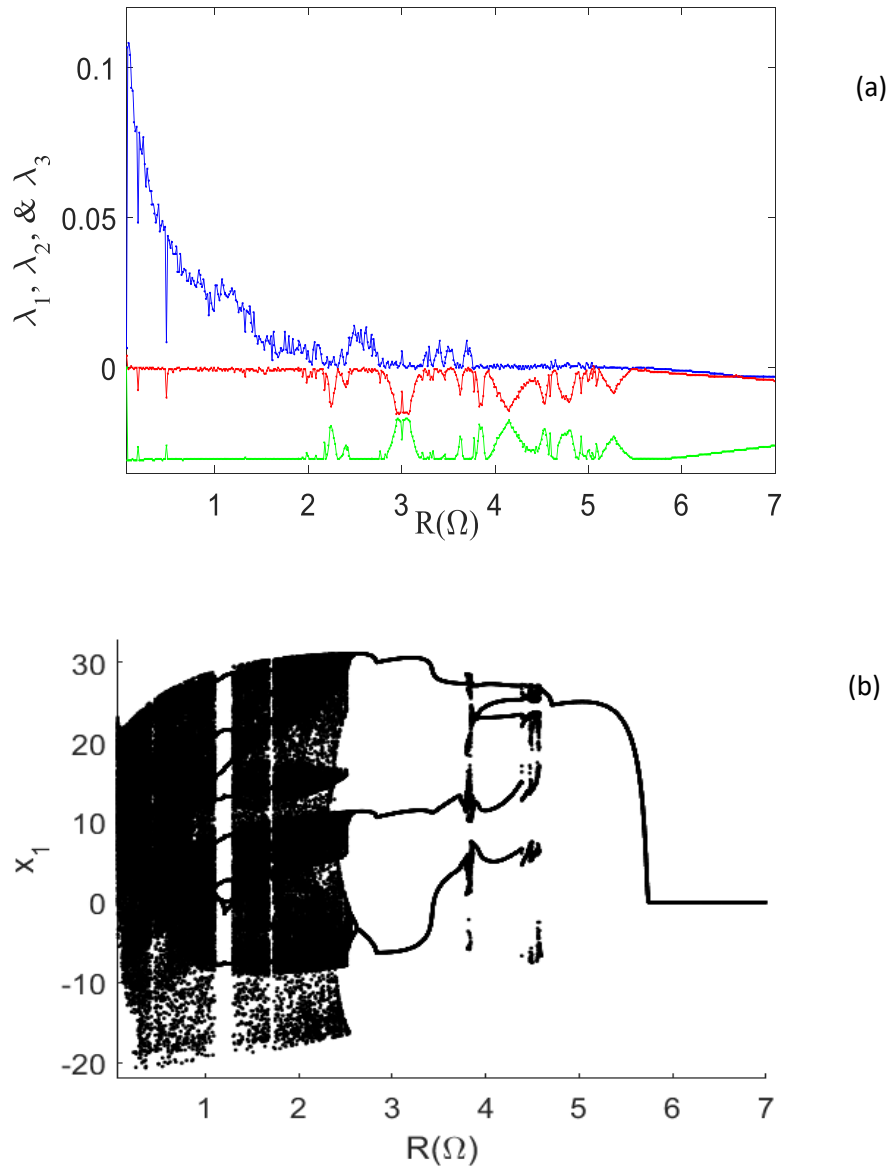


Figure 34: Lyapunov spectra as a function of resistor $R(\Omega)$ (a) and the corresponding bifurcation diagram displaying the local maxima (b) of x_1 as a function of resistor R for $C_1=0.1$ nF and $L=0.8$ pH.

RESULTS AND DISCUSSION

When resistor R varies from 0.052Ω to 6.038Ω , the bifurcation diagram of figure 3.13(b) exhibits reverse period doubling to chaotic and hyper-chaotic regions interspersed with periodic windows. For $6.038 \Omega < R \leq 7.000 \Omega$, there is no oscillation in the circuit. These dynamics are confirmed by the Lyapunov spectra (Figure 3.13 (a)) and can be verified by the plot of the attractor for different values of the control parameter R . To see the two positive Lyapunov exponents of fig. 13a, which confirms the existence of hyperchaotic behavior, the zoom of this figure is illustrated in figure 3.14.

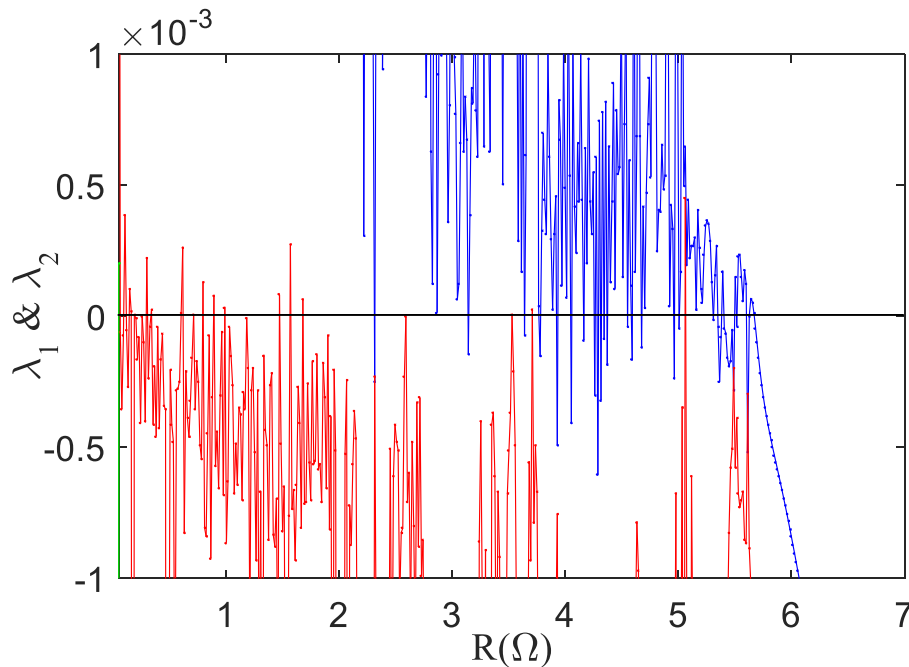


Figure 35: Zoom of the Lyapunov spectra of Figure 3.13 (a).

The phase portraits of hyperchaotic and chaotic attractors for specific values of the resistor R are presented in Figure 3.15.

RESULTS AND DISCUSSION

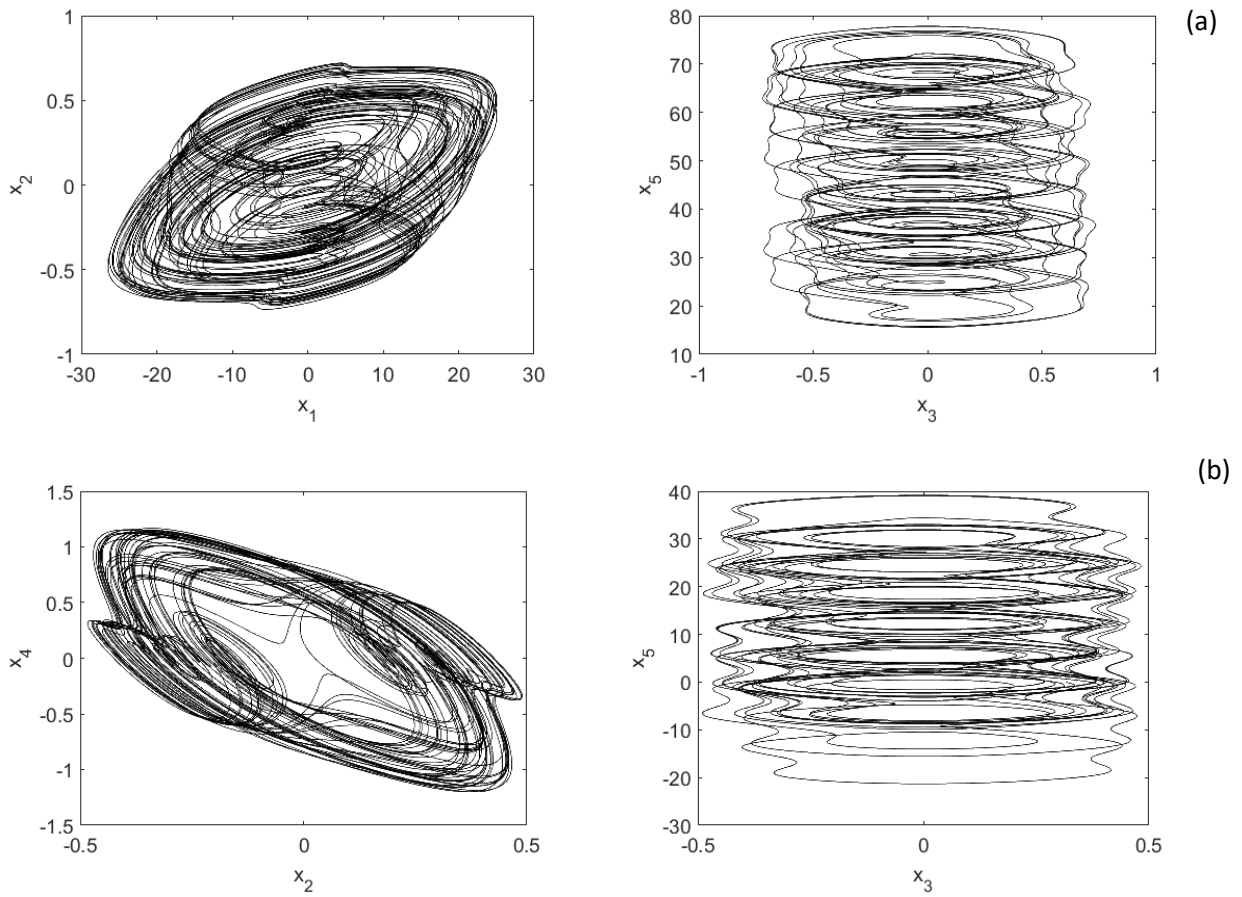


Figure 3.15: Hyperchaotic and chaotic attractors in the plane (x_2, x_4) and (x_3, x_5) :

(a) for $R = 61.78 \times 10^{-2} \Omega$; and (b) for $R = 1.50 \Omega$

LCC-JJ-Op amp circuit exhibits hyperchaotic attractors for $R = 61.78 \times 10^{-2} \Omega$ and chaotic attractors for $R = 1.50 \Omega$, as shown in figure 3.15. Another bifurcation diagram of $x_1(\tau)$ versus C_1 when $L = 0.8 \text{ pH}$; $R = 1.5 \Omega$ is plotted (not shown). This bifurcation diagram reveals similar dynamical behaviors illustrated in figure 3.13.

RESULTS AND DISCUSSION

3.3.2. OrCAD-PSpice simulation of the Colpitts Josephson junction Op amp circuit

The electronic implementation of the LCC-JJ-Op amp circuit is implemented in this section. The circuit of Figure 3.16 is obtained from the set of Eqs. (3.12) using an integrated approach based on operational amplifiers [184, 185].

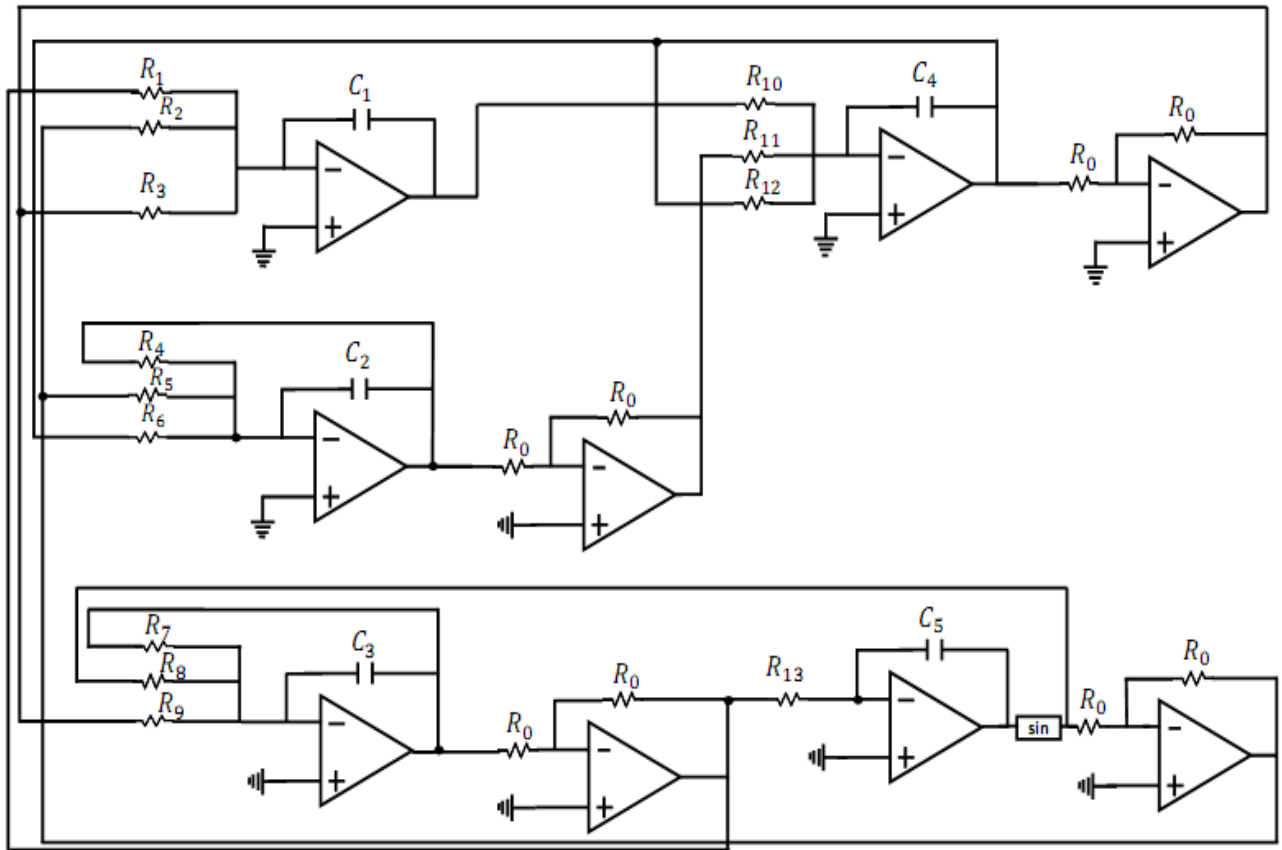


Figure 3.16: Analog circuit of the Colpitts Josephson junction Op amp circuit

Figure 3.16 consists of thirteen resistors (from R_1 to R_{13}), an analogical sinus function, and five inverter circuits made of one operational amplifier with two identical resistors named R_0 . The variables x_1 , x_2 , x_3 , x_4 and x_5 are represented by the voltages across the capacitor of the different integrators. The SIN block is the same described previously in 3.2.4.1. All the capacitors in Figure 3.16 are identical: $C_1 = C_2 = C_3 = C_4 = C_5 = C_6 = C$. By applying Kirchhoff's circuit laws to the electronic circuit of figure 3.16, its circuitual equations can be derived as follows:

RESULTS AND DISCUSSION

$$\dot{x}_1 = \frac{1}{R_1 C \omega_0} x_3 + \frac{1}{R_2 C \omega_0} \sin(x_5) + \frac{x_4}{R_3 C \omega_0}, \quad (3.18a)$$

$$\dot{x}_2 = -\frac{1}{R_4 C \omega_0} x_2 + \frac{1}{R_5 C \omega_0} \sin(x_5) - \frac{1}{R_6 C \omega_0} x_4, \quad (3.18b)$$

$$\dot{x}_3 = -\frac{1}{R_7 C \omega_0} x_3 - \frac{1}{R_8 C \omega_0} \sin(x_5) + \frac{1}{R_9 C \omega_0} x_4, \quad (3.18c)$$

$$\dot{x}_4 = -\frac{1}{R_{10} C \omega_0} x_1 + \frac{1}{R_{11} C \omega_0} x_2 - \frac{1}{R_{12} C \omega_0} x_4, \quad (3.18d)$$

$$\dot{x}_5 = \frac{1}{R_{13} C \omega_0} x_3. \quad (3.18e)$$

By identification between the set of Eqs. (3.12) and the set of Eqs. (3.18), the following expressions are obtained:

$$\begin{aligned} R_1 = R_2 = \frac{1}{\alpha_1 C \omega_0}; \quad R_3 = \frac{1}{\alpha_2 C \omega_0}; \quad R_4 = R_5 = R_6 = R_7 = R_8 = R_9 = \frac{1}{\beta_1 C \omega_0}; \\ R_{10} = R_{11} = \frac{1}{\theta_1 C \omega_0}; \quad R_{12} = \frac{1}{\theta_2 C \omega_0}; \quad R_{13} = \frac{1}{C \omega_0}. \end{aligned} \quad (3.19)$$

Following the values of different parameters in system (3.12), the values of the 13 resistors (R_1 to R_{13}) are recorded in Table 3.2 below.

Table 2.2: Values of resistors of the Colpitts Josephson junction Op amp circuit with $\omega_0 = 10^4$ and $C = 100 \text{ nF}$.

Resistors	Values (Ω)	Resistors	Values (Ω)
$R_1 = R_2$	312.20	$R_{10} = R_{11}$	668.67
R_3	89172.20	R_{12} varying with control parameter R	
$R_4 = R_5 = R_6 = R_7 = R_8 = R_9$	31210.30	$R_{13} = R_0$	1000.00

RESULTS AND DISCUSSION

The circuit of Figure 3.16 is investigated, and the phase portraits obtained from ORCAD PSPice software are illustrated in Figure 3.17.

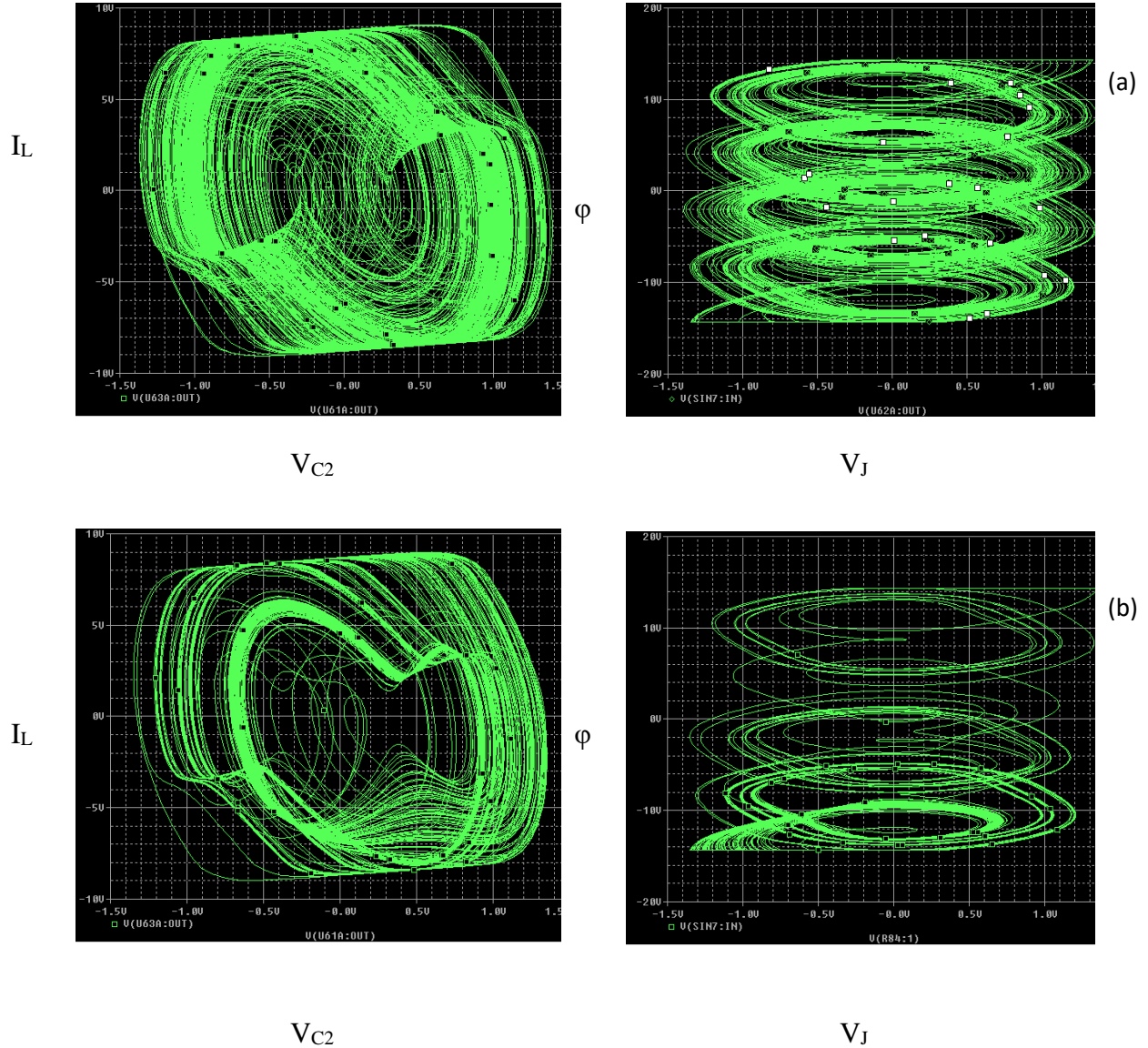


Figure 36: OrCAD-PSpice phase portrait of hyper-chaotic and chaotic attractors in the planes (V_{C_2}, I_L) and (V_J, φ) for (a) $R = 61.78 \times 10^{-2} \Omega$ and (b) $R = 1.50 \Omega$

The hyperchaotic attractor is presented in Figure 3.17(a), while the chaotic attractor is presented in Figure 3.17(b). From Figure 3.17, one can note a qualitatively good agreement between the PSpice results and numerical simulation results (see Figure 3.15).

RESULTS AND DISCUSSION

3.3.3. Partial and total amplitude controls of Colpitts Josephson junction Op amp circuit

In the literature, the partial and total amplitude controls are reported in a few chaotic oscillators [186–190]. They are of great interest for some engineering applications where the desired amplitude level can be achieved. The amplitude of the attractors of the LCC-JJ-Op amp circuit can be adjusted partially or totally.

3.3.3.1. Partial amplitude control

The state variable x_1 appears only in the fifth equation of the set of Eqs. (3.12) and its amplitude can be changed by inserting a boosting controller γ into system (3.12) as follows:

$$\dot{x}_1 = \alpha_1(x_3 + \sin(x_5)) + \alpha_2 x_4, \quad (3.20a)$$

$$\dot{x}_2 = -\beta_1(x_2 - \sin(x_5) + x_4), \quad (3.20b)$$

$$\dot{x}_3 = -\beta_1(x_3 + \sin(x_5) - x_4), \quad (3.20c)$$

$$\dot{x}_4 = -\theta_1((x_1 + \gamma) - x_2) - \theta_2 x_4, \quad (3.20d)$$

$$\dot{x}_5 = x_3. \quad (3.20e)$$

The system (3.20) has two equilibrium points $E_{11}(-\gamma, 0, 0, 0, 0)$ and $E_{12}(-\gamma, 0, 0, 0, \pi)$. The local stability of $E_{12}(-\gamma, 0, 0, 0, \pi)$ reveals that it is unconditionally unstable. The local stability of $E_{11}(-\gamma, 0, 0, 0, 0)$ reveals that system (11) has a Hopf bifurcation when the resistor R passes through the critical value $R_H = 6.038999998 \Omega$. So the stability of equilibrium points E_{11} and E_{12} are independent of boosting controller γ . To check the partial amplitude control of the system (3.20), the plot of the average values of the state variables x_1 , x_2 , x_3 , x_4 and x_5 versus boosting controller γ is shown in figure 3.18.

RESULTS AND DISCUSSION

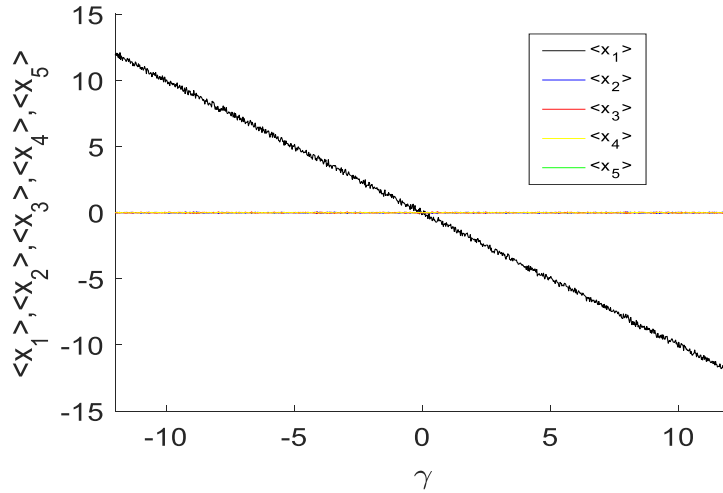


Figure 37: (Color online) The average values of the state variables x_1 (black), x_2 (blue), x_3 (red), x_4 (yellow), and x_5 (green) versus boosting controller γ for $R = 0.6178 \Omega$.

It is shown in Figure 3.18 that the average of the state variable x_1 decreases, and the other four state variables (x_2 , x_3 , x_4 , and x_5) remain unchanged when the boosting controller γ is varied. The phase portraits and time series of the state variable x_1 of the system (3.20) are depicted in Figure 3.19 for different values of the boosting controller γ .

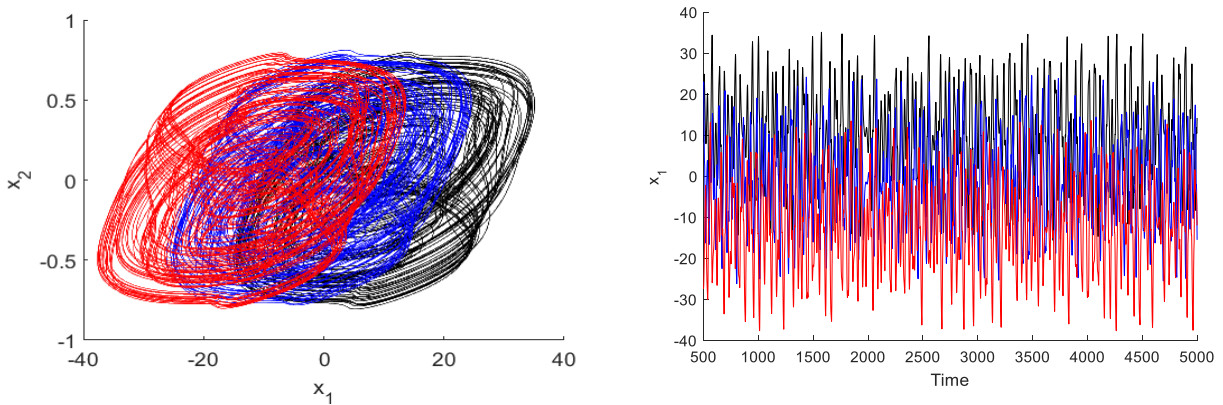


Figure 38: (Colour online) Phase portraits in the plane (x_1, x_2) and time series of the signal x_1 of system (3.20) for $R = 0.6178 \Omega$ and different values of control parameter γ : $\gamma = -10$ (black), $\gamma = 1$ (blue) and $\gamma = 12$ (red); Initial conditions $x_1(0) = 0.02$, $x_2(0) = 0.01$, $x_3(0) = 0.01$, $x_4(0) = 0.01$, $x_5(0) = 0.001$.

RESULTS AND DISCUSSION

The amplitude of the chaotic signal x_1 is boosted from a bipolar signal to a unipolar signal when increasing the boosting controller γ as shown in Figure 3.19.

3.3.3.2. Total amplitude control

LCC-JJ-Op amp circuit also has the feature of total amplitude control by inserting the changing variables: $x_1 \rightarrow x_1/\varepsilon$; $x_2 \rightarrow x_2/\varepsilon$; $x_3 \rightarrow x_3/\varepsilon$; $x_4 \rightarrow x_4/\varepsilon$ and $x_5 \rightarrow x_5/\varepsilon$. We precise that the introduction of the variable epsilon (ε) is an amplitude scaling. The parameter ε remains in the sinusoidal terms as shown in the following system (3.21):

$$\dot{x}_1 = \alpha_1(x_3 + \varepsilon \sin(x_5/\varepsilon)) + \alpha_2 x_4, \quad (3.21a)$$

$$\dot{x}_2 = -\beta_1(x_2 - \varepsilon \sin(x_5/\varepsilon) + x_4), \quad (3.21b)$$

$$\dot{x}_3 = -\beta_1(x_3 + \varepsilon \sin(x_5/\varepsilon) - x_4), \quad (3.21c)$$

$$\dot{x}_4 = -\theta_1(x_1 - x_2) - \theta_2 x_4, \quad (3.21d)$$

$$\dot{x}_5 = x_3. \quad (3.21e)$$

The system (3.21) has two equilibrium points $E_{21}(0,0,0,0,0)$ and $E_{22}(0,0,0,0,\varepsilon\pi)$. The local stability of $E_{22}(0,0,0,0,\varepsilon\pi)$ reveals that it is unconditionally unstable. Otherwise, the local stability of $E_{21}(0,0,0,0,0)$ reveals that system (3.21) has a Hopf bifurcation when the resistor R passes through the critical value $R_H = 6.038999998 \Omega$. So the stability of equilibrium points E_{21} and E_{22} are independent of the boosting controller ε . The phase portraits of the system (3.21) are depicted in Figure 3.20 for different values of the control parameter ε .

RESULTS AND DISCUSSION

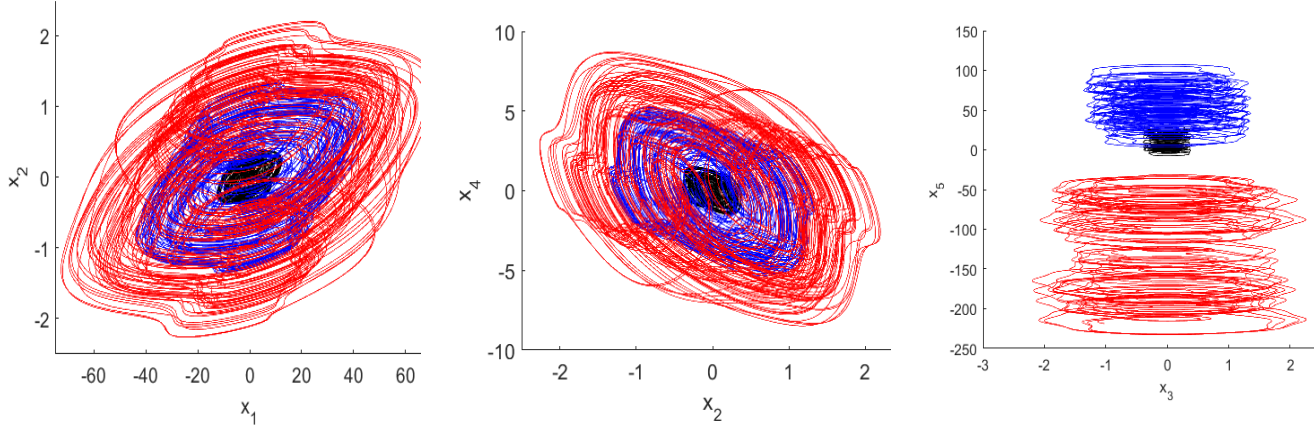


Figure 39 : (Colour online) Phase portraits in the planes (x_1, x_2) , (x_2, x_4) and (x_3, x_5) of system (12) for $R = 0.6178 \Omega$ and different values of control parameter ε : $\varepsilon = 0.5$ (black), $\varepsilon = 1.5$ (blue) and $\varepsilon = 2$ (red); Initial conditions $x_1(0) = 0.02$, $x_2(0) = 0.01$, $x_3(0) = 0.01$, $x_4(0) = 0.01$, $x_5(0) = 0.001$

As shown in Figure 3.20, the amplitude of signal signals x_1 , x_2 , x_3 , x_4 , and x_5 are adjusted simultaneously by the control parameter ε . The control parameter ε adjusts the amplitudes of the attractors for a small value (for $\varepsilon = 0.5$, the amplitudes are small) to large values (for $\varepsilon = 2$, the amplitudes are large).

3.4. Conclusion

In this chapter, we have studied the analysis of a five-component autonomous circuit with the nonlinear and active element a Josephson junction diode that is described by the linear resistive–capacitive–inductance shunted junction model. We have also studied the analysis and electronic implementation of an LCC-Josephson Junction-operational amplifier circuit. The circuits studied here provides additional tools to justify hyperchaos in autonomous circuits with less than four physical linear capacitors and/or inductors, and operating at low frequency. We presented the dynamical behaviors obtained by numerically simulations. These results were confirmed by electronically implementing the proposed circuit in OrCAD-PSPICE software. This can have an impact on the applications of nonlinear electrical signals such as in chaos cryptography, random number generation and mechatronic technology

GENERAL CONCLUSION

This thesis dealt, firstly, with the analysis of a five-component autonomous circuit with the nonlinear and active element of a Josephson junction diode that is described by the linear resistive–capacitive–inductance shunted junction model. Then, with the analysis and electronic implementation of an LCC-Josephson Junction-operational amplifier circuit. In the first part, the proposed circuit consists of one operational amplifier, two capacitors, a Josephson junction, and one inductance with its internal resistors. Meanwhile, in the second part, we have the same circuit only without the inductance. The stability of the equilibrium points of the different proposed circuits was studied using the Routh-Hurwitz criterion. It was found that the two circuits display Hopf bifurcation, periodic oscillations, chaotic, and hyperchaotic oscillations. While many JJ-based circuits displaying hyperchaos are the result of delay coupling or synchronization of two or more single chaotic circuits, the present case is a simple stand-alone one with a Colpitts linear resonator [161]. Its electronic implementation was carried out in OrCAD-PSpice software and a good qualitative agreement was shown between the numerical and analog results. The partial and total amplitude controls were achieved by adding two new parameters described in the second proposed circuit. The microcontroller used in this work appeared like a good way to display real electronic signals from nonlinear dynamical systems. The circuit studied here provides additional tools to justify hyperchaos in autonomous circuits with less than four physical linear capacitors and/or inductors, and operating at low frequency. This can have an impact on the applications of nonlinear electrical signals such as in chaos cryptography, random number generation, and mechatronics technology. This work can have applications in telecommunication for the encryption of information. This will be possible at the normal temperature range for the analog and microcontroller models. But it could also be possible at a low-temperature range for material Josephson junction. In this case, one has in mind the present quest for quantum computers.

EXTENSIONS AND FUTURE WORK

EXTENSIONS AND FUTURE WORK

In this work, we have obtained some interesting results that have opened interesting perspectives for future investigations. For future works, we plan especially:

- The construction of an electrical circuit of sine function which will allow realizing the circuit of JJ. This will allow us to realize experimentally the different circuits proposed in this thesis.
- The use of different proposed chaos/hyperchaos electrical circuits for the encryption of information.
- To exploit the complex high-frequency signals of these circuits for the modulation of semiconductors, and finally
- The use of these autonomous non-linear circuits as a power supply in electromechanical systems (EMS).

BIBLIOGRAPHY

BIBLIOGRAPHY

- [1] D. Gonze, and M. Kaufman, Theory of non-linear dynamical systems. (2012)
- [2] S. Rajasekar, S. Parthasarathy, M. Lakshmanan, Prediction of horseshoe chaos in BVP and DVP oscillators. Chaos, Solitons and Fractals 1992; 2 : 271. (1992).
- [3] M. Levi, F. C. Hoppensteadt, and W. Miranker, Dynamics of the Josephson junction. Quarterly of Applied Mathematics 36:167–198. (1978)
- [4] R. L. Kautz, and R. Monaco, Survey of chaos in the rf-biased Josephson junction. Journal of applied physics 57: 875–889. (1985)
- [5] A. Malishevskii, and S. Uryupin, Current-voltage characteristics of radiating Josephson sandwich. Physics Letters A 384: 126515. (2020)
- [6] D. McCumber, Effect of ac impedance on dc voltage-current characteristics of superconductor weak-link junctions. Journal of Applied Physics 39: 3113–3118. (1968)
- [7] Z. Zhang, K. Chau, Z. Wang, F. Li, and J. Li, Analysis of chaos in Josephson junctions with external magnetic field for high-precision voltage measurement in electric vehicles. IEEE transactions on applied superconductivity 22: 4904704–4904704. (2011)
- [8] H. P. W. Gottlieb, Question# 38. What is the simplest jerk function that gives chaos? Amer. J. Phys 64, 525-525 (1996)
- [9] R. Tchitnga, R. Zebaze Nanfa'a, F.B. Pelap, P.H. Louodop Fotso, and P. Woafu, A novel high-frequency interpretation of a general purpose Op-Amp-based negative resistance for chaotic vibrations in a simple a priori nonchaotic circuit, Journal of Vibration and Control 23, 744-751 (2015).
- [10] B. Muthuswamy, A. Przybylski, C. Feilbach and J. Mossbrucker, Two Element Chaotic and Hyperchaotic Circuits, in 4th International Interdisciplinary Symposium on Chaos and Complex Systems, Antalya, Turkey, April 30th (2012).
- [11] V.-T. Pham, A. Buscarino, L. Fortuna, and M. Frasca, Simple memristive time-delay chaotic systems, Int J Bif. Chaos 23, 1350073-1350081, (2013.).
- [12] R. Tchitnga, H.B. Fotsin, B. Nana, P.H. Louodop Fotso and P. Woafu, Hartley's oscillator: The simplest chaotic two-component circuit," Chaos, Solitons & Fractals 45, 306-313 (2012).

BIBLIOGRAPHY

- [13] B. Muthuswamy and L. O. Chua, "Simplest chaotic circuit," *Int J. Bif. Chaos* 20, 1567-80, (2010).
- [14] R. Barboza & L. O. Chua, The four-element Chua's circuit, *Int. J. Bifurcation and Chaos* 18, 943–955 (2008).
- [15] G.-S. Yim, J.-W. Ryu, Y.-J Park, S. Rim, S.-Y. Lee, W.-H. Kye, and C.-M. Kim, Chaotic behaviors of operational amplifiers," *Phys. Rev. E* 69, 045201 (2004).
- [16] J.R. Piper and J.C. Sprott, Simple Autonomous Chaotic Circuits, *IEEE Transactions on Circuits and Systems-II: Express Briefs* 57, 730-734 (2010).
- [17] R. Tchitnga, T. Nguazon, P.H. Louodop Fotso, and J. A. C. Gallas, Chaos in a Single Op-Amp based jerk circuit: Experiments and simulations, *IEEE Transactions on Circuits and Systems-II: Express Briefs* 63, 239-243 (2016).
- [18] B. Mumuangsaen, B. Srisuchinwong, A minimum five-component five-term single-nonlinearity chaotic jerk circuit based on a twin-jerk single-op-amp technique, *Int. J. Circ. Theor. Appl.* 46, 656-670 (2017).
- [19] T. Kiliyas, K. Kelber, A. Mogel, W. Schwarz. Electronic chaos generators-design and applications, *Int J Electron* 79, 737–53 (1995).
- [20] K. M. Cuomo & A. V. Oppenheim, Circuit implementation of synchronized chaos with applications to communications," *Phys. Rev. Lett.* 71, 65–68 (1993).
- [21] P. Arena, L. Fortuna & M. Frasca, Attitude control in walking hexapod robots: An analogic Spatio-temporal approach," *Int. J. Circ. Th. Appl.* 30, 349–362 (2002).
- [22] M. E. Yalcin, J. A. K. Suykens & J. Vandewalle, True random bit generation from a double-scroll attractor," *IEEE Trans. Circuits Syst.-I: Regular Papers* 51, 1395–1404 (2004).
- [23] J. Clarke, N. N. Cleland, M. H. Devoret, D. Esteve and J. M. Martinis, Quantum Mechanics of a Macroscopic Variable: The Phase Difference of a Josephson Junction, *Science* 239, 992-997 (1988).
- [24] R.L. Kautz, Chaotic states of RF-biased Josephson junctions, *J. Appl. Phys.* 52, 6241–6246 (1981).
- [25] S. K. Dana, Spiking and Bursting in Josephson Junction, *IEEE Transactions on Circuits and Systems II: Express Briefs* 53, 1031–1034 (2006).

BIBLIOGRAPHY

- [26] A. B. Cawthorne, C. B. Whan, and C. J. Lobb, Complex dynamics of resistively and inductively shunted Josephson junctions, *Journal of Applied Physics* 84, 1126–1132 (1998).
- [27] S.T. Kingni, G. F. Kuate, R. Kengne, R. Tchitnga, and P. Wofo, Analysis of a non equilibrium linear resistive-capacitive-inductance shunted junction model, dynamics, synchronization and application to digital cryptography in its fractional-order form, *Complexity* 2017, Article ID 4107358, 12 pages DOI.org/10.1155/2017/4107358 (2017)
- [28] M. Canturk, I. Askerzade, Chaotic dynamics of externally shunted Josephson junction with unharmonic CPR, *J. Supercond, Novel Magn.* 26, 839–843 (2013).
- [29] S. T. Kingni, G. Fautso Kuate, V. Kamdoum Tamba, A. V. Monwanou and J. Bio Chabi, Analysis of a fractal Josephson junction with unharmonic current-phase relation, *Journal of Superconductivity and Novel Magnetism* 32, 2295–2301 (2019).
- [30] E. N. Lorenz, *The essence of chaos*, UCL Press, (1993)
- [31] J. C. Sprott, Some simple chaotic flows, *Phys Rev E* 50, R647-R650 (1994).
- [32] J. C. Sprott, Simple chaotic systems and circuit, *Am J. Phys* 68, 758-763 (2000)
- [33] Z. Fu, and J. Heidel, Non-chaotic behavior in three-dimensional quadratic systems, *Nonlinearity* 12, 739-740 (1999)
- [34] B. J. West, *Fractal Physiology and Chaos in Medicine, Studies of Nonlinear Phenomena in Life Science* (2nd Ed.), World Scientific, Singapore, 16 (2012)
- [35] E. N. Lorenz, Deterministic Nonperiodic Flow, *J. Atmos Sci* 20, 130–141 (1963)
- [36] A. L. Golberger, Non-linear dynamics for clinicians: chaos theory, fractals, and complexity at the bedside, *The Lancet* 347, 1312-1314 (1996)
- [37] G. M. Somfai, E. Tátrai, L. Laurik, B. E. Varga, V. Ölvedy, W. E. Smiddy, *et al*, Fractal-based analysis of optical coherence tomography data to quantify retinal tissue damage, *BMC bioinformatics* 15, 295-304 (2014)
- [38] D. Levy, *Chaos theory and strategy: Theory, application, and managerial implications*, *Strategic Management Journal* 15, 167-167 (1994)
- [39] R. M. Goodwin, *Chaotic economic dynamics*. Oxford University Press: Oxford (1990)
- [40] J. Larsson and B. Dahlin, Educating far from equilibrium: Chaos philosophy and the quest for complexity in education, *Forma Mente: Rivista Internazionale di Ricerca sul Futuro digital*, 9, (2012).

BIBLIOGRAPHY

- [41] O. E. Rössler, Continuous chaos - four prototype equations, *Ann. New York Acad. Sci.* 316, 376-392 (1979)
- [42] J. Kengne, L. K. Kengne, J. C. Chedjou, & K. Nosirov, A simple anti-parallel diodes based chaotic jerk circuit with arcsinh function: theoretical analysis and experimental verification, *Analog Integrated Circuits and Signal Processing* 108, 597-623 (2021)
- [43] H. Tanaka, S. Sato, & K. Nakajima, Integrated circuits of map chaos generators, *Analog Integrated Circuits and Signal Processing* 25, 329-335 (2000)
- [44] S. H. Strogatz, , *Nonlinear dynamics and chaos: with applications to physics, biology, chemistry, and engineering*, Westview press. (2014)
- [45] B. Nana, S. B. Yamgoué, R. Tchitnga, and P. Wofo, On the modeling of the dynamics of electrical hair clippers, *Chaos, Solitons & Fractals* 112, 14-23 (2018)
- [46] R. M. Nguimdo and P. Colet, Electro-optic phase chaos systems with an internal variable and a digital key, *Optics express* 20, 25333-25344 (2012)
- [47] Y. C. Kouomou, P. Colet, L. Larger, and N. Gastaud, Electro-optic phase chaos systems with an internal variable and a digital key, *IEEE journal of quantum electronics* 41, 156-163 (2005)
- [48] L. O. Chua, *The genesis of Chua's circuit*, Stuttgart: Hirzel-Verlag 46, 250-257 (1992)
- [49] J. H. B. Deane, D. C. Hamill, Instability, subharmonics, and chaos in power electronics systems, *IEEE T Power Electron* 5, 260-268 (1990)
- [50] M. Joshi, & A. Ranjan, An autonomous chaotic and hyperchaotic oscillator using OTRA. *Analog Integrated Circuits and Signal Processing* 101, 401-413 (2019)
- [51] E. Tlelo-Cuautle, A. Gaona-Hernández, & J. García-Delgado, Implementation of a chaotic oscillator by designing Chua's diode with CMOS CFOAs, *Analog Integrated Circuits and Signal Processing* 48, 159-162 (2006)
- [52] B. Nana, S. B. Yamgoué, R. Tchitnga, and P. Wofo, Simple Mathematical Model for Ferromagnetic Core Inductance and Experimental Validation, *American Journal of Electrical and Electronic Engineering* 3, 29-36 (2015)
- [53] B. Nana, S. B. Yamgoué, I. Kemajou, R. Tchitnga, and P. Wofo, Dynamics of an RLC series circuit with hysteretic iron-core inductor, *Chaos, Solitons & Fractals* 106, 184-192 (2018)
- [54] A. Azzouz, M. Hasler, Orbits of the R-L-diode circuit, *IEEE T Circ Syst* 37, 1330-9 (1990).

BIBLIOGRAPHY

- [55] P. Louodop, H. Fotsin, M. Kountchou, E. B. M. Ngouonkadi, H. A. Cerdeira, & S. Bowong, Finite-time synchronization of tunnel-diode-based chaotic oscillators, *Physical Review E* 89, 032921 (2014)
- [56] S. Gopal and Y. C. Lai, Finite-time synchronization of tunnel-diode-based chaotic oscillators, *Circuits, Systems & Signal Processing* 28, 535-545 (2009)
- [57] R. W. Tapche, Z. T. Njitacke, J. Kengne, & F. B. Pelap, Complex dynamics of a novel 3D autonomous system without linear terms having a line of equilibria: coexisting bifurcations and circuit design, *Analog Integrated Circuits and Signal Processing* 103, 57-71 (2020)
- [58] A. O. Semenov, A. V. Osadchuk, I. A. Osadchuk, K. O. Koval, & M. O. Prytula, The chaos oscillator with inertial non-linearity based on a transistor structure with negative resistance, 17th International Conference of Young Specialists on Micro/Nanotechnologies and Electron Devices (EDM, 2016)
- [59] F. C. Talla, R. Tchitnga, R. Kengne, B. Nana, and A. Fomethé, Prytula, The chaos oscillator with inertial non-linearity based on a transistor structure with negative resistance, *Heliyon* 5, e02715 (2019)
- [60] R. Tchitnga, R. Zebaze Nanfa'a, F. B. Pelap, P. Louodop, P. Wofo, Chaotic behaviors of operational amplifiers, *Journal of Vibration and Control* 23, 744-751 (2017)
- [61] R. Zebaze Nanfa'a, R. Tchitnga, P. H. Louodop Fotso, R. Kengne, F. C. Talla, B. Nana, and F. B. Pelap, Non-periodic oscillations, bistability, coexistence of chaos and hyperchaos in the simplest resistorless Op-Amp based Colpitts oscillator. *Heliyon* 6, e03482 (2020)
- [62] A. S. Elwakil and A. M. Soliman, Two modified for chaos negative impedance converter Op-Amp oscillators with symmetrical and antisymmetrical nonlinearities, *Int. J. Bifurcation Chaos* 8, 1335-1346 (1998)
- [63] L. O. Chua, Memristor-The missing circuit element, *IEEE Trans. Circuit Theory*, *IEEE Trans. Circuit Theory*, CT-18, 507-519 (1971)
- [64] D. B. Strukov, G. S. Snider, D. R. Stewart, and Williams, The missing memristor found, *Nature* 453, 80-83 (2008)
- [65] M. P. Sah, C. Yang, H. Kim, B. Muthuswamy, J. Jevtic and L. Chua, A generic model of memristors with parasitic components, *IEEE Transactions on Circuits and Systems I: Regular Papers* 62, 891-898 (2015)

BIBLIOGRAPHY

- [66] B. A. Mezatio, M. Motchongom Tingue, R. Kengne, A. T. Kouanou, T. F. Fonzin & R. Tchitnga, A generic model of memristors with parasitic components, *International Journal of Dynamics and Control* 8, 70-90 (2020)
- [67] S. K. Dana, D. C. Sengupta, and K. D. Edoh, Chaotic dynamics in Josephson junction. *IEEE Transactions on Circuits and Systems I: Fundamental Theory and Applications* 48: 990–996 (2001)
- [68] P. Louodop, R. Tchitnga, F. F. Fagundes, M. Kountchou, V. K. Tamba, H. A. Cerdeira, Extreme multistability in a Josephson-junction-based circuit, *Physical Review E* 99, 042208 (2019)
- [69] S. Nikolov, S. Clodong, Hyperchaos–chaos–hyperchaos transition in modified Rössler systems, *Chaos, Solit. Fractals* 28, 252-263 (2006)
- [70] M. T. Levinsen, R. Y. Chiao, M. J. Feldman and B. A. Tucker. An inverse ac Josephson effect voltage standard. *Appl. Phys. Lett.* 31, 776-778 (1977).
- [71] X. F. Meng, Y. D. Dai, H. M. Jiang, X. M. Ren, Y. Zhang, M. X. Yan, *et al.* Observations of the ac Josephson effect in Y-Ba-Cu-O superconductors at 77 K. *Solid state communications* 63, 853-855 (1987).
- [72] J. X. Jin, Y. Xin, Q. L. Wang, Y. S. He, C. B. Cai, Y. S. Wang, and Z. M. Wang. Enabling high-temperature superconducting technologies toward practical applications. *IEEE Transactions on Applied Superconductivity* 24, 1-12 (2014).
- [73] R. Kengne, R. Tchitnga, S. A. Kammogne Tewa, G. Litak, A. Fomethé, and C. Li, Fractional-order two-component oscillator: stability and network synchronization using a reduced number of control signals, *European Physical Journal B* 91, 304 (2018)
- [74] M. S. Krishna, S. Das, K. Biswas, & B. Goswami, Fabrication of a fractional-order capacitor with desired specifications: a study on process identification and characterization, *IEEE Transactions on Electron Devices* 58, 4067-4073 (2011)
- [75] J. C. Sprott, A proposed standard for the publication of new chaotic systems, *Int. J. Bifurcation. Chaos* 21, 2391-2394 (2011)

BIBLIOGRAPHY

- [76] J. Kengne, G. D. Leutcho, & A. N. K. Telem, Reversals of period-doubling, coexisting multiple attractors, and offset boosting in a novel memristive diode bridge-based hyperjerk circuit, *Analog Integrated Circuits and Signal Processing* 101, 379-399 (2019)
- [77] F. M. Salamand, S. S. Sastry, "Dynamics of the forced Josephson junction circuit: the regions of chaos," *Institute of Electrical and Electronics Engineers. Transactions on Circuits and Systems*, 32, (8), 784–796, (1985).
- [78] C. B. Whan, C. J. Lobb, & M. G. Forrester, Spiking and bursting in Josephson junction, *Journal of applied physics* 77, 382-389 (1995)
- [79] M. Octavio, Bifurcating, chaotic, and intermittent solutions in the RF based Josephson junction, *Phys. Rev. B* 29, 1231-1242 (1984)
- [80] T. P. Valkering, C. L. A. Hooijer, and M. F. Kroon, Bifurcating, chaotic, and intermittent solutions in the RF based Josephson junction, *Physica D* 135, 137-153 (2000)
- [81] R. T. Siewe, U. S. Domguia, & P. Woafu, Microcontroller control/synchronization of the dynamics of van der Pol oscillators submitted to disturbances, *International Journal of Nonlinear Sciences and Numerical Simulation*, 19, 153-163 (2018)
- [82] J. M. Martinis, M. H. Devoret and J. Clarke, Experimental tests for the quantum behavior of a macroscopic degree of freedom: The phase difference across a Josephson junction, *Phys. Rev. B* 35, 4682-4698 (1987).
- [83] R. Chiu, M. Mora-Gonzalez and D. Lopez-Mancilla, Microcontroller control/synchronization of the dynamics of van der Pol oscillators submitted to disturbances, *Conf. Electron. Eng. Comput. Science, IERI Procedia* 4, 247-252 (2013)
- [84] M. Z. De la Hoz, L. Acho and Y. Vidal, An experimental realization of a chaos-based secure communication using Arduino microcontrollers, *Scientific. World J.* 10, 123080 (2015).
- [85] H. Hamiche, S. Guermah, R. Saddaoui, K. Hannoun, M. Laghrouche, and S. Djennoune, Analysis and implementation of a novel robust transmission scheme for private digital communications using Arduino Uno board, *Nonlinear Dyn.* 81, 1921-1932 (2015)
- [86] R. T. Siewe, U. S. Domguia, & P. Woafu, Generation of pulse-like and bursting-like oscillations from nonlinear systems using embedded technologies and applications to excite

BIBLIOGRAPHY

- mechanical arms, *Communications in Nonlinear Science and Numerical Simulation* 69, 343-359 (2019)
- [87] M. A. Murillo-Escobar, C. Cruz-Hernández, F. F. Abundiz-Pérez and R. M. López-Gutiérrez, A robust embedded biometric authentication system based on fingerprint and chaotic encryption, *Expert Syst. Appl.* 42, 8198-8211 (2015)
- [88] T. Visser, Modelling and Analysis of Long Josephson Junctions, Ph/D thesis, 2002 [cited at p. 7]
- [89] B. D. Josephson. “Possible new effects in superconductive tunneling”, *Phys. Lett*, 1(7), 251–253, (1962).
- [90] B. D. Josephson. “The discovery of tunneling super-currents”, *Rev. Mod. Phys*, 46, (2), 251–254, (1974).
- [91] L. N. Cooper. “Bound electron pairs in a degenerate Fermi gas”, *Phys. Rev*, 104, (4), 1189–1190, (1956).
- [92] L. Burke. “On the tunnel effect (Abstract)”, *The Quarterly Journal of Experimental Psychology*, 4, (3), 121–138, (1952).
- [93] A. Mostefai. Modélisation et caractérisation électrique de la jonction Josephson par approximation au sens des moindres carrés. *Carpathian Journal of Electronic & Computer Engineering* , 12(2), (2019).
- [94] P. Woaf, Transitions to chaos and synchronization in a nonlinear emitter-receiver system. *Physics Letters A*, 267(1), 31-39 (2000).
- [95] B. A. Huberman, J. P. Crutchfield, & N. H. Packard, Noise phenomena in Josephson junctions. *Applied Physics Letters*, 37(8), 750-752 (1980).
- [96] H. D. Jensen, A. Larsen, & J. Mygind, Chaos in self-pumped resonator coupled Josephson junctions. *Physica B: Condensed Matter*, 165, 1661-1662 (1990).
- [97] C. B. Whan, C. J. Lobb, & M. G. Forrester, Effect of inductance in externally shunted Josephson tunnel junctions. *Journal of applied physics*, 77(1), 382-389 (1995)
- [98] K. K Likharev, *Dynamics of Josephson Junctions and Circuits* (New York: Gordon and Breach) (1981)
- [99] D. T. Ngatcha, A. A. Oumate, A. S. Kemnang Tsafack, and S. T. Kingni, Dynamical analysis and microcontroller implementation of linear resistor-capacitor shunted Josephson junction model. *Chaos Theory and Applications*, 3(2), 55-58, (2021).

BIBLIOGRAPHY

- [100] J. Clarke, "A superconducting galvanometer employing Josephson tunneling," *Philosophical Magazine*, vol. 13, no. 121, pp. 115–127, (1966).
- [101] W. C. Stewart, "Current-voltage characteristics of Josephson junctions," *Applied Physics Letters*, vol. 12, no. 8, pp. 277–280, (1968).
- [102] A. B. Cawthorne, C. B. Whan, et C. J. Lobb, Influence et évaluation de l'inductance parasite dans les jonctions Josephson shuntées. *Transactions IEEE sur la supraconductivité appliquée*, 7 (2), 2355-2358 (1997).
- [103] C. B. Whan, , & C. J. Lobb, Complex dynamical behavior in RCL-shunted Josephson tunnel junctions. *Physical Review E*, 53(1), 405 (1996).
- [104] A. D. Smith, R. D. Sandell, A. H. Silver, and J. F. Burch, "Chaos and Bifurcation in Josephson Voltage-Controlled Oscillators," *IEEE Transactions on Magnetics*, vol. 23, no. 2, pp. 1267–1270, (1987).
- [105] S. K. SHRIVASTAVA, et G. KUMAR, Application of high-Tc superconducting Josephson junction devices. *International Journal of Emerging Technologies and innovative research (JETIR)*, vol.7. (2019)
- [106] A. P. Kuznetsov, S. P. Kuznetsov, E. Mosekilde, and N. V. Stankevich, "Co-existing hidden attractors in a radio- physical system," *J. Phys. A. Math. Theor.*, 48, (12), 125101-18, Mar. (2015).
- [107] J. S. Pei, P. W. Joseph, D. T. Michael, F. M. Sami, and G. B. Francois, "Understanding memristors and memcapacitors in engineering mechanics applications," *Nonlinear Dyn.*, vol. 80, no. 1, pp. 457_489, Apr. (2015).
- [108] S. Duan, X. Hu, L. Wang, S. Gao, and C. Li, "Hybrid memristor/RTD structure-based cellular neural networks with applications in image processing," *Neural Comput. Appl.*, vol. 25, no. 2, pp. 291_296, Aug. (2014).
- [109] J. X. Zha, H. Huang, and Y. J. Liu, "A novel window function for memristor model with application in programming analog circuits," *IEEE Trans. Circuits Syst. II, Exp. Briefs*, vol. 63, no. 5, pp. 423_427, Mar. (2016).
- [110] B. Arindam, "Small-signal neural models and their applications," *IEEE Trans. Biomed. Circuits Syst.*, 6, (1), 64-75, Feb. (2012).

BIBLIOGRAPHY

- [111] M. Gotz, U. Feldmann, and W. Schwarz, "Synthesis of higher dimensional Chua circuit," *IEEE Trans. Circuits Syst. I, Fundam. Theory Appl.*, 40, (11), 854-860, Nov. (1993).
- [112] D. Premraj, K. Suresh, T. Banerjee, and K. Thamilmaran, "An experimental study of slow passage through Hopf and pitchfork bifurcations in a parametrically driven nonlinear oscillator," *Commun. Nonlinear Sci. Numer. Similar.*, 37, 212-221, May (2016).
- [113] A. Arulgnanam, K. Thamilmaran, and M. Daniel, "Chaotic dynamics with high complexity in a simplified new nonautonomous nonlinear electronic circuit," *Chaos Solitons Fractals*, 42, (4), 2246-2253, Nov. (2009).
- [114] T. Banerjee, "Single amplifier biquad based inductor-free Chua's circuit," *Nonlinear Dyn.*, 68, (4), 565-573, Jun. (2012).
- [115] T. A. Matsumoto, chaotic attractor from Chua's circuit. *IEEE Trans Circuit Syst*; 31, 1055–8. (1984)
- [116] M. P. Kennedy, Three steps to chaos. Part I: Evolution. *IEEE Trans Circuit Syst*; 40, 640–56 (1993)
- [117] K. Murali K, M. Lakshmanan, L. O. Chua, Bifurcation and chaos in the simplest dissipative non-autonomous circuit. *Int J Bifurcat Chaos*; 4, 1511–24 (1994).
- [118] A. S. Elwakil, & M. P Kennedy, A semi-systematic procedure for producing chaos from sinusoidal oscillators using diode-inductor and FET-capacitor composites. *IEEE Transactions on Circuits and Systems I: Fundamental Theory and Applications*, 47(4), 582-590 (2000)
- [119] A. S. Elwakil, & M. P. Kennedy, Construction of classes of circuit-independent chaotic oscillators using passive-only nonlinear devices. *IEEE Transactions on Circuits and Systems I: Fundamental Theory and Applications*, 48(3), 289-307 (2001)
- [120] J. C. Sprott, A new class of chaotic circuits. *Physics Letters A*, 266(1), 19-23 (2000)
- [121] M. P. Kennedy, Robust op-amp realization of Chua's circuit. *Frequency*; 46:66–80 (1992)
- [122] K. Thamilmaran, M. Lakshmanan, K. Murali, Rich variety of bifurcation and chaos in variant of Murali–Lakshmanan–Chua circuit. *Int J Bifurcat Chaos*, 10:1781–5 (2000)
- [123] L. O. Chua, C. A. Desoer, and E. S. Kuh, *Linear and nonlinear circuits*, New York: McGraw-Hill; (1987).

BIBLIOGRAPHY

- [124] G. Q. Zhong, and F. Ayrom, Experimental confirmation of chaos from Chua's circuit. *International journal of circuit theory and applications*, 13(1), 93-98 (1985)
- [125] T. Matsumoto, L. O. Chua, M. Komuro, The double scroll. *IEEE Trans Circuits Syst*, 32, 797–818 (1985)
- [126] M. Lakshmanan, K. Murali, *Chaos in nonlinear oscillators: controlling and synchronization*. Singapore: World Scientific Publishing Company; (1996)
- [127] Y. Ueda, N. Akamatsu, Chaotically transitional phenomena in the forced negative-resistance oscillator. *IEEE Trans Circuit Syst*, 28, 217–23 (1981)
- [128] P. S. Linsay, Period doubling and chaotic behavior in a driven anharmonic oscillator. *Phys Rev Lett*, 4, 1349–52 (1981)
- [129] Testa J, Perez J, Jeffries C. Evidence for universal chaotic behavior of a driven nonlinear oscillator. *Phys Rev Lett* 48, 714–7 (1982)
- [130] N. Inaba, S. Mori, Chaos via torus breakdown in a piecewise-linear forced van der Pol oscillator with a diode. *IEEE Trans Circuit Syst* 38, 398–409 (1991)
- [131] J. G. Lacy, A simple piecewise-linear nonautonomous circuit with chaotic behavior. *Int J Bifurcation Chaos* 6, 2097–100 (1996)
- [132] K. Thamilmaran, M. Lakshmanan, Classification of bifurcation and routes to chaos in a variant of Murali–Lakshmanan–Chua circuit. *Int J Bifurcat Chaos* 12, 783–813 (2002)
- [133] K. Thamilmaran, D. V. Senthilkumar, A. Ishaq Ahmed, M. Lakshmanan, Strong chaos in a forced negative conductance series LCR circuit. *Int J Bifurcation Chaos*, 15, 637–51 (2005)
- [134] E. Kurt, Nonlinearities from the non-autonomous chaotic circuit with a non-autonomous model of Chua's circuit. *Phys Scr*, 74, 22–7 (2006)
- [135] A. I. Ahamed and M. Lakshmanan, "Nonsmooth bifurcations, transient hyperchaos and hyperchaotic beats in a memristive Murali- Lakshmanan- Chua circuit," *Int. J. Bifurc. Chaos*, vol. 23, no. 6, pp. 1350098-1_1350098-28, Jun. 2013.
- [136] B. Bao, P. Jiang, H. Wu, and F. Hu, "Complex transient dynamics in periodically forced memristive Chua's circuit," *Nonlinear Dyn.*, vol. 79, no. 4, pp. 2333_2343, Mar. 2015.
- [137] A. I. Ahamed, K. Srinivasan, K. Murali, and M. Lakshmanan, "Observation of chaotic beats in a driven memristive Chua's circuit," *Int. J. Bifurc. Chaos*, vol. 21, no. 3, pp. 737_757, Mar. 2011.

BIBLIOGRAPHY

- [138] Mahmoud, M. Gamal, E. Mansour, Ahmed, and Nabil Sabor. "On autonomous and nonautonomous modified hyperchaotic complex Lü systems." *International Journal of Bifurcation and Chaos* 21.07 (2011) 1913-1926.
- [139] C. Barbara, & C. Silvano, "Hyperchaotic behavior of two bi-directionally Chua's circuits," *Int. J. Circuits Theor. Appl.* 30, 625–637 (2002)
- [140] S. Cang, G. Qi, & Z. Chen, "A four-wing hyperchaotic attractor and transient chaos generated from a new 4-D quadratic autonomous system," *Nonlin. Dyn.* 59, 515–527 (2010)
- [141] J. D. Gibbon, & M. J. McGuinnes, "The real and complex Lorenz equations in rotating fluids and laser" *Physica D* 5, 108–121 (1982).
- [142] A. C. Fowler, J. D. Gibbon, & M. J. McGuinnes, "The real and complex Lorenz equations and their relevance to physical systems," *Physica D* 7, 126–134 (1983)
- [143] H. Zeghlache, & P. Mandel, "Influence of detuning on the properties of laser equations," *J. Opt. Soc. Amer. B* 2, 18–22 (1985)
- [144] A. Rauh, L. Hannibal, & N. Abraham, "Global stability properties of the complex Lorenz model," *Physica D* 99, 45–58 (1996)
- [145] G. M. Mahmoud, T. Bountis, M. A. Al-Kashif, & S. A. Aly, "Dynamical properties and synchronization of complex non-linear equations for detuned laser," *J. Dyn. Syst.* 24, 63–79. (2009)
- [146] G. M. Mahmoud, & T. Bountis, "The dynamics of systems of complex nonlinear oscillators," A Review, *Int. J. Bifurcation and Chaos* 14, 3821–3846 (2004)
- [147] G. M. Mahmoud, H. A. Abdusalam, & A. A. M. Farghaly, "Chaotic behavior and chaos control for a class of complex partial differential equations," *Int. J. Mod. Phys. C* 12, 889–899 (2001)
- [148] BELIC, M. R. Deterministic chaos. *Sv. Fiz. Nauka*, vol. 3, p. 1-186. (1990)
- [149] H. Fotsin, S. Bowong, & J. Daafouz, Adaptive synchronization of two chaotic systems consisting of modified Van der Pol–Duffing and Chua oscillators. *Chaos, Solitons & Fractals*, 26(1), 215-229 (2005).
- [150] G. P. King, S. T. Gaito, Bistable chaos. I. Unfolding the cusp. *Phys Rev A* 1992;46:3093–599 (2005).

BIBLIOGRAPHY

- [151] H. B. Fotsin, P. Wofo, Adaptive synchronization of a modified and uncertain chaotic Van der Pol–Duffing oscillator based on parameter identification. *Chaos, Solitons & Fractals*;24(5), 1363–71 (2005)
- [152] R. Femat, G. Solis-Perales. Synchronization of chaotic systems with different order. *Phys Rev E*; 65, 036226–33 (2002)
- [153] S. Bowong, F. M. Moukam, Stability and duration time of chaos synchronization of a class of nonidentical oscillators. *Phys Scr*; 68, 326–32 (2003)
- [154] G. P. Jiang, W. X. Zheng, G. Chen, Jiang, G. P., Zheng, Integral-observer-based chaos synchronization. *IEEE Transactions on Circuits and Systems II: Express Briefs*, 53(2), 110–114 (2006).
- [179] T. A. Matsumoto, chaotic attractor from Chua's circuit. *IEEE Trans Circ Syst*; 31, 1055–8 (1984)
- [156] G. Q. Zhong, Implementation of Chua's circuit with cubic nonlinearity. *Int J Bifur Chaos*; 41, 934–41 (1994)
- [157] R. N. Madan, Chua's circuit: a paradigm for chaos. Singapore: World Scientific; 1993
- [158] G. P. Jiang, W. X. Zheng, G. Chen, Global chaos synchronization with channel time-delay. *Chaos, Solitons & Fractals*, 20, 267–75 (2004)
- [159] L. Li, Y. Yu, G. J. Ye, Q. Ge, X. Ou, H. Wu, D. Feng, X. H. Chen, and Y. Zhang, 'Black phosphorus field-effect transistors', *Nature nanotechnology* 9(5), 372 (2014)
- [160] A. Javey, J. Guo, Q. Wang, M. Lundstrom, and H. Dai, 'Ballistic carbon nanotube field-effect transistors', *nature* 424(6949), 654 (2003)
- [161] R. TCHITNGA, Robert, T. NGUAZON, P. H. L. FOTSO, *et al.* Chaos in a single op-amp–based jerk circuit: Experiments and simulations. *IEEE Transactions on Circuits and Systems II: Express Briefs*, vol. 63, n° 3, p. 239-243 (2015).
- [162] Q. XU, Q. ZHANG, B. BAO, *et al.* Non-autonomous second-order memristive chaotic circuit. *Accès IEEE*, vol. 5, p. 21039-21045 (2017)
- [163] Q. Xu, Y. Lin, B. C. Bao, and M. Chen, "Multiple attractors in a non-ideal active voltage-controlled memristor based Chua's circuit," *Chaos Solit. Fractals*, vol. 83, pp. 186–200, (Feb. 2016).

BIBLIOGRAPHY

- [164] Kitio, Theoretical and experimental studies of the dynamics of nonlinear electromechanical systems with flexible arms, thesis 107 (2008)
- [165] C. Hayashi Nonlinear oscillations in physical systems. New York: Mc Graw-Hill (1964).
- [166] J. B. Mogo, and P. Woafu. "Dynamics of a nonlinear electromechanical device with a pendulum arm." *Computational and Nonlinear Dynamics*, 374-378 (2007)
- [167] R. Yamapi, J. B. Chabi Orou, and P. Woafu, "Harmonic Oscillations, Stability and Chaos Control in a Nonlinear Electromechanical System," *J. Sound Vib.*, 259(5), pp. 1253–1264 (2003)
- [168] I. Petráš, "Fractional-order memristor-based Chua's circuit," *IEEE Trans. Circuits Syst. II, Exp. Briefs*, vol. 57, no. 12, pp. 975_979, Dec. (2010).
- [169] A. L. Fitch, D. Yu, H. H. Iu, and V. Sreeram, "Hyperchaos in a memristor-based modified canonical Chua's circuit," *Int. J. Bifurc. Chaos*, vol. 22, no. 6, pp. 1250133-1-1250133-8, Dec. (2012).
- [170] J. Ma, Z. Q. Chen, Z. L. Wang, and Q. Zhang, "A four-wing hyperchaotic attractor generated from a 4-D memristive system with a line equilibrium," *Nonlinear Dyn.*, vol. 81, no. 3, pp. 1275_1288, Aug. (2015).
- [171] L. Zhou, C. H. Wang, and L. L. Zhou, "Generating hyperchaotic multi-wing attractor in a 4D memristive circuit," *Nonlinear Dyn.*, vol. 85, no. 4, pp. 2653_2663, Aug. (2016).
- [172] J. Kengne, Z. N. Tabekoueng, V. K. Tamba, and A. N. Negou, "Periodicity, chaos, and multiple attractors in a memristor-based Shinriki's circuit," *Chaos*, vol. 25, no. 10, pp. 103126-1-103126-10, Oct. (2015).
- [173] Q. Xu, Y. Lin, B. C. Bao, and M. Chen, "Multiple attractors in a non-ideal active voltage-controlled memristor-based Chua's circuit," *Chaos Solit. Fractals*, vol. 83, pp. 186_200, Feb. (2016).
- [174] P. Saha, D. C. Saha, A. Ray, and A. R. Chowdhury, "Memristive non-linear system and hidden attractor," *Eur. Phys. J. Special Top.*, vol. 224, no. 8, pp. 1563_1574, Jul. (2015).
- [175] B. C. Bao, Z. H. Ma, J. P. Xu, Z. Liu, and Q. Xu, "A simple memristor chaotic circuit with complex dynamics," *Int. J. Bifurc. Chaos*, vol. 21, no. 9, pp. 2629_2645, Sep. (2011).
- [176] N. F. F. Foka, B. Ramakrishnan, A. R. Tchamda, S. T. Kingni, K. Rajagopal, & V. K. Kuetche, Dynamical analysis of Josephson junction neuron model driven by a thermal signal

BIBLIOGRAPHY

- and its digital implementation based on microcontroller. *The European Physical Journal B*, 94(12), 1-7 (2021).
- [177] A. Wolf, J. B. Swift, H. L. Swinney, and J. A. Vastano, ‘Determining Lyapunov exponents from a time series, *Physica D: Nonlinear Phenomena* 16(3), 285–317. (1985)
- [178] J. C Sprott, *Elegant chaos: algebraically simple chaotic flows*, World Scientific. (2010)
- [179] F. Faure, “systèmes dynamiques, Chaos et Applications”, cours de Master I de l’Université de Joseph Fourier, Grenoble, France. (2015)
- [180] https://fr.wikipedia.org/wiki/Electric_component
- [181] R. Yamapi and P. Wofo. Nonlinear Electromechanical Devices: Dynamics and Synchronization, in *Mechanical Vibrations: Measurement, Effects, and Control*. Eds. R. C. Sapri, Nova Publishers; (2008).
- [182] C. A. Kitio Kwuimy and P. Wofo. Dynamics of a self-sustained electromechanical system with flexible arm and cubic coupling. *Communication in Nonlinear Science and Numerical Simulation*, 12 (8): 1504-1517, (2007).
- [183] M. Conti and C. Turchetti, “Approximate identity neural networks for the analog synthesis of nonlinear dynamical systems,” *IEEE Trans. Circuits Syst. I Fundam. Theory Appl.*, vol. 41, no. 12, pp. 841–858, (1994).
- [184] L. Fortuna, M. Frasca, M. G. Xibilia, Chua’s Circuit Implementations: Yesterday, Today and Tomorrow, Singapore: World Scientific 65, (2009)
- [185] J. C. Chedjou, H. B. Fotsin, P. Wofo, & S. Domngang, Analog simulation of the dynamics of a van der Pol oscillator coupled to a Duffing oscillator, *IEEE Transactions on Circuits and Systems I: Fundamental Theory and Applications* 48, 748-757 (2001)
- [186] C. Li, J. C. Sprott. Variable-boostable chaotic flows. *Optik Int J Light Electron Opt.* 27, 10389-10398 (2016).
- [187] A. Akif, L. Chunbiao, P. Ihsan. Amplitude control analysis of a four-wing attractor, its electronic circuit designs, and microcontroller-based random number generator. *J Circuits Syst Comput.* 26, 1750190-1750209 (2017).

BIBLIOGRAPHY

- [188] C. Li, J. Sprott, Z. Yuan, et al. Constructing chaotic systems with total amplitude control. *Int J Bifurcation Chaos* 25, 1530025–1530039 (2015).
- [189] V. Kamdoum Tamba, R. Karthikeyan, V-T Pham, et al. Chaos in a system with an absolute nonlinearity and chaos synchronization. *Adv Math Phys.* (2018). doi:10.1155/2018/5985489
- [190] J. R. Mboupda Pone, S. T. Kingni, G. R. Kol & V-T Pham. Hopf bifurcation, antimonotonicity and amplitude controls in the chaotic Toda jerk oscillator: analysis, circuit realization, and combination synchronization in its fractional-order form, *Automatika*, 60,149-161 (2019).
- [191] C. B. Whan and C. J. Lobb, “Complex dynamical behaviors in RCLshunted Josephson tunnel junction,” *Phys. Rev. E*, vol. 53, no. 1, pp. 405–413 (1996).
- [192] N. F. F. Foka, B. Ramakrishnan, A. C. Chamgoué, A. F. Talla, & V. K. Kuetche. Neuronal circuit based on Josephson junction actuated by a photocurrent: dynamical analysis and microcontroller implementation. *The European Physical Journal B*, 95(6), 1-8 (2022)

LIST OF PUBLICATIONS OF THE THESIS

LIST OF PUBLICATIONS OF THE THESIS

1. Publication of the thesis

- **Y.J., Monkam**, S.T. Kingni, S. T., R. Tchitnga, and P. Wofo, “Electronic simulation and microcontroller real implementation of an autonomous chaotic and hyperchaotic system made of a Colpitts-Josephson junction-like circuit”, *Analog Integrated Circuits and Signal Processing* 110 (3), 395-407 (2022)

2. Other publication

- G.B.M. Soh, **Y.J. Monkam**, P.R.N. Tuwa, R. Tchitnga, and P. Wofo, “Study of a piezoelectric plate-based self-sustained electric and electromechanical oscillator”, *Mechanic Research Communication*, 105, 103504-13 (2020).